

**NASA**  
**Technical**  
**Paper**  
**2625**

December 1986

# Description of Data on the Nimbus 7 LIMS Map Archive Tape

## *Ozone and Nitric Acid*

Ellis E. Remsberg,  
Robert J. Kurzeja,  
Kenneth V. Haggard,  
James M. Russell III,  
and Larry L. Gordley

(NASA-TP-2625) DESCRIPTION OF DATA ON THE  
NIMBUS 7 LIMS MAP ARCHIVE TAPE: OZONE AND  
NITRIC ACID (NASA) 73 p CSCL 04A

N87-13022

H1/46 44679  
Unclas

**NASA**

**NASA  
Technical  
Paper  
2625**

1986

# Description of Data on the Nimbus 7 LIMS Map Archive Tape

## *Ozone and Nitric Acid*

Ellis E. Remsberg  
*Langley Research Center  
Hampton, Virginia*

Robert J. Kurzeja  
*Savannah River Laboratory  
Aiken, South Carolina*

Kenneth V. Haggard and  
James M. Russell III  
*Langley Research Center  
Hampton, Virginia*

Larry L. Gordley  
*The College of William and Mary  
Williamsburg, Virginia*

**NASA**

National Aeronautics  
and Space Administration

Scientific and Technical  
Information Branch

## Introduction

The Limb Infrared Monitor of the Stratosphere (LIMS) experiment on the Nimbus 7 spacecraft consisted of a thermal infrared limb scanning radiometer with six channels centered at wavelengths ranging from 6.2 to 15  $\mu\text{m}$  (Gille and Russell 1984). The experiment functioned in orbit from October 24, 1978, until May 28, 1979. Radiance profiles measured by LIMS were later processed at Langley Research Center to infer middle atmosphere temperature profiles and the concentrations of key compounds believed to be important in stratospheric ozone photochemistry. The results of this analysis are available on the LIMS Map Archival Tape (LAMAT), which contains Fourier coefficient representations of these atmospheric variables at selected pressures (100, 70, 50, 30, 16, 10, 7, 5, 3, 2, 1.5, 1.0, 0.7, 0.5, 0.4, 0.2, 0.1, 0.05 mbar) and every 4° of latitude. The Fourier coefficients were determined with a Kalman filter technique in order to estimate synoptic maps from asymptotic satellite data. This approach is discussed in detail in Haggard et al. (1986) and applied to temperature and geopotential heights in that report. The pertinent LAMAT analysis notation, formats, and terminology are also available there. The LAMAT, as well as the LIMS Inverted Profile Archival Tape (LAIPAT), is archived at the National Space Sciences Data Center (NSSDC), NASA Goddard Space Flight Center, Greenbelt, MD 20771.

This report concentrates on the Kalman filter results for two other LIMS species—ozone ( $\text{O}_3$ ) and nitric acid ( $\text{HNO}_3$ ). These results are available for ozone from 100 to 0.05 mbar, and for nitric acid from 100 to 2 mbar. Topics that are discussed include the input parameters to the Kalman filter algorithm, special data properties that affect maps derived from the coefficients, an overview of the map results, and comparison of the mixing ratios with the original data. Strengths and weaknesses of the mapped results are noted.

## Symbols

<b>K</b>	vector defined in equation (2)
<b>M</b>	order of the Fourier series, less than or equal to 6
<b>p</b>	pressure, mbar
<b>S</b>	error covariance matrix
<b>T</b>	temperature, K
<b>t</b>	time
<b>X</b>	vector of Fourier coefficients $X_j$ ( $j = 1, 2, 3, \dots, 2M + 1$ )

<b>Z</b>	ozone mixing ratio, ppmv
<b><math>\theta</math></b>	latitude, deg
<b><math>\lambda</math></b>	longitude, deg east
<b><math>\sigma^2</math></b>	variance
<b><math>\sigma_{\text{obs}}</math></b>	observed standard deviation at noon GMT between synoptic field and asymptotic data
<b><math>\sigma_{\text{wave}}</math></b>	longitudinal variations about the zonal mean expressed as a root-mean-square deviation
<b><math>\tau</math></b>	relaxation time
Subscripts:	
<b>e</b>	estimate
<b>m</b>	measured
<b>n</b>	index of data points (see eq.(3))
Superscript:	
<b>T</b>	transpose
Abbreviations:	
<b>FOV</b>	field of view
<b>GMT</b>	Greenwich Mean Time
<b>LAIPAT</b>	LIMS Inverted Profile Archival Tape
<b>LAMAT</b>	LIMS Map Archival Tape
<b>LIMS</b>	Limb Infrared Monitor of the Stratosphere
<b>NLTE</b>	nonlocal thermodynamic equilibrium
<b>OSB</b>	out of spectral band
<b>PSC</b>	polar stratospheric cloud
<b>RMSD</b>	root-mean-square difference between LAMAT and LAIPAT data
<b>S/N</b>	signal-to-noise
<b>ZMT</b>	zonal mean trend

## Ozone

The quality of the ozone data on the LIMS Inverted Profile Archival Tape (LAIPAT) has been reported by Remsberg et al. (1984a) and is generally excellent. The ozone data have already been the subject of scientific investigations (Leovy et al. 1985). This section reviews the characteristics of the ozone data and considers the quality of the Fourier coefficients derived from those data.

### Nimbus 7 Orbit and LIMS Data Set

The Sun-synchronous Nimbus 7 orbit imposes two basic limitations on the use of the LAIPAT data to

calculate a synoptic map. First, there are at most 28 measurements at a given latitude per day, limiting the number of horizontal wavelengths that can be resolved. In addition, the measurements occur at two local solar times—near 1 p.m. and 11 p.m. at the Equator. The synoptic fields can be represented by a set of Fourier coefficients calculated for noon GMT at each latitude and pressure level.

The ozone mixing ratio field  $Z$  at a particular time (GMT)  $t$ , latitude  $\theta$ , and pressure  $p$ , is given in vector form by

$$Z_{t,\theta,p}(\lambda) = \mathbf{K}^T(\lambda) \cdot \mathbf{X}_{t,\theta,p} \quad (1)$$

where

$$\mathbf{K}^T(\lambda) = [1 \quad \cos \lambda \quad \sin \lambda \quad \cos 2\lambda \quad \cdots \quad \sin M\lambda] \quad (2)$$

where  $M \leq 6$  and the superscript  $T$  denotes the transpose of the vector. Synoptic data are required to calculate  $\mathbf{X}$  in equation (1) exactly. Here, the discrete form is actually used to solve for  $\mathbf{X}$ :

$$Z_n = \mathbf{K}_n^T \cdot \mathbf{X}_n \quad (3)$$

where  $Z_n$  is the measured value of the field at time  $t_n$  and longitude  $\lambda_n$ . The Kalman filter algorithm, described in detail by Haggard et al. (1986), was used to develop for noon GMT a best fit field  $\mathbf{X}$  to the ozone data. For reference purposes, the ascending (generally daytime data) segment of an orbit is that part of the LIMS tangent track where the tangent point moves from south to north, the descending (generally nighttime data) segment is that part where the tangent point moves from north to south, and the whole orbit, or combined data, includes both segments. The corresponding segments of the orbit are termed modes (inadvertently named nodes in Haggard et al. 1986). (Note also that the months were reversed in fig. 11 of Haggard et al.: fig. 11(a) is for May 1979; fig. 11(b), for January.)

The ozone data sampling was sufficient to calculate 9 Fourier coefficients for modes 1 (ascending) and 2 (descending) and 13 coefficients for mode 3 (combined) for all standard LAMAT pressure levels except 100 and 0.05 mbar. At most latitudes, the ascending mode data were taken near midday and the descending mode data near midnight. There were insufficient data at 100 mbar to calculate any coefficients at low latitudes, while at the topmost level (0.05 mbar), coefficients were calculated at only a few latitudes for mode 1 and at about one-half of the latitudes for mode 2. The greater latitude coverage of mode 2 arises because the relatively large nighttime ozone concentrations in the mid-mesosphere yield

better signal-to-noise ratios than do the daytime concentrations.

When day-night differences are small, the data for modes 1 and 2 can be combined to yield a map (mode 3) that is generally superior to maps of either mode 1 or 2 because enough data exist to calculate additional waves (5 and 6). On the other hand, at levels where the day-night differences are large compared with the zonal mean value, for example, at 0.2, 0.1, and 0.05 mbar, the combined mode maps must be viewed with caution. Day-night differences also cause the root-mean-square difference (RMSD) between the data and the Kalman filter approximation to the data to be larger for the combined mode than for the ascending or the descending mode. This characteristic of the combined mode data is important because the RMSD is one measure of the "goodness of fit" of the mapping procedure. This point will be discussed further in the following paragraphs.

There are indications based on the work of Solomon et al. (1986a) that nonlocal thermodynamic equilibrium (NLTE) effects must be considered at least for the LIMS daytime ozone mixing ratio inferred at 0.4 to 0.05 mbar. Corrections for the NLTE effects would decrease daytime ozone mixing ratios to values that are more consistent with theory, but such corrections have not been applied to the archived data. Remsberg et al. (1984a) also discuss some systematic day-night differences that were seen in the ozone radiances and the retrieved concentrations at low latitudes for all months. The average March difference (their fig. 17) is a maximum of 7 percent at about 7 to 10 mbar near the Equator, with the daytime concentration exceeding the nighttime value. Such variations can affect the combined mode data in the equatorial stratosphere.

Estimates of the vertical resolution of the ozone data on the LAIPAT were discussed in Remsberg et al. (1984a). It was shown that a 15-percent amplitude perturbation in ozone mixing ratio for a wavelength of 5 km (half-wavelength of 2.5 km) centered at 30 mbar would produce a perturbed radiance signal-to-noise ratio of about 2. Further analysis yields an effective vertical resolution (half-wavelength) for the LAIPAT ozone mixing ratios of 2.9 km. Because of the approximately 3.5-km spacing for the LAMAT pressure levels, this resolution is degraded, with waves shorter than 7 km (half-wavelength of 3.5 km) having their features aliased to longer waves.

### Kalman Filter

The Kalman filter is a sequential estimator. It is assumed that an estimate of the ozone mixing ratio

field  $\mathbf{X}_{n,e}$  and its uncertainty, represented by an error covariance matrix  $\mathbf{S}_{n,e}$ , are initially available, and those estimates are updated by the assimilation of each measurement in the data time series. Since the estimates of  $\mathbf{X}_{n-1}$  and  $\mathbf{S}_{n-1}$  are known from a previous time step, it is possible to estimate these terms at time  $t_n$  by using

$$\mathbf{X}_{n,e} = \mathbf{X}_{n-1} + (t_n - t_{n-1})d\mathbf{X}/dt \quad (4)$$

and

$$\mathbf{S}_{n,e} = \mathbf{S}_{n-1} + |t_n - t_{n-1}| d\mathbf{S}/dt \quad (5)$$

These expressions are then used to estimate the measurement at  $t_n$ , that is,  $Z_{n,e}$  (from eq. (3)), and the variance of that estimate  $\sigma_{n,e}^2$  where

$$\sigma_{n,e}^2 = \mathbf{K}_n^T \mathbf{S}_{n,e} \mathbf{K}_n \quad (6)$$

The amount by which  $\mathbf{X}_n$  and  $\mathbf{S}_n$  are incremented for the next time step is determined by considering the difference between the measured and estimated ozone values, weighted by the variances of the measured data  $\sigma_{n,m}^2$  and the estimates  $\sigma_{n,e}^2$ . As defined in Haggard et al. (1986), several parameters must be determined as part of the input data. The zonal mean trend,  $dX_1/dt$  in equation (4), was calculated directly from the data. Measured variances  $\sigma_{n,m}^2$  were obtained from data precision estimates in Remsberg et al. (1984a), and this parameter was considered to be adjustable in the Kalman filter runs (see later). The factor  $d\mathbf{S}/dt$  in equation (5) contains the variances of the amplitudes of the waves and the zonal mean, calculated from a preliminary Kalman filter run over an appropriate time increment  $\Delta t$ , or relaxation time  $\tau$ . That increment was calculated by considering the autocorrelation of each wave amplitude at each latitude and noting the time for the autocorrelation to reach the noise level. The parameters  $\sigma_{n,m}^2$  and  $d\mathbf{S}/dt$ , are considered virtual data because they were not known exactly from the LAIPAT information.

At each pressure level, the virtual data were contained in a  $38 \times 7$  matrix of amplitude variances, a 7-element vector of relaxation times, and a measurement standard deviation. The virtual data set affects the LAMAT results in several ways. The relaxation times, amplitude variances, and measurement precision affect the closeness with which the filter matches the data, as measured by the RMSD of the fit. For example, a decrease in the relaxation time or an increase in the amplitude variances shortens the response time of the filter and reduces the RMSD of the fit to the data. The RMSD also varies with the input measurement precision. In addition, the amplitude variances and the relative sizes of the seven

elements in the relaxation vector determine the fraction of the filter correction to be apportioned to the zonal mean and the six waves.

The amplitude variances and zonal mean trends for the final Kalman filter runs were obtained from a preliminary Kalman filter run, where its input amplitude variances were independent of wave number and also several orders of magnitude larger than their expected values. These large variances decreased the time smoothing of the preliminary filter and produced "exact" fits to the data. Final input amplitude variances, zonal mean trends, and relaxation times were calculated for each latitude from the preliminary run. The relaxation times obtained in this manner varied excessively with latitude and pressure, and more representative values were obtained by averaging the results in three pressure intervals (100–10, 10–1, and 1–0.05 mbar) over latitude and pressure. The January values are shown in table 1.

The calculated amplitude variances were smoothed with latitude and used as input to the final run; results for 100, 10, 1, and 0.1 mbar are shown in table 2. Both ascending and descending mode data were used in the preliminary runs except at 0.2, 0.1, and 0.05 mbar, where only descending mode (nighttime) data were used. This procedure was followed because the nighttime measurements are more reliable at these pressure-altitudes and because the day-night differences result in spuriously larger amplitude variances in the combined mode.

The data precision specified in the virtual data set was determined by comparing results obtained from a set of test runs which used a range of input precisions. Remsberg et al. (1984a, fig. 4) estimated the precision of the ozone measurements from sets of six consecutive scans near the same location along an orbit. Those precision estimates were averaged with latitude, multiplied by either 1.0, 1.5, or 2.0, and then used in Kalman filter test runs. A comparison of the resulting maps indicated that the  $1.5 \times$  precisions yielded the "best" results, but the overall differences were not large, indicating rather weak sensitivity to the actual precision estimates. Accordingly, the precisions used for all final runs were the  $1.5 \times$  values, which are shown in table 3.

### Ozone Mapping Criteria

The criteria used to determine the final measurement precision are related to the broader question of how the overall quality of the maps was determined. Both subjective and objective criteria were used to judge the quality of the fit. The most important objective criterion was the RMSD between the data and the mapped field, which is a measure

of the closeness of the empirical fit to the data. Although the RMSD can be made arbitrarily small by a suitable choice of the virtual data set, an exact fit of the filter to the data is neither desirable nor statistically justified. Only under ideal conditions, that is, when the time and spatial variation inherent in the atmospheric phenomena have been sampled with sufficient resolution, should one expect the RMSD to be comparable to the measurement precision. Thus, the measurement precision is an approximate lower limit for the RMSD. For practical reasons the RMSD was not routinely calculated, but rather the deviation  $\sigma_{\text{obs}}$ , which, in general, exceeds the RMSD because it is a comparison of the noon GMT fit with all data for the day. Nevertheless,  $\sigma_{\text{obs}}$  is a suitable approximate measure of the closeness of fit, and a comparison of  $\sigma_{\text{obs}}$  with the measurement precision indicates how far the fit is from the ideal.

The most important subjective measures of the quality of fit are continuity in space, time, and mode. A prominent feature seen at more than one latitude, longitude, or day was assumed to be real, and adjustments, if any, to the Kalman filter input which reproduced the feature were favored. Of course, all such features could not be studied, so only selected subsets of the maps were inspected. The method used to determine the appropriate measurement precision for the Kalman filter runs illustrates this approach. As mentioned before, Kalman filter maps at 10 mbar for all days in January were obtained for the combined mode with the  $1.0 \times$  precision of Remsberg et al. (1984a) and also with  $1.5 \times$  and  $2.0 \times$  precisions. Features in these maps were inspected for continuity with respect to latitude, longitude, and mode. It was concluded that many of the features obtained with the precision in that reference lacked this continuity, probably because the LAIPAT scans spaced  $4^\circ$  in latitude along an orbit vary more than scans spaced  $0.8^\circ$  as analyzed therein. Moreover, it was found that the runs made with the  $2.0 \times$  precision unnecessarily smoothed real features. For example, highs and lows in the ozone field were reduced by 5–10 percent and gradients smoothed. It was, therefore, concluded that the runs made with the  $1.5 \times$  precisions were preferable, even though the maps looked more “noisy” than the  $2.0 \times$  maps.

In summary, the most important objective criterion for judging the quality of the fit was  $\sigma_{\text{obs}}$ . The maps were also subjectively evaluated on the basis of resolution of real features, as defined above. Examples of the application of these criteria follow.

The average closeness of fit can be seen in figure 1, which shows the  $\sigma_{\text{obs}}$  for the January combined mode. The RMSD is roughly three times the precision input into the filter runs (table 3). As noted

above, this difference is due to day-night differences, time variations during the course of the day, and temporal and spatial variations too small to be adequately resolved by the filter. The fraction of the RMSD due to day-night differences can be seen by comparing figure 2, which shows  $\sigma_{\text{obs}}$  for the ascending mode, with figure 1. This comparison reveals that the day-night difference in these January data accounts for about 30 percent of the total  $\sigma_{\text{obs}}$  for the combined mode.

The quality of the fit of the Fourier coefficients to the synoptic data is difficult to determine unambiguously; however, the quantity  $\sigma_{\text{obs}}$  provides a conservative estimate of the fit. Since the zonal mean coefficient is always much larger than  $\sigma_{\text{obs}}$  while the wave coefficients are more nearly the same or smaller, the zonal mean coefficient has a better precision than the wave components. Of course, the confidence that one has in the accuracy of any specific coefficient depends on the history of all the coefficients according to equations (4) and (5).

In the winter hemisphere, planetary wave amplitudes are often large and transient. An example of the longitudinal variations (waves) of ozone mixing ratio about the zonal mean is shown in figure 3 for January and is expressed as root-mean-square wave standard deviation  $\sigma_{\text{wave}}$ . The ability of the Kalman filter to fit the data does not depend on the size of the wave amplitudes, but rather on the temporal variation of the field, assuming that the Kalman filter model resolves the waves. Thus, the filter can have some difficulty fitting even large waves in the winter hemisphere. On the other hand, those same large coefficients are better defined in terms of the data precision. For this reason, the accuracy of the winter coefficients is normally better than that in the summer hemisphere or at low latitudes, where the wave amplitudes are typically of the order of or less than the precision of the data.

### Data Screening

Data that were “flagged” on the LAIPAT due to signal-to-noise problems were not used in the LAMAT analysis. Strict adherence to the header indices for each scan on the LAIPAT eliminated such data. Before the Kalman filter algorithm was applied to the data, a maximum-minimum mixing ratio criterion was also applied. At 10 mbar for January, that range was from 12 to 1 ppmv. At 100 mbar, the range decreased to 4 to 0.2 ppmv, and at 0.1 mbar, it was 3 to 0.1 ppmv. Data were also discarded during the Kalman filter processing whenever the difference between a measurement  $Z_{n,m}$  and the Kalman filter estimate of the measurement  $Z_{n,e}$  exceeded a 5-sigma test (see eq. (7) of Haggard et al. 1986, and

discussion thereof). Less than 0.01 percent of the data were removed according to these tests. Quite a few profiles at low latitudes near 70 and 100 mbar were rejected because of cloud interference or because retrieved mixing ratios fell below 0.1 ppmv. For this reason, many fewer LAMAT profiles extend down to 70 mbar between  $\pm 16^\circ$  latitude and down to 100 mbar between  $\pm 32^\circ$ . Even though fewer data were screened out at 50 mbar, there were usually insufficient profiles for calculating all 13 coefficients there for the combined mode near the Equator.

A special procedure was used to delete data contaminated by polar stratospheric clouds (PSC's). The effects of PSC's (McCormick et al. 1982) could clearly be seen in the LIMS ozone data at high latitudes in the lower stratosphere. PSC-type signatures were found in the LAIPAT from November 27 to December 4 and from December 26 to January 23. The occurrence of PSC's in the LIMS ozone data has been mentioned in Hamill and McMaster (1984). Because these spurious data could result in serious errors in the mapping coefficients for all the LIMS parameters except temperature, an attempt was made to remove all data (including temperature) that could be attributed to PSC's.

The apparent ozone mixing ratio retrieved in the PSC regions occasionally exceeded ozone mixing ratios in neighboring regions by a factor of 4 or more. The PSC signatures could be distinguished by very large horizontal gradients in ozone mixing ratio. For example, at the edges of the PSC's, the retrieved ozone mixing ratio often varied by 15 percent or more over  $10^\circ$  or less of longitude. In addition, the PSC's were invariably found in very cold regions with temperatures less than 195 K.

Occasionally, the apparent ozone mixing ratio was so large that the retrieval algorithm "failed" and the PSC-contaminated data segments were considered outside the first and last good data points (the header indices on the LAIPAT) for that scan. Those few scan segments, which represented situations where the data were highly contaminated by PSC's, were not included in the LAMAT preparation. In the remaining instances where PSC signatures were noted, the PSC flags on the LAIPAT (see appendix A) were ignored in the preliminary Kalman filter run. Boundaries of the PSC's were located instead by inspecting the daily noon GMT ozone maps from those preliminary Kalman filter runs at pressure levels of 16, 30, 50, 70, and 100 mbar. Frequently, they appeared as "bull's-eye" patterns on the preliminary ozone maps, as shown in figure 4(a) ( $72^\circ\text{N}$ ,  $0^\circ\text{E}$ ) for January 5 at 30 mbar. The latitude and longitude boundaries of the clouds found by this inspection of the daily maps were used to define a set of "PSC cloud boxes"

for each pressure-altitude. (The scan segments that were deleted because of retrieval "failure" and, thus, not included in these preliminary runs, were also located in the cloud boxes.) Because the errors in the retrieval at one pressure-altitude were likely to contaminate the result at lower altitudes, the cloud box for each lower level was taken to be at least as large as that of the level above. The cloud boxes obtained from the maps were assumed to apply to the entire day (0.00 GMT to 24.00 GMT), and all LIMS data within the specified box on that day were removed before making a final Kalman filter run.

The above procedure seemed to remove all the PSC-contaminated data, but it also removed some apparently "good" data near the edges of the PSC signature. Unfortunately, no objective way was found for deciding whether ozone data near the edges of the clouds were contaminated by the cloud or merely were larger than the surrounding data. It was deemed preferable to delete some potentially good data rather than to allow PSC-contaminated data into the analysis, especially since those contaminated segments are still available on the LAIPAT, if closer analysis is desired. Removal of such data meant that certain regions or latitudes might not contain enough data to calculate coefficients for all the wave numbers. Even the zonal mean may be biased slightly in such instances, because the deleted data are concentrated in a specific longitude sector rather than distributed evenly. Figure 4(b) presents the combined mode 30-mbar ozone field for January 5 after removal of the PSC feature. Enough data were present to calculate coefficients for all six wave numbers. A similar plot from only the ascending mode coefficients contained no information from wave number 4 at  $76^\circ\text{N}$  and  $80^\circ\text{N}$ . Fortunately, the PSC's were not so extended or persistent that ozone information could not be obtained from nearby days and thereby extrapolated by the Kalman filter to the day of interest. Therefore, the combined mode LAMAT ozone data should not exhibit large sampling biases because of PSC removal. An excellent argument in favor of the present PSC removal technique is the good continuity with latitude and pressure of waves after PSC removal. Results from ascending and descending modes were also found to be more consistent after PSC removal.

Because information about the coverage and persistence of PSC's is of scientific interest in its own right, a tabulation of the cloud boxes is presented in appendix A (table 6), and the approximate area for each box is also plotted daily. In general, the occurrence of PSC's matched the sightings reported by McCormick et al. (1982) and was correlated with

regions of low stratospheric temperatures  $T$  less than 195 K.

### Quality of LAMAT Ozone Results

Although the average closeness of the empirical fits to the data was indicated in figures 1 and 2, it is of interest to know how well the Kalman filter resolves some of the special features found in the LIMS ozone data set. A better picture of the quality of the maps can be obtained by evaluating the fit on specific days. Figures 5 and 6 show 10-mbar contour plots on January 2. A striking feature of the Northern Hemisphere (fig. 5) is the very tight packing of the contours in a mid-latitude band about  $10^\circ$  wide. The latitude of tight packing also varies with longitude and, moreover, was seen on many other days in the winter. It must, therefore, be a real feature of the data (see Leovy et al. 1985, for further discussion). The success with which this feature is resolved is thus an excellent indication of the quality of the Kalman filter analysis. Southern Hemisphere fields in figure 6 have contours that are nearly circular, with ozone mixing ratios decreasing poleward. This character is consistent with predictions of only very weak wave activity at 10 mbar in the summer hemisphere.

The results in figures 5 and 6 have been smoothed with a latitude filter (weighted 1-2-1) applied to LAMAT data spaced at the  $4^\circ$  latitude increments in order to yield less "noisy" plots for display purposes. To show what this smoothing process has done to the original coefficient fields, the unsmoothed values are plotted in figure 7 (cf., fig. 5). The gradients are slightly weaker near  $40^\circ\text{N}$  after smoothing, but all the important features have been retained.

Figure 8 shows the Kalman filter results and the data at  $48^\circ\text{S}$ , the Equator, and  $48^\circ\text{N}$  for 10 mbar on January 2. The weak wave 2 feature in figure 8(a) and in the corresponding contour plot (fig. 6) can be seen in both ascending and descending modes despite the systematic differences between the two modes. At the Equator (fig. 8(b)), the two modes exhibit a substantial day-night difference (about 0.4 ppmv) and dissimilar patterns in longitudinal variations. The significance of the longitudinal variations in the combined mode curve is, therefore, questionable. This finding for the Equator (10 mbar) is consistent with the fact that the wave amplitudes are of the order of the data precision there. The Kalman filter approximation to the data at  $48^\circ\text{N}$  is much better. In the region between  $0^\circ\text{E}$  and  $90^\circ\text{E}$ , which cuts across the tightly packed contours shown in figures 5 and 7, the ozone gradient can be seen in the data of both modes and is well represented by the filter fit. Both the ascending and the descending mode in figure 8(c) shows a slight minimum at  $80^\circ\text{E}$  and

a second maximum at  $130^\circ\text{E}$ . The data suggest a somewhat greater difference between this maximum and minimum than was obtained with the filter.

Figure 8 illustrates differences in the separate Kalman filter fits to the ascending and descending mode data. Figure 8(c) shows that the sharp ozone gradient between  $0^\circ\text{E}$  and  $50^\circ\text{E}$  and the second maximum at  $130^\circ\text{E}$  are both resolved better by the combined mode. In this case the greater horizontal resolution afforded by the wave 6 fit has resulted in a superior fit to the data. This result contrasts with the results obtained for the Southern Hemisphere and the Equator (figs. 8(a) and 8(b), respectively), where systematic differences between the data of the two modes were too large to produce a better fit when the data were combined.

Because a principal reason for using the Kalman filter was to interpolate asymptotic satellite data to a single GMT, the noon maps can be compared properly only with data gathered near noon GMT, that is, for a longitude band about  $30^\circ$  in width or narrower. This constraint limits the longitudinal width suitable for comparisons between the LAMAT and LAIPAT data. Note, however, that a substantial number of data points are collected nearly simultaneously along an orbit. A stringent test of the filter fit is, therefore, a comparison of the ozone observations along an orbit with the LAMAT results, evaluated at the time and longitudes of the orbit. Since filter results are available only at noon GMT, it is necessary to choose an orbit as close as possible to the Greenwich meridian so that the orbit time is as close as possible to noon GMT (see also fig. 3 of Haggard et al. 1986).

A portion of the ascending mode of orbit 972 was selected for this comparison. The orbit tangent point locus (or track) sketched in figure 7 not only passes close to the Greenwich meridian but also cuts across the region of high ozone gradients discussed earlier. Data were taken between 14:17 and 14:43 GMT. Contours of the data for this orbit (from the LAIPAT) have been plotted in figure 9 and show quite clearly the region of high gradients near 10 mbar that was seen at mid-latitudes in figure 7. The large mixing ratios near  $76^\circ\text{N}$ , at 100–30 mbar are due to a PSC event. Figure 10 shows the Kalman filter fits (PSC's removed) evaluated at the longitudes of the tangent height crossing at each latitude. The orbital section shown in figure 9 is a daytime orbit and, therefore, should agree better with the ascending mode fit (fig. 10(a)) than with the descending mode fit (fig. 10(b)).

Comparison of figure 9 with figure 10 is significant for several reasons. First, the filter maps are smoother than the orbit data, as expected, even though no 1-2-1 smoothing with latitude has been

applied in the generation of figure 10. The "wiggles" in the isopleths of figure 9 are due, in part, to uncertainties in the pressure registration of each ozone radiance profile on the LAIPAT (spaced  $4^\circ$  in latitude). Some of that "wobble" then is artificial, and it was reduced in the LAMAT processing by specifying input precisions that were poorer than "observed" by a factor of 1.5. Truncation of the Kalman filter output to four or six waves (depending on the mode) plus the inherent time smoothing of the filter also reduces the wiggles, especially that part due to medium-scale atmospheric transients. Second, the mid-latitude region of tightly packed contours is reproduced in both modes but with a diminished gradient. Finally, the comparison provides another independent test of the accuracy of the Kalman filter. Note, for example, that the small 9.0-ppmv isopleth that appears in figure 9 near the Equator at 10 mbar is not found in the descending mode analysis, where the maximum contour is 8.0 ppmv. The implied error in the empirical fit is near 10 percent. On the other hand, the maximum mixing ratio contour for the ascending mode empirical fit is 9.0 ppmv, which is close to the measured value, as expected, since the orbital segment in figure 9 is for an ascending mode. Generally, combined mode results differ from the LAIPAT data by  $\pm 5$  percent.

The quality of the LAMAT ozone data during stratospheric warming events is of particular interest because of the transient nature of these phenomena. Figure 11 is a 10-mbar contour map for January 26, where in addition to the tight packing of the ozone contours in mid-latitudes discussed earlier, a splitting of the polar ozone vortex is evident with an important wave 2 component. Figure 12 compares the filter results with data for January 26 at  $52^\circ\text{N}$ ,  $56^\circ\text{N}$ , and  $60^\circ\text{N}$ . Good coherency exists between the data at adjacent latitudes and between the ascending and descending modes. The combined mode analysis contains important short wave components that are lacking in the ascending and descending mode curves. Inspection of the data indicates that these features are probably real since they appear at adjacent latitudes.

The time evolution of the ozone mixing ratio is shown in figure 13 at  $56^\circ\text{N}$  for January 25, 26, and 27. Examination of the data and fits reveals that while the longer wave components change slowly with time and are resolved well in all three mode analyses, the shorter waves (4-6) in the combined mode are more transient.

The split vortex pattern in figure 11, a weak feature at 10 mbar, is more pronounced at 3 mbar. This feature is reproduced quite well by the filter as can be seen in figure 14, which shows the combined

mode fit at  $72^\circ\text{N}$  on January 26. The comparison with the data is also good for the descending and ascending modes (not shown), because the shorter waves are much less important at this level.

From about January 24 onward, the sampling at high latitudes was excellent and the data appear accurate in that even highly anomalous LIMS ozone profiles agreed well with the few correlative data profiles that were available there (Remsburg et al. 1984a). No data were eliminated in the LAMAT due to PSC's during this period. Some data were lost between 30 and 100 mbar at the highest Northern Hemisphere latitudes due to signal-to-noise problems in the ozone retrievals, which most likely were due to biases in retrieved temperature profiles or calculated horizontal temperature gradients. These instances occurred on February 3-6 ( $80^\circ$ - $130^\circ\text{E}$ ) and February 26 ( $80^\circ$ - $110^\circ\text{E}$ ). Data that were retained at altitudes just above those deleted segments showed rather large variations with time and between modes.

An example of such variations is shown in figure 15 for the combined mode fits at  $76^\circ\text{N}$  and 16 mbar for February 25, 26, and 27. This period was characterized by transient dynamics and rapid ozone transport as indicated in figure 16 by the tongue of ozone being advected toward the pole at  $80^\circ\text{E}$ . This feature is believed to be a result of nonlinear transport processes and has been discussed by Leovy et al. (1985). As the data in figure 15(b) show, there was a large amount of scatter near  $80^\circ\text{E}$  on February 26. None of these data points were screened out during the Kalman filter analysis according to the criteria discussed earlier. A pressure-latitude cross section (fig. 17) for orbit 1734 (near  $80^\circ\text{E}$  in fig. 16) contains an ozone contour of 7.0 ppmv extending from Equator to pole, so that strong northward transport is suggested for that time. Therefore, the transient behavior of the Kalman filter results may be a good approximation to what was actually happening in the atmosphere at that time. On the other hand, the lack of correspondence between the ascending and the descending mode data between  $250^\circ\text{E}$  and  $330^\circ\text{E}$  on February 27 (fig. 15(c)) indicates inaccuracies with the ozone retrieval in that situation, perhaps due to not accounting for horizontal ozone gradients. These results must be kept in perspective, however, since figure 15 represents the most difficult situation that was encountered in the LAMAT ozone processing. Even here, if the data near  $80^\circ\text{E}$  are assumed correct, the Kalman filter followed them well, and near  $330^\circ\text{E}$  the combined mode results represent an average value with an uncertainty of only about 15 percent. Just as in the case of the January 2 orbital comparisons (figs. 9-10), it is again useful to compare the Kalman filter results with the actual orbital cross

section shown in figure 17. Because orbit 1734 occurred near 18:00 GMT, the combined mode Kalman filter results in figure 18 were selected for comparison. Again, even in this highly disturbed atmospheric period, the mapped coefficients represent a good approximation to the original retrieved profiles that were used to obtain figure 17. Ozone gradients have been smoothed somewhat and the 8 ppmv values at mid to high latitudes near 10 mbar are reduced by 0.5 to 1.0 ppmv in figure 18. Such a reduction is largely a result of the difficulty of the present mapping algorithm in approximating the transient and highly localized tongue of ozone shown in figure 16.

A final important criterion for judging the quality of the LAMAT ozone data is the coherence between the modes. Since the entire time series is used to determine the coefficients at each latitude, a certain amount of coherency in calculated coefficients with time is expected. Conversely, the mapping is independent of latitude and, therefore, the coherency in the derived coefficients with latitude is a better test of the significance of the analysis. Figure 19 shows the wave 1, 3, and 5 amplitudes and phases for January 5. The ascending (dotted) and descending (dashed) modes agree reasonably well for wave 1, even in the Southern Hemisphere, where the amplitudes are weak. Similar conclusions apply to wave 3. Although only the combined mode included wave 5, coherency of the amplitude and phase with latitude in the Northern Hemisphere for figure 19 (where the amplitudes are significant) implies that the wave 5 result is also meaningful.

## Nitric Acid

### Nitric Acid Mapping Criteria

The accuracy and precision of the LAIPAT nitric acid data have been reported by Gille et al. (1984a). They conclude that near the peak mixing ratio (at about the 30-mbar level) the precision is approximately 2 to 4 percent and that the data agree with the correlative measurements to approximately 20 percent. The high precision of the data suggests that the Kalman filter should produce good results if the measured fields are consistent with the assumptions made in the filtering process. Although specific simulations of the vertical resolution for the nitric acid fields have not been conducted, the final values for the LAIPAT and LAMAT should be analogous to those given for the ozone fields because both channels have the same field-of-view width. However, signal-to-noise ratio from the tangent layer continues to be good in the lower stratosphere for nitric acid, because its spectral signature remains optically thin there (as opposed to ozone's).

The Fourier coefficients for nitric acid were calculated for all three modes for the 10 LAMAT pressure levels from 100 to 2 mbar. For most levels, latitudes, and days, sampling was sufficient to calculate 13 Fourier coefficients for the combined mode, and 9 coefficients each for the ascending and descending modes. However, at the 2-mbar level and in the equatorial regions from 100 to 50 mbar, the data were very sparse and fewer coefficients were calculated. At some of these latitudes, no maps were produced because of the sparse data field.

The mapping procedure for nitric acid was similar to that just described for ozone, but the data precision, expressed here as a variance  $\sigma_{n,m}^2$ , was determined differently. The initial precision estimates were taken from Gille et al. (1984a). They were then increased slightly to allow for effects that were not accounted for explicitly in the LAMAT processing. These effects include rapid wave transience, errors in pressure registration of the radiance profiles, and errors due to not interpolating the LAIPAT profile to the exact latitudes (see Haggard et al. 1986). A series of Kalman filter runs were conducted using a range of  $\sigma_{n,m}^2$ . The results of these runs were analyzed, and a set of  $\sigma_{n,m}^2$  values was selected that seemed to result in a best fit between the data and the mapped results. Unlike the procedure followed for ozone, these final values of  $\sigma_{n,m}^2$  were not determined as a fixed factor times the initial estimate; instead, the values of  $\sigma_{n,m}^2$  were adjusted, as necessary, to account for the changing variability of the wave field as the data were mapped for different time periods. In no case was the precision set to a value less than that given in Gille et al. (1984a). The values used for both the relaxation times and the amplitude variances (in  $dS/dt$  in eq. (5)), the zonal mean trends ( $dX_1/dt$  in eq. (4)), and  $\sigma_{n,m}$  are listed in tables 4 and 5.

As was noted in the ozone discussion, all the data that were contained within regions contaminated by polar stratospheric clouds were removed before the mapping was begun. In addition, a few profile data segments were removed because the mixing ratios were judged to be either too large or too small, or because they exceeded a 5-sigma error range determined by the Kalman filter for nitric acid (see Haggard et al. 1986). All the data removed in this way together represented less than 0.01 percent of the total data.

### Quality of the LAMAT Nitric Acid Results

The quality of the nitric acid data on the LAMAT is considered very good, except perhaps at the 2- and 3-mbar levels, where Gille et al. (1984a) noted that the LAIPAT nitric acid mixing ratios were too large.

The cause of this artificial increase is explained in appendix B.

Particular attention is given in this section to instances when the nitric acid gradients were large and, therefore, potentially subject to error in the mapping analysis. Nitric acid maps are shown in figure 20 for the Northern Hemisphere at 10 mbar for February 5, 6, and 7. The maps in figures 20(a) to 20(c) are unsmoothed. The effect of smoothing in the meridional direction using a 1-2-1 filter can be noted by comparing figure 20(b) with figure 20(d), which has been smoothed. These fields contain excellent examples of the large gradients that frequently occur in nitric acid mixing ratio. The region of sharp gradients starting near 40°N, 310°E and running east and north to the pole is associated with a sudden stratospheric warming that was under way (see Haggard et al. 1986).

The data for February 6 are compared with the derived LAMAT field in figure 21. The ascending mode data are presented in figure 21(a); the symbol marked with a plus sign was taken at 0:48 GMT on February 6 and is the first data point on this day. The time order of the data is from right to left; thus, the two leftmost data points were each taken within an hour of the time for which the map was produced. The  $\sigma_{\text{obs}}$  is only 0.32 ppbv. On the descending mode map (fig. 21(b)), the first data point of the day is near 300°E, and the data point at 114°E is within 40 minutes of the map time, that is, noon GMT ( $\sigma_{\text{obs}}$  is 0.34 ppbv). The combined mode fit in figure 21(c) contains more detail, and its  $\sigma_{\text{obs}}$  is 0.51 ppbv. This slightly less accurate combined mode fit is a result of using ascending and descending mode data taken in the same local region but during a period when the field was changing more rapidly than was assumed for the Kalman filter. Note, however, that the combined mode results in the region of the steep gradient fall between the ascending mode and the descending mode measurements taken after noon. A short wave structure is more pronounced in figure 21(c) than in figures 21(a) or 21(b), and despite its larger standard deviation, figure 21(c) is still a better estimate of the field at this time. The results in figure 21 are an excellent indication of the high quality of the nitric acid maps.

The meridional gradient of the zonal mean of nitric acid mixing ratio is often quite large in mid-latitudes. A large gradient, coupled with north-south action of waves, can produce large latitudinal gradients in the wave components of the nitric acid fields. Such situations are potential sources of error for the maps because the selected LAIPAT profiles, while being within 1° of the nominal latitude (i.e., the 4° latitude increments), were not interpolated to

the nominal latitude before being inserted into the Kalman filter algorithm.

Figures 22 to 24 show the amplitudes of the zonal mean and waves 1 and 2, as a function of latitude at 30 mbar, on January 25, 26, and 27. This period provides one of the sharpest latitudinal gradients in waves 1 and 2 and contains an inflection in the zonal mean value near 44°N. The significance of the uncertainties in latitude was tested by observing the results for each of the three modes for each day. The zonal mean coefficients for January 25 for each mode are overlaid in figure 22 and are in excellent agreement. Results for the other two days are similar. Results obtained for this pressure level do not seem to depend on the particular distribution of the data with time, and there is no significant day-night difference that might cause an error in the combined mode fit. The large meridional gradient of the zonal mean mixing ratio yields even sharper gradients in the non-zonal wave amplitudes (figs. 23 and 24). The wave 1 and 2 amplitudes are large between about 12°N and 30°N near the inflection in figure 22 and then decrease near 44°N. The rapid latitudinal variation of the wave 2 amplitude on January 25 is noteworthy, and the consistency of the amplitudes of waves 1 and 2, as calculated from each of the three modes, denotes real features. The occurrence of these rapid variations must be considered when smoothing the LAMAT field. Even a 1-2-1 smoothing with latitude can affect derived meridional structure.

Another example of the fit for large gradients is shown in figure 25 for January 25 combined mode data. A  $\sigma_{n,m}$  of 0.22 ppbv was estimated for these latitudes. This precision is approximately equal to  $\sigma_{\text{obs}}$  for the lowest latitudes, where the meridional gradient is small. Even though the zonal mean and the wave structure is changing rapidly, the fit between the curve and the data remains good even at the higher latitudes.

In the tropical lower stratosphere (50 to 100 mbar), there are not enough data to calculate the higher wave number coefficients. Both the sine and the cosine coefficients have been set to zero for those waves, and calculations of meridional transport of species can yield discontinuities with latitude where this occurs. Figures 26 and 27 present the zonal mean of combined mode nitric acid results for January and May, respectively, and figures 28 and 29 show the difference between the ascending and the descending mode (in terms of a fraction of the zonal mean) for those months. Modal differences centered near the Equator are expected between 2 and about 30 mbar due to photochemistry, but residual differences at 50 to 70 mbar in the Northern and Southern Hemispheres of about 5 percent also

appear and do not seem to be explained by a diurnal cycle. The differences are negative (descending mode value greater than ascending mode value) almost everywhere except in the lower stratosphere of the Southern Hemisphere. The differences are of the order of the estimated precision in the measurement, but much smaller than the estimated accuracy (Gille et al. 1984a), and the differences between 50 and 70 mbar do not change sign between January and May. Further analysis indicates that this feature of the data is likely to be an artifact of the retrieval process. For example, figure 30 shows that there are also maxima in the day-night temperature differences for January near 30°S and 30°N at about 70 mbar, just where the nitric acid differences are noticeable, and the sign of the differences is the same for both temperature and nitric acid. This analysis behavior is unexpected because a positive temperature difference should yield a negative nitric acid difference through the constituent retrieval.

Several explanations are possible:

1. Some extra emission present at low latitudes due to thin clouds may not have been detected and flagged by the cloud top criterion used in the LIMS processing. Such emission could contribute to both the carbon dioxide (CO<sub>2</sub>) (used for temperature) and nitric acid channel radiances. Because of the much different view directions for the descending and ascending modes (see figs. 31 and 32), the effects of any extra emission may vary accordingly.
2. The LIMS temperatures near 70 mbar are too warm at low latitudes (Gille et al. 1984b), and such a bias can affect the two viewing modes differently.
3. The horizontal (Equator to pole) gradients of temperature and nitric acid divided by their zonal means ( $\Delta T/T\Delta y$ ) are largest near  $\pm 30^\circ$  in the lower stratosphere, and these gradients reverse for the two hemispheres. Although temperature gradients were accounted for to a first order in both the temperature and the nitric acid retrievals, no account was made for nitric acid gradients in the nitric acid retrieval. An estimate of this gradient effect at 70 mbar has been made by scaling arguments based on similar effects seen at 7 mbar for nitrogen dioxide (NO<sub>2</sub>) (see fig. 3(a) of Solomon et al. 1986b). Both nitrogen dioxide and nitric acid are optically thin in the stratosphere, but because the mixing ratio peak for nitrogen dioxide occurs some 15 km higher than that for nitric acid, the 7-mbar or nitrogen dioxide results have been used for interpretation of the 70-mbar nitric acid results. Neglect of the gradient effect in nitrogen dioxide led to an approximate maximum

error of 40 percent near the terminator, and scaling shows that nitric acid mixing ratio can be in error by about 10 percent, which is about what is observed in figures 28 and 29.

Given the foregoing potential error mechanisms, more direct interpretations of the lower stratospheric modal differences in nitric acid are not advised.

Finally, a point of omission is noted. The ascending and descending mode nitric acid coefficients at 3 mbar were inadvertently not calculated (and thus set to zero for the LAMAT) for March 9, 1979, through April 4, 1979. The combined mode coefficients were calculated and archived.

## Conclusions

In summary, the following conclusions can be drawn about the ozone and nitric acid synoptic maps on the LAMAT.

1. When the data were characterized by long (wave numbers less than 4) and slowly changing (time scales greater than 2 days) components, the Kalman filter fit approached the optimum expected, that is, the standard deviation between the synoptic maps and asynoptic data is about equal to the estimated data precision. When transient features with time scales of the order of 2 days or less were present, the  $\sigma_{\text{obs}}$  was several times larger than the estimated data precision.
2. When the day-night differences were small and when the short wavelengths were significant, the combined mode maps were generally superior to the maps for either the ascending or the descending mode. At pressure-altitudes above about 0.4 mbar, the combined mode ozone maps are not meaningful because of the large day-night differences that occur there.
3. Comparison of LAIPAT orbital ozone data with the Kalman filter LAMAT results, evaluated at the same latitudes and longitudes of the orbital data, indicated errors in the Kalman filter analysis of generally less than 5 percent, with 15 percent being a maximum error.
4. There is continuity with latitude and mode for both nitric acid and ozone coefficients, even when strong gradients are present. This finding confirms the utility and fidelity of the LAMAT algorithm, because data for each mode and latitude were processed independently.

NASA Langley Research Center  
Hampton, VA 23665-5225  
August 27, 1986

## Appendix A

### Frequency and Distribution of Polar Stratospheric Cloud Signatures in the LIMS Data

Sightings of polar stratospheric clouds (PSC's) during 1978 and 1979 were documented by McCormick et al. (1982). PSC signatures observed with the LIMS ozone channel were noted on the LAIPAT (Remsberg et al. 1984a) and in the preparation of the LAMAT. Whereas the determinations by McCormick et al. (1982) were limited to a narrow latitude band near 66°N, the broader coverage of the LIMS experiment yielded a more comprehensive picture of the PSC distribution. Because most PSC sightings occurred near 22 km, it is appropriate to characterize PSC's using the LAIPAT profiles interpolated to 30 mbar (altitudes of 22–23 km for high latitude winter) and then mapped using the Kalman filter algorithm.

For the preliminary ozone analysis, "bad" data, or data at pressures outside the header indices, on the LAIPAT scans were removed, but data containing PSC flags were retained. During the preliminary Kalman filter run, no additional data were deleted because they exceeded prescribed limits on the ozone mixing ratios. Values of  $dS/dt$  for the LIMS ozone data in the Kalman filter equations (Haggard et al. 1986) were set large so that the filter was forced to fit the LAIPAT data and thereby represent the PSC signatures more exactly in the preliminary maps (large values of  $dS/dt$  override any effect of  $\sigma_{n,m}$  in the filter runs). The 5-sigma limits between the filter results and the data were calculated and used to remove a very small number of the profiles. Ozone maps at 30 mbar were plotted and the location of significant maxima (typically bull's-eye patterns) in ozone mixing ratio were noted (see fig. 4(a)). Segments of profiles contributing to those patterns were removed from the data set before a second processing with the Kalman filter for the creation of the LAMAT. These second runs made use of more realistic values of  $dS/dt$  and also limits on measured ozone mixing ratio (9 and 1.5 ppmv at 30 mbar).

Data that were excluded from the final LAMAT 30-mbar Kalman filter runs are listed in table 6. The locations in table 6 are approximate, and they were specified more exactly in the production software. Data were also deleted according to a similar procedure at 50, 70, and 100 mbar, but sometimes the latitude-longitude boundaries were larger at those levels. Data deletions that began at 50 mbar rather than 30 mbar occurred at several latitude-longitude locations on December 30 and on January 6, 13, 18,

23, and 24. Occasionally, data were also deleted at 16 mbar when the preliminary maps contained bull's-eye patterns at locations that were approximately coincident with the 30-mbar signatures. Data were deleted beginning at 16 mbar ( $\approx 26$  km) on January 2, 4, 8, 9, and 19.

Figure 33 indicates the approximate area coverage and persistence of the PSC's at 30 mbar as derived from LIMS data. Signatures were present from November 27 through December 3 and from December 25 through January 23, except for January 6. No LIMS data were obtained on December 29 and 31 and on January 12. Generally, the PSC signatures persisted from late December to the minor warming in late January, but they were confined to the highest latitudes. Their coverage, however, was of the order of or less than 3 percent of the hemisphere. Because the PSC's only occurred north of 54° latitude, the areas in figure 33 must be multiplied by 5.24 to determine the percent area covered by clouds from there to the pole. The maximum area in that case is 17 percent at 30 mbar. The Nimbus 7 SAM II sightings in table 1 of McCormick et al. (1982) often agree with LIMS locations in table 6, although the areas deleted in developing the LAMAT are likely overestimates.

Scan segments that contained PSC signatures were also deleted for the other LIMS species and temperature. Simulations showed that the presence of PSC signatures was barely detectable in the carbon dioxide channel radiances and that the retrieved temperatures in those instances would be too warm. An estimate of this temperature bias was made by considering the temperature profile segments that were within the cloud boxes listed in table 6. First the minimum 30-mbar temperatures in each cloud box were determined from the LAIPAT data interpolated to 30 mbar for each day when PSC's existed. From December 25 to January 16, the average minimum temperature from the interpolated LAIPAT data was 190.1 K with a range of +1.6 to -1.8 K.

Then the maximum apparent ozone mixing ratio from the interpolated LAIPAT data in each daily cloud box at 30 mbar was determined. It was assumed that the PSC emission would be directly proportional to the mass of cloud material along the line of sight in the tangent layer. This assumption was made despite the fact that when a relatively opaque PSC occurs at minimum temperatures, it attenuates radiances from warmer rather than colder regions of the atmosphere along the line of sight. It was also assumed that the occurrence of this material would be inversely correlated with temperature in that layer (i.e., largest apparent ozone mixing ratio and coldest LIMS temperatures). Such a consistent

inverse relationship was not found, however; the average retrieved temperature where ozone emission was high was 193.2 K (with a range of +1.5 to -2.9 K), an increase of 3.1 K over the average minimum cloud box temperature of 190.1 K (a value that may also suffer some contamination). Thus, the decision to delete all potentially PSC-contaminated temperature profile segments along with all the species profile segments seems to have been justified for the production of the LAMAT.

At 190.1 K, the saturation vapor pressure over ice is  $33.2 \times 10^{-5}$  mbar, which requires a water vapor mixing ratio of 11.1 ppmv at 30 mbar (List 1958). A value of 11.1 ppmv is above the upper limit of the high-latitude water vapor mixing ratios reported by Remsberg et al. (1984b) and disagrees somewhat with the theoretical predictions for PSC formation as reported by Steele et al. (1983). Temperatures closer to 187 K seem to be required. It may also be possible that actual PSC formation and growth occurs at lower temperatures but that the particles do not sublimate immediately after the temperature increases.

The interpolated LAIPAT data at 30 mbar were examined further for those locations where pro-

nounced (greater than 12 ppmv) apparent ozone signatures occurred; these locations are listed in table 7. By using this more restrictive definition for a PSC, the areas defined in table 6 and figure 33 are reduced. The locations in table 7 from December 30 through January 11 are generally to the north of the SAM II tangent latitude point, while on January 19 and 20 they are to the south (see McCormick et al. 1982, table 1). The longitudes are in general agreement, however.

As pointed out in Haggard et al. (1986), the final LAMAT data, with the contaminated regions removed, contain temperatures that are colder by up to 3 K where the anomalously high ozone signatures had been and temperatures that are warmer by up to 4 K where the minimum temperatures in the cloud boxes had been. The effect on minimum values occurs because for a given latitude, the Kalman filter algorithm interpolates across cloud box regions of low temperatures from adjacent longitudes (spaced  $20^\circ$  to  $60^\circ$ , table 6) that had warmer temperatures. If the regions of very cold temperatures were of a short duration, then the "memory" of the Kalman filter may also have induced a slight warm bias. Therefore, the LAMAT temperatures are considered inappropriate for studying PSC saturation effects.

## Appendix B

### Systematic Errors in Nitric Acid in the Mid to Upper Stratosphere

Gille et al. (1984a) and Austin et al. (1986) discuss the presence of a positive radiance bias at upper altitudes for the nitric acid channel. The effect of this bias on the retrieved mixing ratio is clearly noted in figure 34 as an increasing value above about 2 mbar. Figure 34 represents the result of averaging radiance profiles over a  $60^\circ$  longitude sector for January 5–9 at  $64^\circ\text{N}$  in order to improve signal-to-noise ratio in the upper stratosphere before retrieval; the actual archived data only extend upward to 2 mbar. Furthermore, Austin et al. (1986) go on to explain that the secondary maximum in figure 34 at 4 mbar is largely real and not a result of radiance biases. The following analysis gives more detail about possible error effects.

An error budget for the retrieved LIMS nitric acid results has been reported by Gille et al. (1984a) in their table 1 for nitric acid profiles typical of mid-latitudes. Random noise is  $0.0015 \text{ W/m}^2\text{-sr}$  and the 4-mbar radiances ( $0.009$  to  $0.014 \text{ W/m}^2\text{-sr}$ ) associated with the high-latitude retrieval in figure 34 give signal-to-noise (S/N) ratios of 6 to 9, values that are considerably greater than the 2–3 used for the error simulations at 3 mbar reported by Gille et al. (1984a) for a “typical” nitric acid profile. Thus, random errors are not important for the high-latitude secondary maximum in the upper stratosphere in figure 34.

The systematic uncertainties reported by Gille et al. in their table 1 were principally from out of spectral band (OSB) signal errors and from the 1-sigma error in the nitrogen dioxide field-of-view (FOV) side lobe of the nitric acid channel (see also fig. 3 of Gille et al.), both for a “typical” nitric acid mixing ratio of 1 ppbv at 3 mbar. The 45-percent OSB uncertainty at 3 mbar is considered a possible problem because of the inability to know the nitric acid filter characteristics more accurately for regions outside of the  $11.3\text{-}\mu\text{m}$  band. Their calculated FOV error of 45 percent at 3 mbar is not due so much to uncertainties in the knowledge of the FOV function, but rather to the sensitivity of the procedure for deconvolving that function from the measured radiances when the vertical radiance gradient is large. Of course, since the nitric acid values for the secondary maximum in figure 34 are much greater than 1 ppbv, the 45-percent error reported by Gille et al. from both the OSB and FOV effects must be reduced considerably for that feature. Estimates of that error are developed below as a function of latitude.

Efforts to deconvolve the FOV function from the nitric acid channel radiance can cause a significant bias in the nitric acid radiance in the upper stratosphere at low latitudes (see fig. 35). When the LIMS instrument scanned vertically downward across the horizon, the spatial side lobe due to the nitrogen dioxide channel (which makes a negative contribution to the total nitric acid FOV function) was “viewing” radiances emerging from a tangent layer some 32–36 km below where the main nitric acid lobe was viewing at the same time. Although the uncertainty (1 sigma) of the measurement of the side lobe is less than 0.2 percent of the total FOV function, the radiance levels viewed by the side lobe are at least 2 orders of magnitude greater than seen by the main lobe when the main lobe is viewing around the 1.5-mbar level.

Figure 35 shows the typical character of the total nitric acid channel radiance profile for three latitudes— $4^\circ\text{N}$ ,  $44^\circ\text{N}$ , and  $80^\circ\text{N}$ . Like the result at  $64^\circ\text{N}$  in figure 34, these profiles were obtained by averaging radiance profiles over a  $60^\circ$  longitude sector for a 5-day period in order to decrease the random noise component and thus improve S/N ratio at the upper altitudes. The oscillation in the radiance near 1.5 mbar for the  $4^\circ\text{N}$  profile is due to difficulties in deconvolving accurately the radiance contribution of the nitrogen dioxide side lobe that was viewing the sharp increase in radiance at 200 to 300 mbar when the main nitric acid FOV lobe was viewing 1.5 to 2 mbar. (Also, since the total radiance level near 1 mbar is of the order of the digitization step size or one radiance count (equivalent to  $0.0015 \text{ W/m}^2\text{-sr}$ ), any radiance bias at tops of profiles can affect the results even for an averaged radiance profile (see below).) The secondary maximum near 1 mbar shown in figure 36 for the  $4^\circ\text{N}$  profile in figure 35(a) is primarily a result of not being able to deconvolve this side lobe contribution adequately. Conversely, because the vertical radiance gradient at 200 mbar for  $44^\circ\text{N}$  and  $80^\circ\text{N}$  in figure 35 is much less pronounced, a similar radiance oscillation at 1.5 mbar does not arise and hence no corresponding artifact appears in the nitric acid retrievals at those latitudes.

Finally, one additional systematic error can affect the nitric acid radiance profile in the upper stratosphere, so that the retrieved nitric acid does not decrease with height at the expected rate above 35 km (Austin et al. 1986). Specifically, most nitric acid radiance profiles show a 1 or 2 count radiance level at altitudes well above where the first side lobe (due to nitrogen dioxide) should be seeing any significant atmospheric signal. This bias then persists throughout the profile even after the FOV function has been deconvolved from the data. Since the archived data

have not been corrected for this type of radiance bias error, radiance levels of the order of a S/N ratio of 4 or less can be in error by 50 percent or more. Radiances at all latitudes in figure 35 are rendered less certain by this additional bias, but the radiance value

at 4 mbar and 80°N is still clearly significant. Simulations of the possible effects of FOV deconvolution error and this small radiance bias give no more than a 20-percent error in the nitric acid mixing ratio at 80°N and 4 mbar in figure 35.

## References

- Austin, J.; Garcia, R. R.; Russell, J. M., III; Solomon, S.; and Tuck, A. F.: On the Atmospheric Photochemistry of Nitric Acid. *J. Geophys. Res.*, vol. 91, no. D5, Apr. 30, 1986, pp. 5477-5485.
- Gille, John C.; and Russell, James M., III: The Limb Infrared Monitor of the Stratosphere: Experiment Description, Performance and Results. *J. Geophys. Res.*, vol. 89, no. D4, June 30, 1984, pp. 5125-5140.
- Gille, John C.; Russell, James M., III; Bailey, Paul L.; Remsberg, Ellis E.; Gordley, Larry L.; Evans, Wayne F. J.; Fischer, Herbert; Gandrud, Bruce W.; Girard, Andre; Harries, John E.; and Beck, Sharon A.: Accuracy and Precision of the Nitric Acid Concentrations Determined by the Limb Infrared Monitor of the Stratosphere Experiment on Nimbus 7. *J. Geophys. Res.*, vol. 89, no. D4, June 30, 1984a, pp. 5179-5190.
- Gille, John C.; Russell, James M., III; Bailey, Paul L.; Gordley, Larry L.; Remsberg, Ellis E.; Lienesch, James H.; Planet, Walter G.; House, Frederick B.; Lyjak, Lawrence V.; and Beck, Sharon A.: Validation of Temperature Retrievals Obtained by the Limb Infrared Monitor of the Stratosphere (LIMS) Experiment on Nimbus 7. *J. Geophys. Res.*, vol. 89, no. D4, June 30, 1984b, pp. 5147-5160.
- Haggard, Kenneth V.; Remsberg, Ellis E.; Grose, William L.; Russell, James M., III; Marshall, B. T.; and Lingenfeller, G.: *Description of Data on the Nimbus 7 LIMS Map Archive Tape—Temperature and Geopotential Height*. NASA TP-2553, 1986.
- Hamill, Patrick; and McMaster, Leonard R.: *Polar Stratospheric Clouds—Their Role in Atmospheric Processes*. NASA CP-2318, 1984, pp. 18-26.
- Leovy, C. B.; Sun, C.-R.; Hitchman, M. H.; Remsberg, E. E.; Russell, J. M., III; Gordley, L. L.; Gille, J. C.; and Lyjak, L. V.: Transport of Ozone in the Middle Stratosphere: Evidence for Planetary Wave Breaking. *J. Atmos. Sci.*, vol. 42, no. 3, Feb. 1, 1985, pp. 230-244.
- List, Robert J.: *Smithsonian Meteorological Tables*. Smithsonian Inst. Press, 1958.
- McCormick, M. P.; Steele, H. M.; Hamill, Patrick; Chu, W. P.; and Swissler, T. J.: Polar Stratospheric Cloud Sightings by SAM II. *J. Atmos. Sci.*, vol. 39, no. 6, June 1982, pp. 1378-1397.
- Remsberg, Ellis E.; Russell, James M., III; Gille, John C.; Gordley, Larry L.; Bailey, Paul L.; Planet, Walter G.; and Harries, John E.: The Validation of Nimbus 7 LIMS Measurements of Ozone. *J. Geophys. Res.*, vol. 89, no. D4, June 30, 1984a, pp. 5161-5178.
- Remsberg, Ellis E.; Russell, James M., III; Gordley, Larry L.; Gille, John C.; and Bailey, Paul L.: Implications of the Stratospheric Water Vapor Distribution as Determined From the Nimbus 7 LIMS Experiment. *J. Atmos. Sci.*, vol. 41, no. 19, Oct. 1, 1984b, pp. 2934-2945.
- Solomon, S.; Kiehl, J. T.; Kerridge, B.; Remsberg, E. E.; and Russell, J. M., III: Evidence for Non-Local Thermodynamic Equilibrium in the  $\nu_3$  Mode of Mesospheric Ozone. *J. Geophys. Res.*, vol. 91, no. D9, Aug. 20, 1986a, pp. 9865-9876.
- Solomon, S.; Russell, J. M., III; and Gordley, L. L.: Observations of the Diurnal Variation of Nitrogen Dioxide in the Stratosphere. *J. Geophys. Res.*, vol. 91, no. D5, Apr. 30, 1986b, pp. 5455-5464.
- Steele, H. M.; Hamill, Patrick; McCormick, M. P.; and Swissler, T. J.: The Formation of Polar Stratospheric Clouds. *J. Atmos. Sci.*, vol. 40, no. 8, Aug. 1983, pp. 2055-2067.

Table 1. Relaxation Times for Ozone Analysis for January

Pressure, mbar	Relaxation time, days, for wave number—						
	0	1	2	3	4	5	6
100-10	3.3	4.0	2.5	2.2	2.0	1.6	1.5
10-1	3.0	2.8	1.8	1.6	1.5	1.5	1.5
1-0.05	2.2	2.0	1.8	1.7	1.5	1.5	1.5

Table 2. Input Amplitude Variances and Zonal Mean Trend (ZMT) for Ozone Analysis for December-January

Pressure, mbar	Latitude, deg	Variances, ppmv <sup>2</sup> , for wave number—							ZMT, ppmv per day
		0	1	2	3	4	5	6	
100	60S	0.0014	0.0035	0.0011	0.0015	0.0019	0.0022	0.0009	-0.004
	0	.0035							
	60N	.0066	.0123	.0163	.0092	.0050	.0050	.0037	.003
10	60S	.0040	.0069	.0047	.0017	.0014	.0016	.0019	.001
	0	.0069	.0100	.0034	.0035	.0048	.0064	.0054	.015
	60N	.0173	.0817	.0253	.0111	.0069	.0079	.0051	.012
1	60S	.0011	.0010	.0004	.0006	.0004	.0004	.0004	0
	0	.0024	.0016	.0013	.0015	.0014	.0014	.0016	-.003
	60N	.0206	.0126	.0121	.0053	.0039	.0036	.0037	-.003
0.1	60S	.0023	.0013	.0016	.0011	.0014	.0020	.0020	.001
	0	.0037	.0014	.0028	.0026	.0031	.0007	.0007	.004
	60N	.0243	.0221	.0095	.0012	.0111	.0119	.0119	.004

Table 3. Ozone Measurement Precision  $\sigma_{n,m}$  Used in the Final Kalman Filter Runs

Pressure, mbar	Precision, ppmv
100-3	0.14
2.0	.10
1.5	.09
1.0	.09
.7	.07
.5	.07
.4	.07
.2	.05
.1	.07
.05	.14

Table 4. Relaxation Times for Nitric Acid Analysis for January

Pressure, mbar	Relaxation time, days, for Wave Number—						
	0	1	2	3	4	5	6
100	3.03	3.98	3.00	3.00	3.00	3.00	3.00
30	3.42	5.00	4.36	4.31	3.00	3.00	3.00
10	3.40	3.82	3.00	1.52	1.31	1.00	1.00
3	2.72	4.90	3.3	2.59	2.50	2.50	2.50

Table 5. Input Amplitude Variances, Zonal Mean Trend (ZMT), and Measurement Precision  $\sigma_{n,m}$  for Nitric Acid Analysis for January

Pressure, mbar	Latitude, deg	Variances, ppbv <sup>2</sup> , for wave number—							ZMT, ppbv per day	$\sigma_{n,m}$ , ppbv
		0	1	2	3	4	5	6		
100	60S	0.059	0.055	0.066	0.075	0.056	0.097	0.065	-0.002	0.17
	0									
30	60N	.242	.305	.291	.292	.301	.229	.216	-.001	.17
	60S	.089	.065	.042	.059	.044	.053	.066	.013	.12
	0	.034	.034	.037	.040	.046	.040	.040	-.009	.12
10	60N	.317	.344	.333	.213	.282	.287	.180	-.002	.16
	60S	.051	.052	.030	.033	.027	.034	.044	.111	.12
	0	.067	.064	.050	.064	.063	.068	.074	-.006	.12
3	60N	.244	.363	.273	.240	.341	.343	.270	-.002	.17
	60S	.054	.030	.030	.041	.041	.054	.051	.004	.22
	0	.092	.092	.080	.079	.089	.080	.076	.002	.22
	60N	.171	.322	.123	.105	.135	.106	.096	-.109	.17

Table 6. Approximate Location of Polar Stratospheric Clouds on the 30-mbar Map From the Preliminary Kalman Filter Run

Date	Latitude, deg N	Longitude, deg E
Nov. 27	$62 \pm 4$	$0 \pm 15$
28	$68 \pm 6$	$0 \pm 30$
29	$72 \pm 10$	$10 \pm 30$
30	$74 \pm 8$	$15 \pm 30$
Dec. 1	$74 \pm 8$	$25 \pm 32$
2	$76 \pm 2$	$357 \pm 27$
	$68 \pm 2$	$40 \pm 20$
3	$76 \pm 6$	$358 \pm 32$
25	$80 \pm 6$	$350 \pm 40$
26	$80 \pm 6$	$350 \pm 40$
27	$80 \pm 6$	$350 \pm 40$
28	$78 \pm 4$	$340 \pm 62$
30	$78 \pm 4$	$340 \pm 62$
Jan. 1	$74 \pm 8$	$344 \pm 44$
2	$74 \pm 8$	$340 \pm 55$
3	$74 \pm 8$	$340 \pm 55$
4	$72 \pm 6$	$342 \pm 45$
5	$72 \pm 6$	$352 \pm 37$
7	$78 \pm 8$	$324 \pm 61$
8	$78 \pm 8$	$324 \pm 61$
9	$78 \pm 8$	$321 \pm 81$
10	$76 \pm 10$	$312 \pm 81$
11	$74 \pm 12$	$293 \pm 57$
13	$74 \pm 12$	$273 \pm 34$
	$80 \pm 2$	$340 \pm 10$
14	$78 \pm 8$	$277 \pm 43$
	$80 \pm 2$	$340 \pm 10$
15	$76 \pm 10$	$271 \pm 29$
	$80 \pm 2$	$330 \pm 20$
16	$76 \pm 10$	$271 \pm 29$
	$80 \pm 2$	$330 \pm 20$
17	$76 \pm 8$	$296 \pm 46$
	$66 \pm 14$	$44 \pm 20$
18	$72 \pm 6$	$35 \pm 35$
19	$64 \pm 10$	$45 \pm 30$
20	$58 \pm 4$	$57 \pm 28$
21	$58 \pm 4$	$62 \pm 20$
22	$66 \pm 8$	$355 \pm 25$
23	$64 \pm 2$	$352 \pm 37$

Table 7. Locations of Pronounced PSC Signatures From LIMS

Date	Latitude, deg N	Longitude, deg E	Apparent ozone mixing ratio, ppmv
December 30	76	351	13.8
January 1	72	11	21.8
2	72	343	22.0
	76	346	13.7
3	68	333	18.2
	72	310	24.3
4	72	313	14.6
8	80	351	14.5
9	72	338	19.3
	76	341	15.6
	80	353	16.3
10	76	284	18.3
	80	295	17.2
11	72	281	17.4
	76	280	18.0
19	60	54	19.8
20	56	49	17.5
22	68	1	12.4

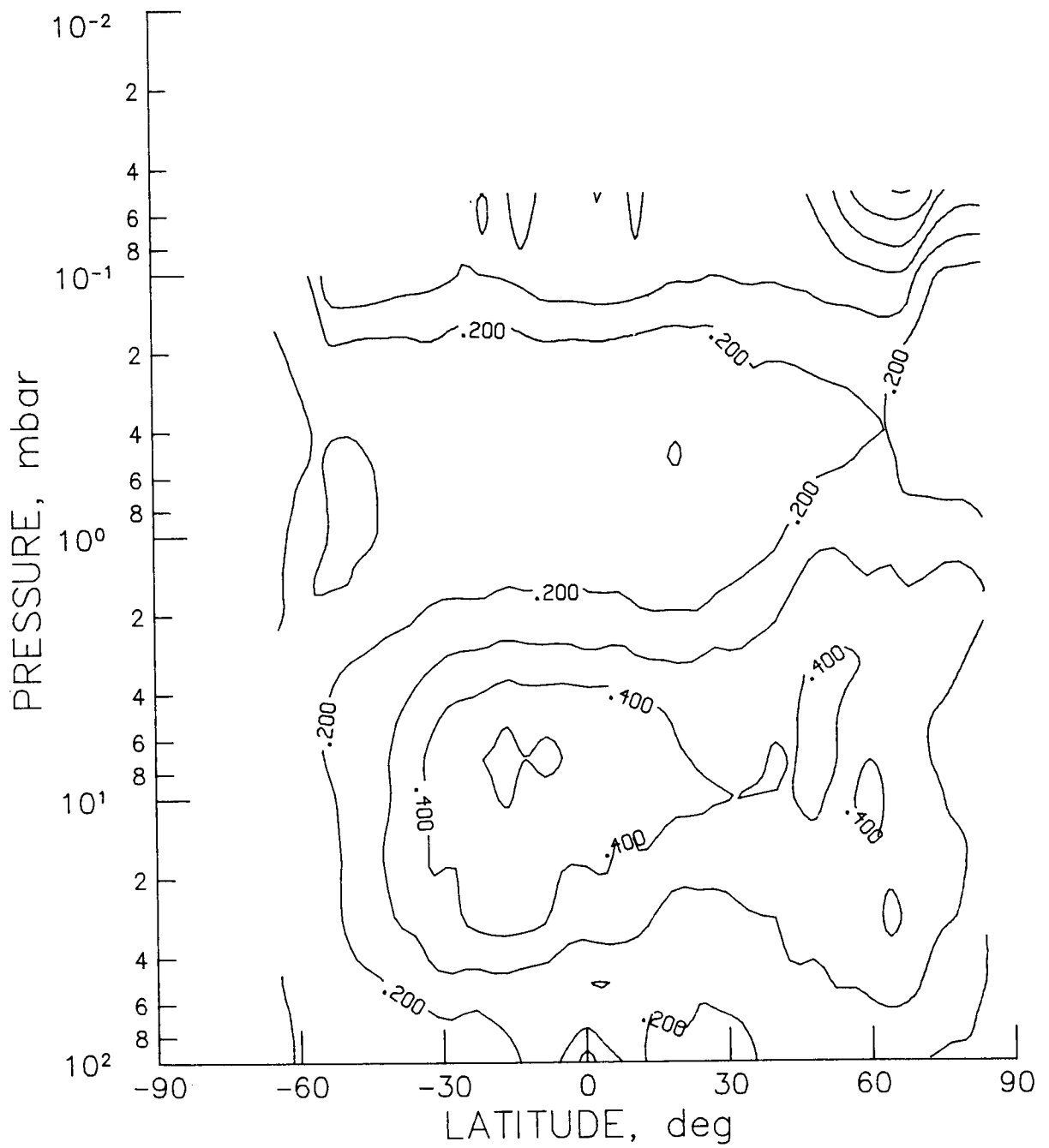


Figure 1. January means of standard deviation  $\sigma_{\text{obs}}$  of combined mode LAMAT ozone mixing ratio from the LAIPAT observations. Contour spacing is 0.1 ppmv.

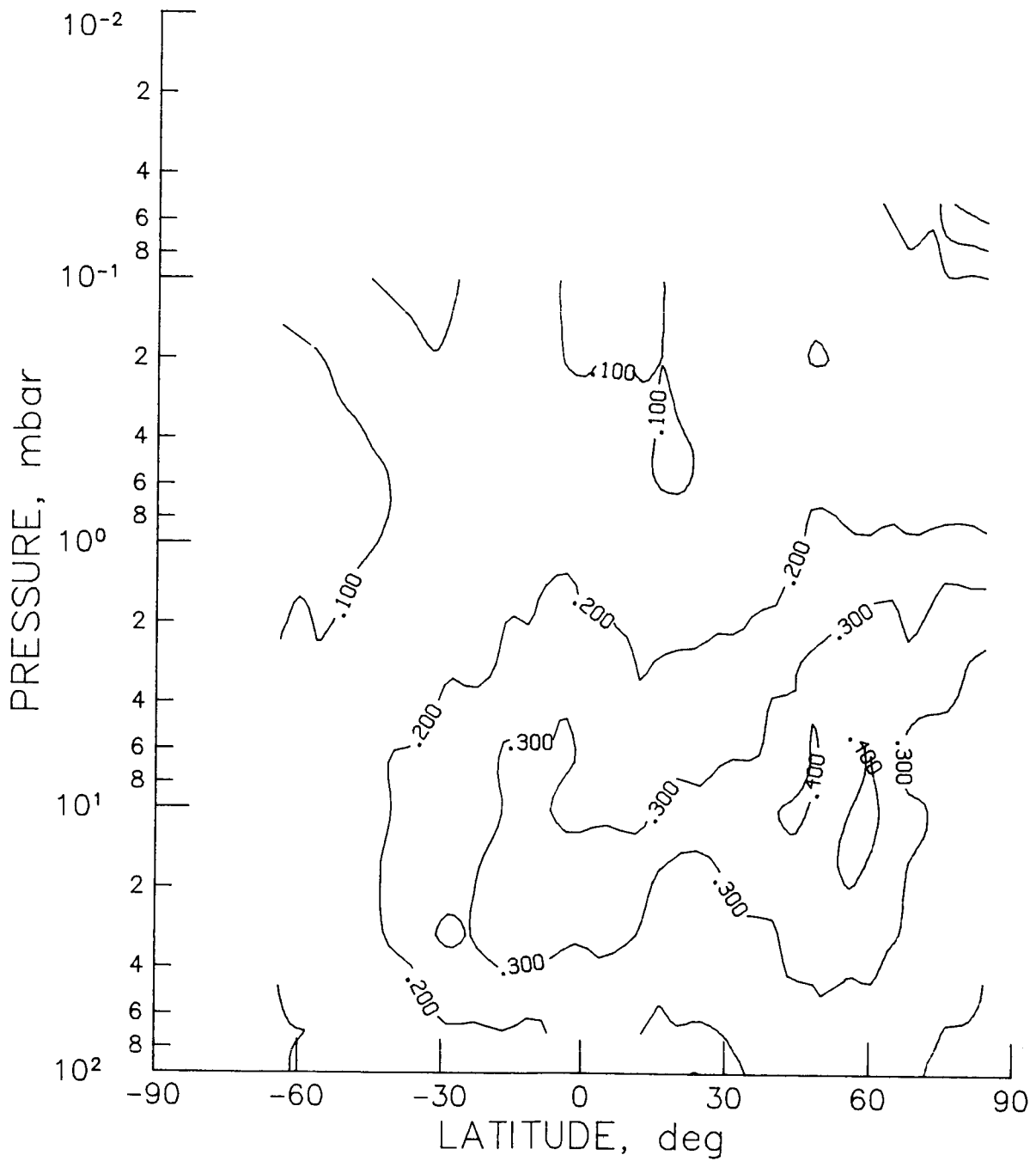


Figure 2. January means of standard deviation  $\sigma_{\text{obs}}$  of ascending mode LAMAT ozone mixing ratio from the LAIPAT observations. Contour spacing is 0.1 ppmv.

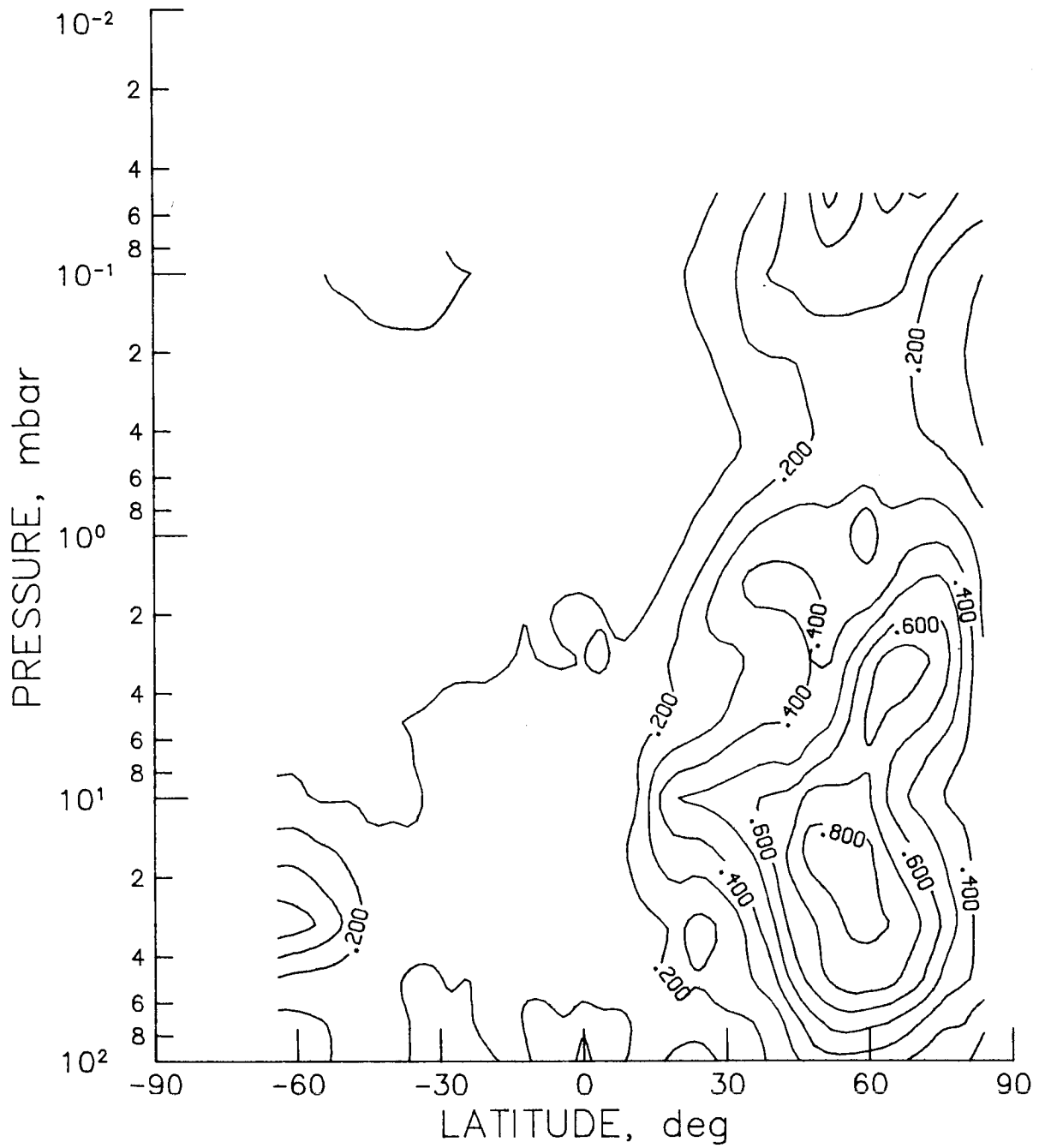
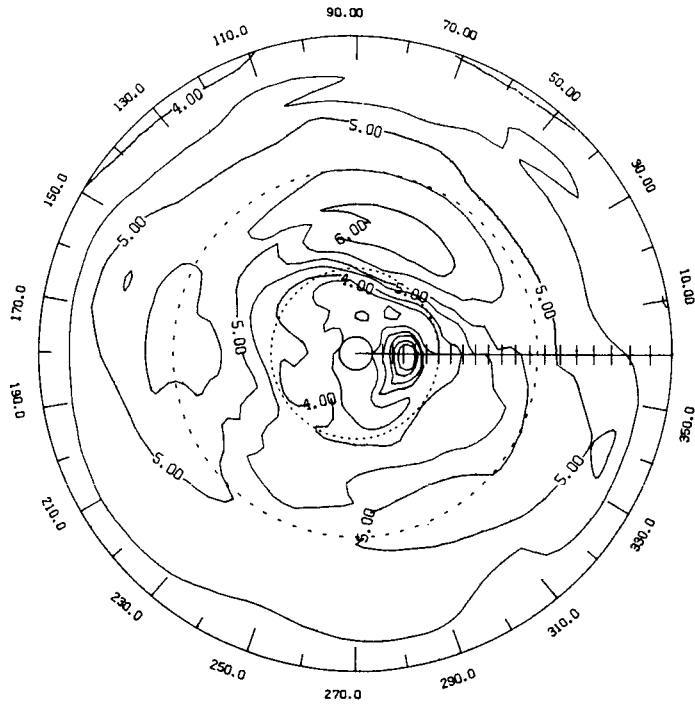
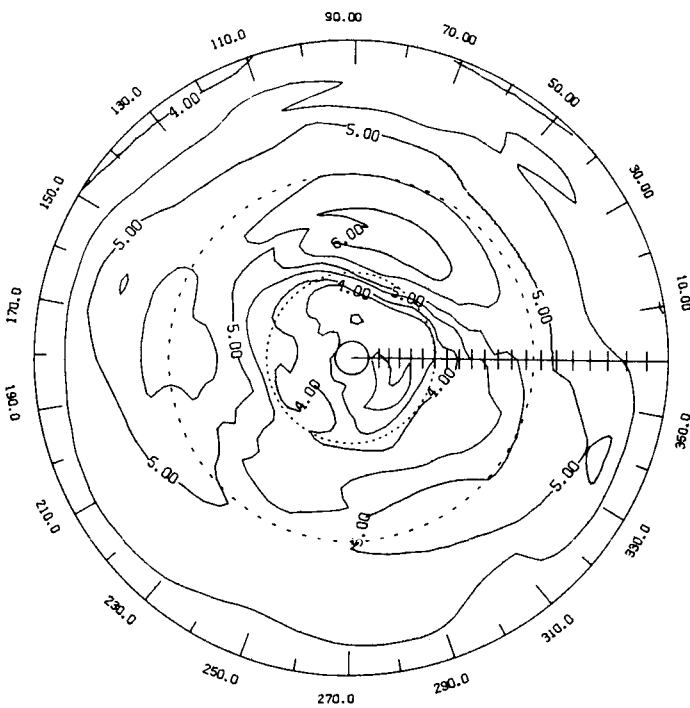


Figure 3. January mean of standard deviation  $\sigma_{\text{wave}}$  of the combined mode LAMAT ozone mixing ratio from its daily zonal means. Contour spacing is 0.1 ppmv.



(a) With PSC signature centered at 72°N, 0°E.



(b) With PSC signature removed.

Figure 4. Plots of ozone mixing ratio at 30 mbar for Jan. 5. Contour spacing is 0.5 ppmv. Greenwich meridian is marked at 4° intervals from 0° to 84°N with dashed circles at 30°N and 60°N.

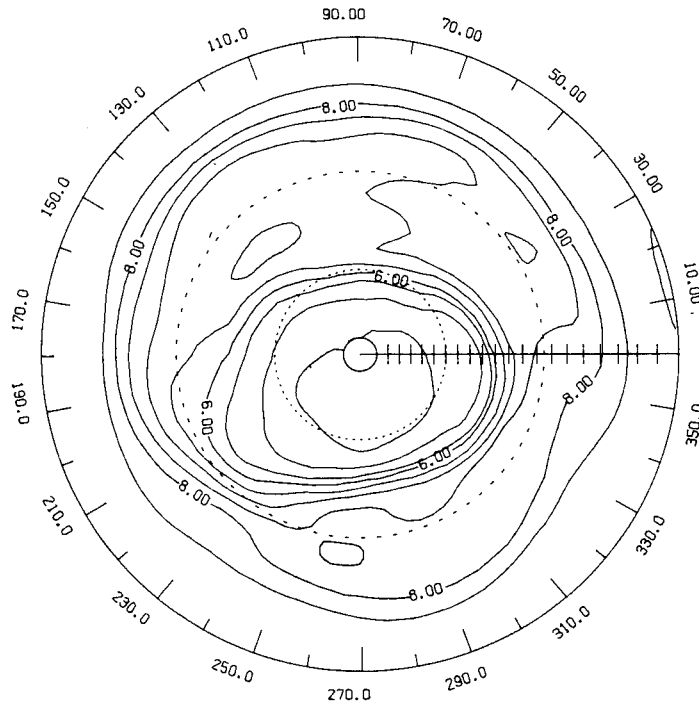


Figure 5. Combined mode LAMAT ozone mixing ratio at 10 mbar for Jan. 2 in Northern Hemisphere with 1-2-1 latitude smoothing. Greenwich meridian is marked at 4° intervals from 0° to 84°N with dashed circles at 30°N and 60°N. Contour spacing is 0.5 ppmv.

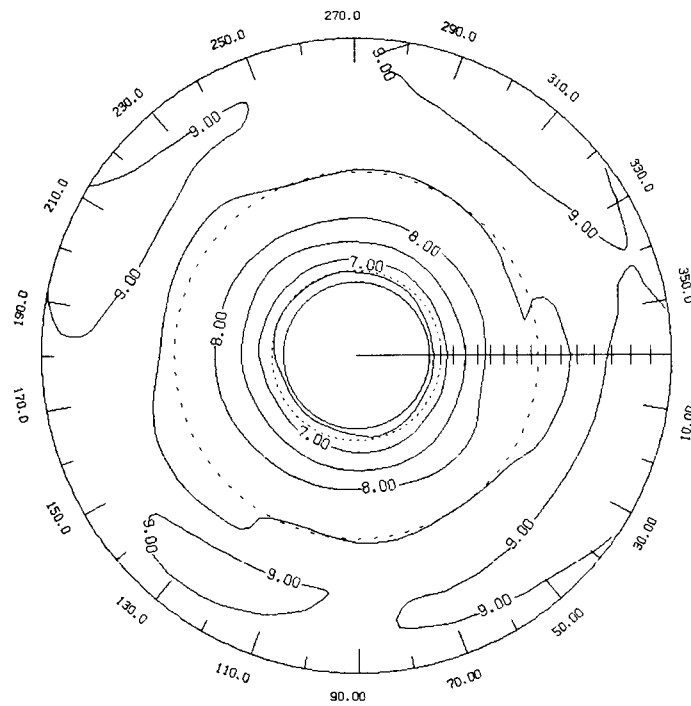


Figure 6. Combined mode LAMAT ozone mixing ratio at 10 mbar for Jan. 2 in Southern Hemisphere with 1-2-1 latitude smoothing. Greenwich meridian is marked at 4° intervals from 0° to 84°S with dashed circles at 30°S and 60°S. Contour spacing is 0.5 ppmv.

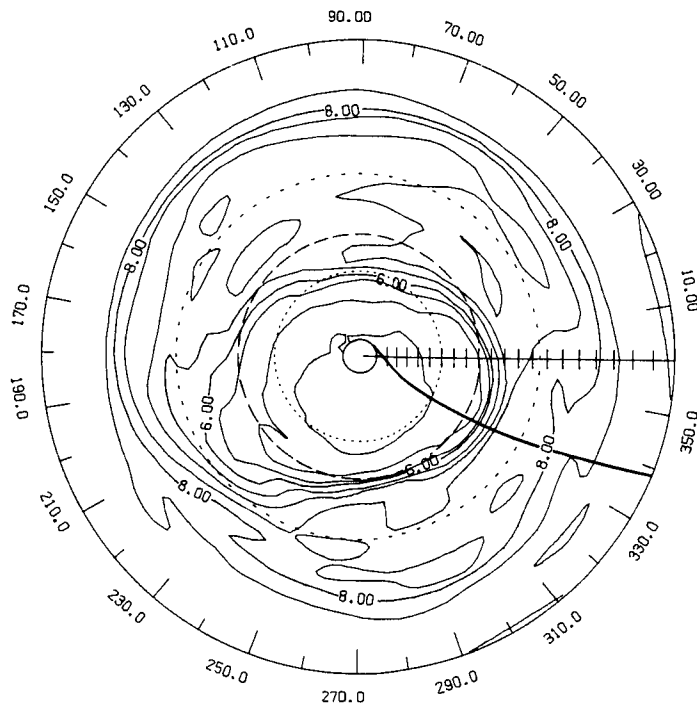
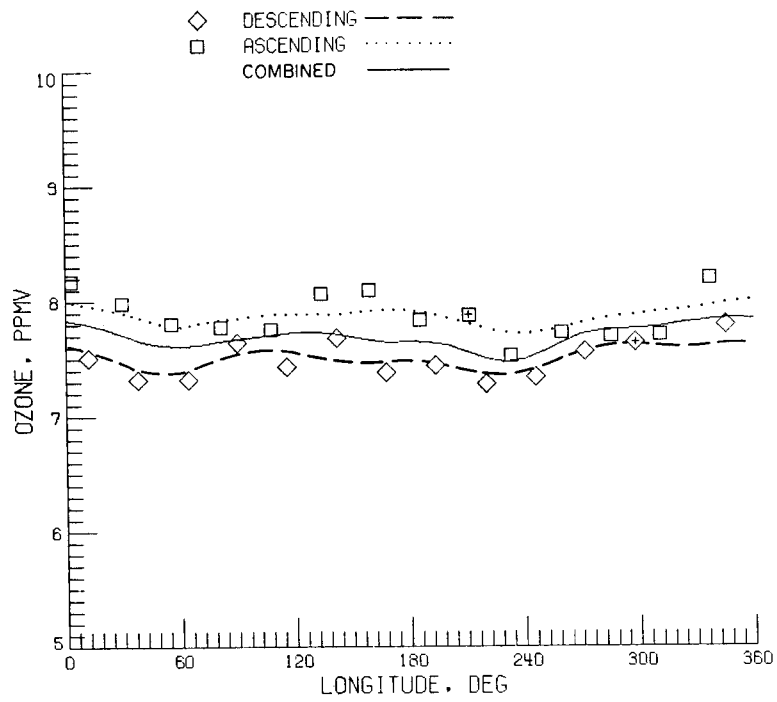
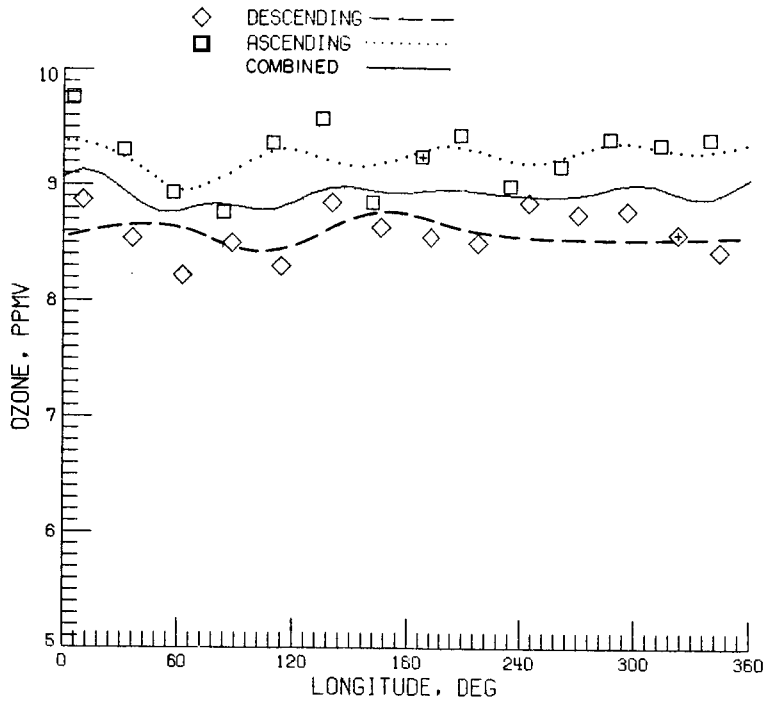


Figure 7. Combined mode LAMAT ozone mixing ratio at 10 mbar for Jan. 2 in Northern Hemisphere without smoothing. Greenwich meridian is marked at 4° intervals from 0° to 84°N with dashed circles at 30°N and 60°N. Contour spacing is 0.5 ppmv. Long-dashed curve is 48°N latitude and solid curve is locus of tangent points for orbit 972.

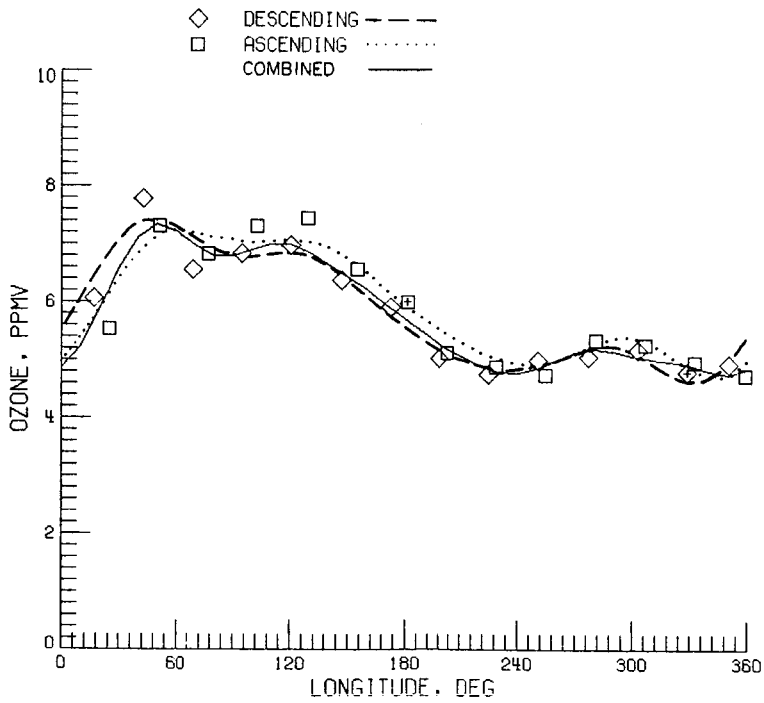


(a) At 48°S.

Figure 8. Kalman filter fit to ozone data at 10 mbar on Jan. 2. Plus signs indicate earliest data points for each mode.



(b) At Equator.



(c) At 48°N (see fig. 7 for latitude position).

Figure 8. Concluded.

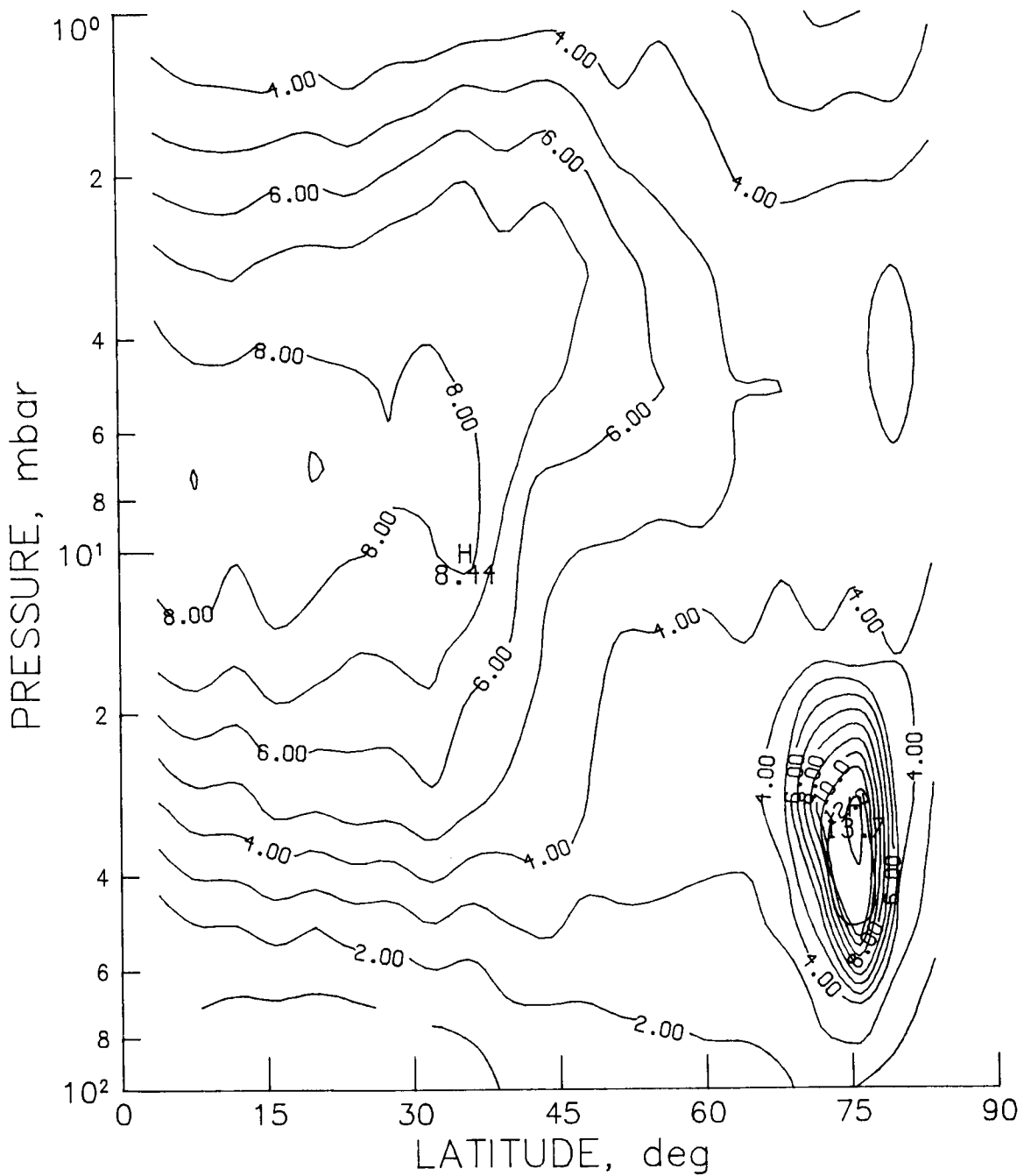
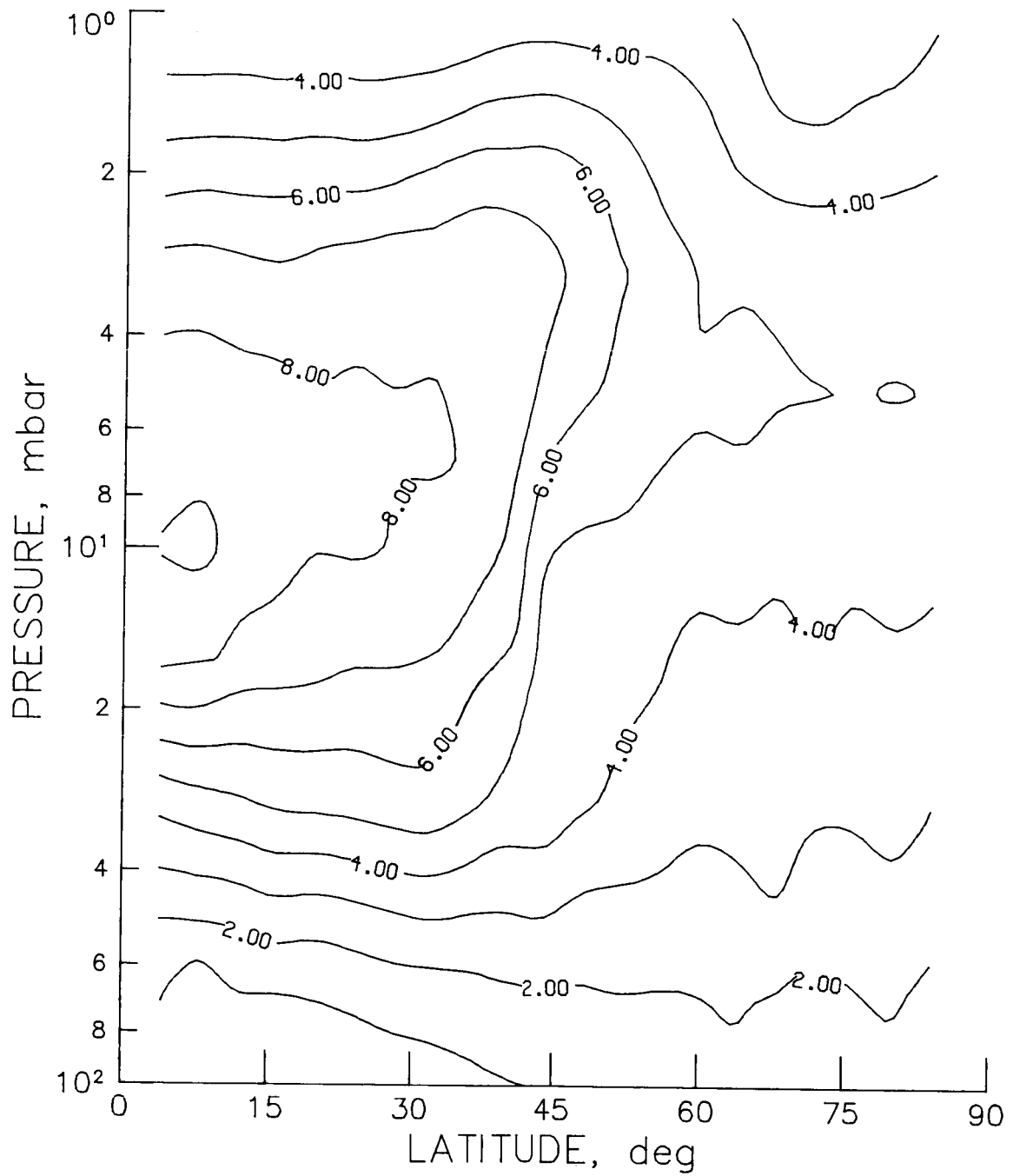
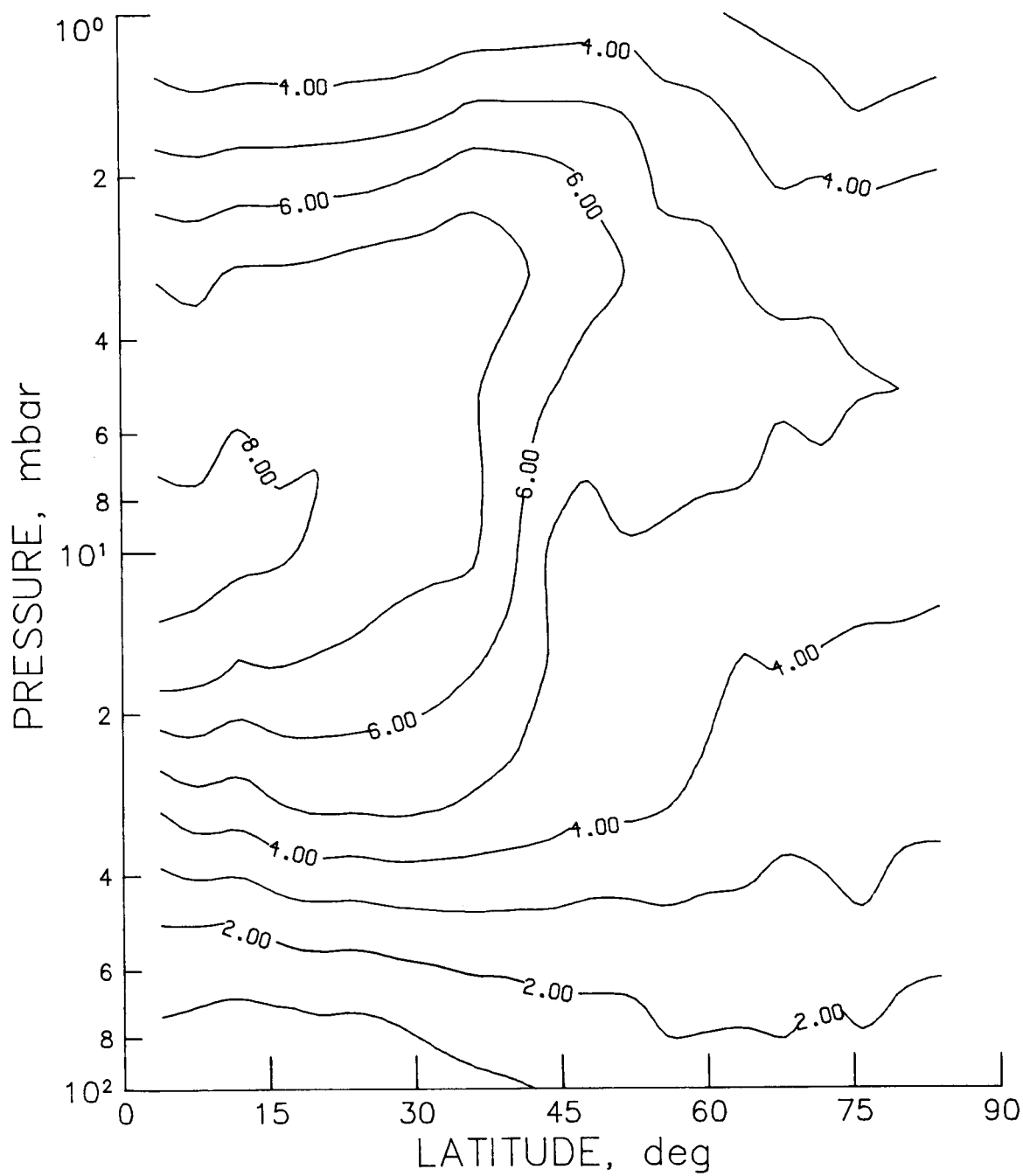


Figure 9. LIMS ozone mixing ratio for ascending mode of orbit 972 (Jan. 2, see fig. 7). Contour spacing is 1.0 ppmv.



(a) Ascending mode.

Figure 10. LAMAT ozone mixing ratio at the longitudes of orbit 972 (Jan. 2, see fig. 7). Contour interval is 1.0 ppmv.



(b) Descending mode.

Figure 10. Concluded.

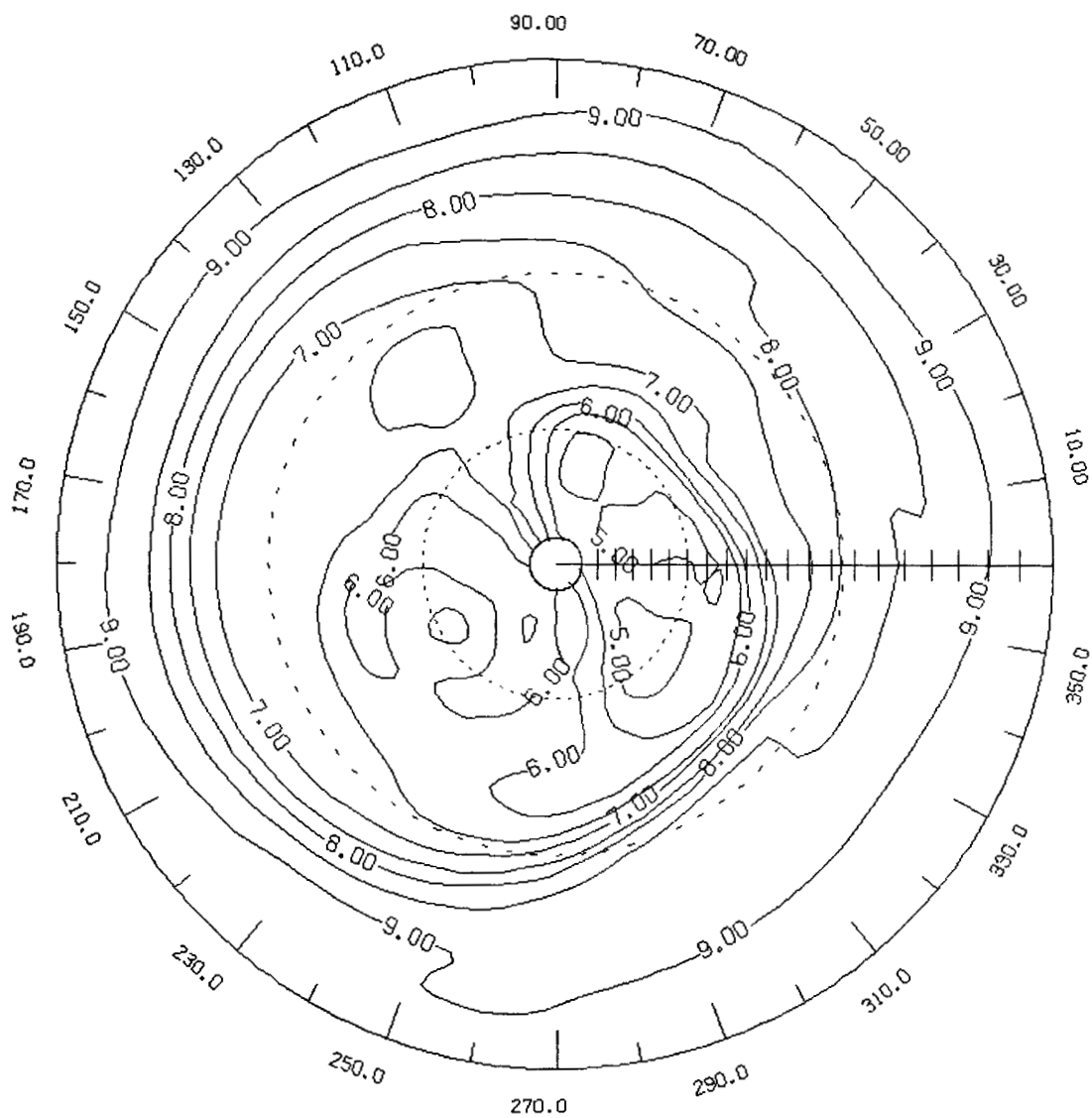
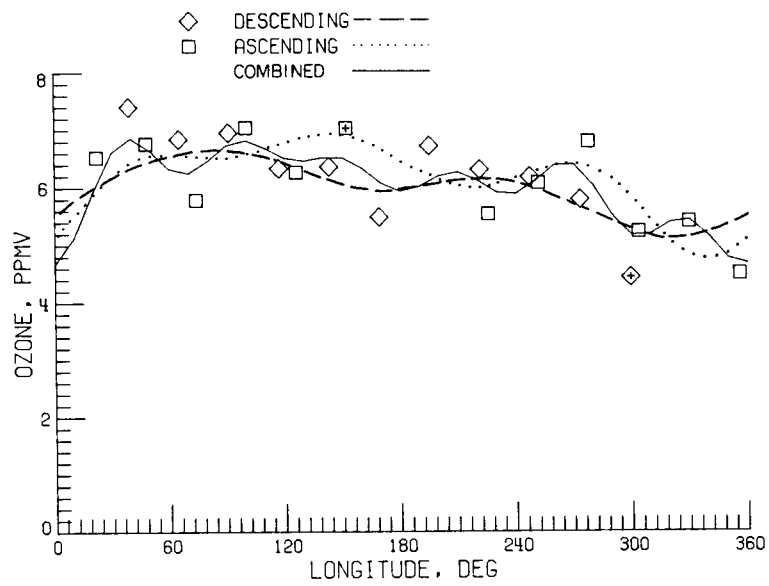
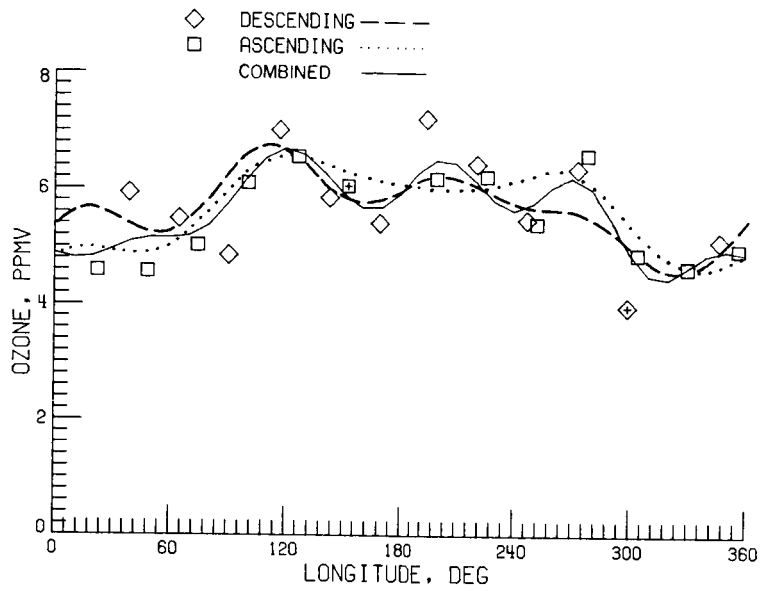


Figure 11. Combined mode LAMAT ozone mixing ratio at 10 mbar for Jan. 26 in Northern Hemisphere with 1-2-1 latitude smoothing. Greenwich meridian is marked at 4° intervals from 0° to 84°N with dashed circles at 30°N and 60°N. Contour spacing is 0.5 ppmv.

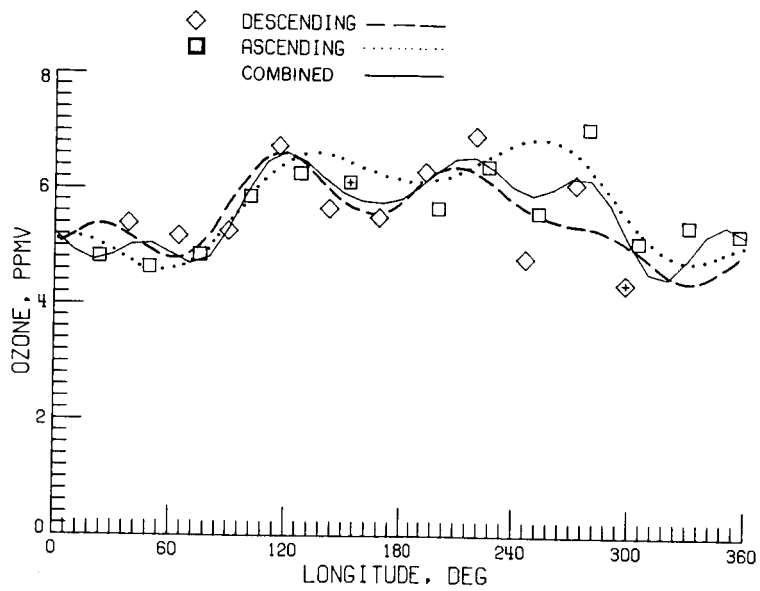


(a) 52°N.

Figure 12. Kalman filter fit to ozone data at 10 mbar on Jan. 26. Plus signs indicate earliest data points for each mode.

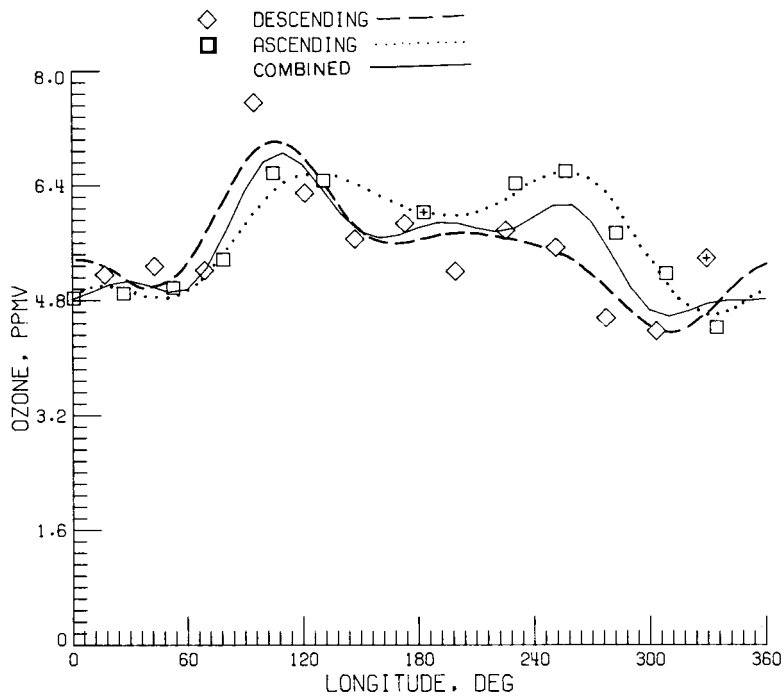


(b) 56°N.



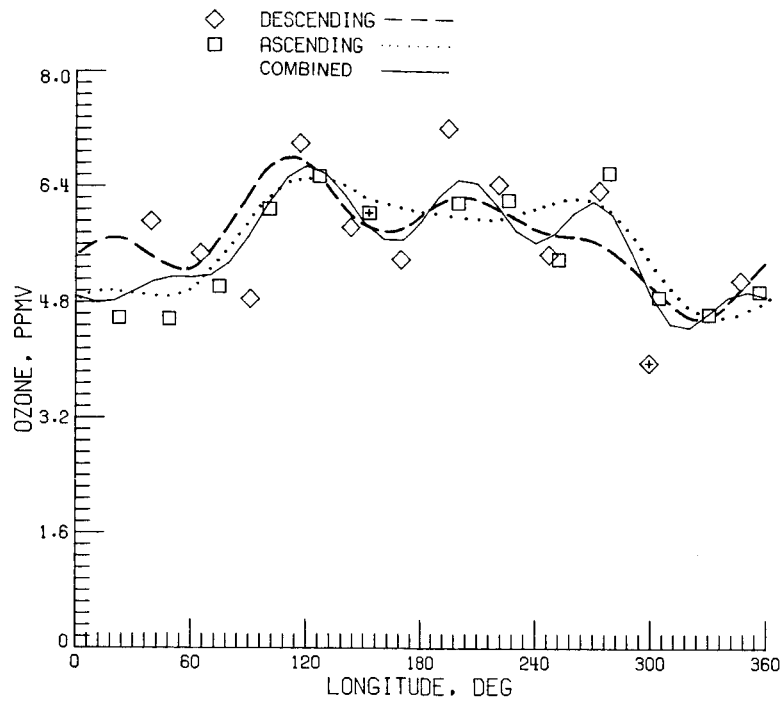
(c) 60°N.

Figure 12. Concluded.

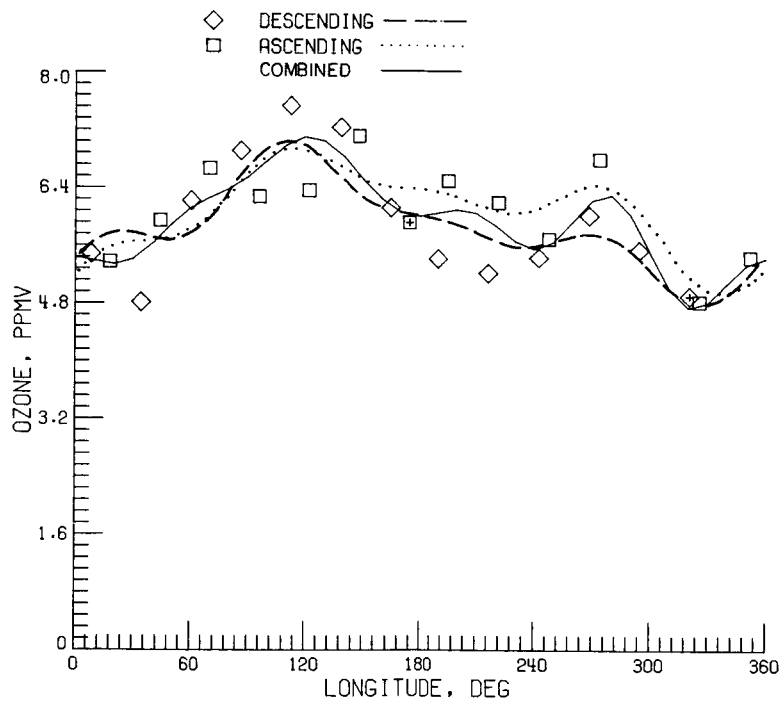


(a) Jan. 25.

Figure 13. Kalman filter fit to ozone data at 10 mbar at 56°N. Plus signs indicate earliest data points for each mode.



(b) Jan. 26.



(c) Jan. 27.

Figure 13. Concluded.

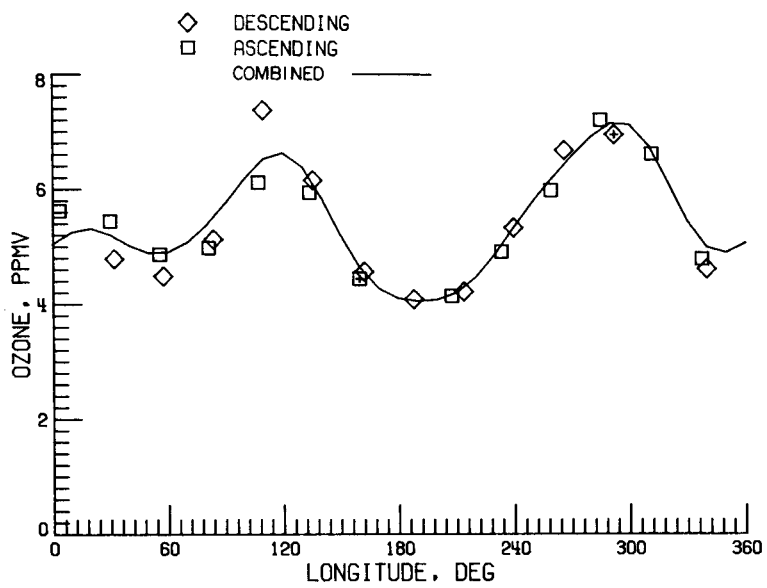
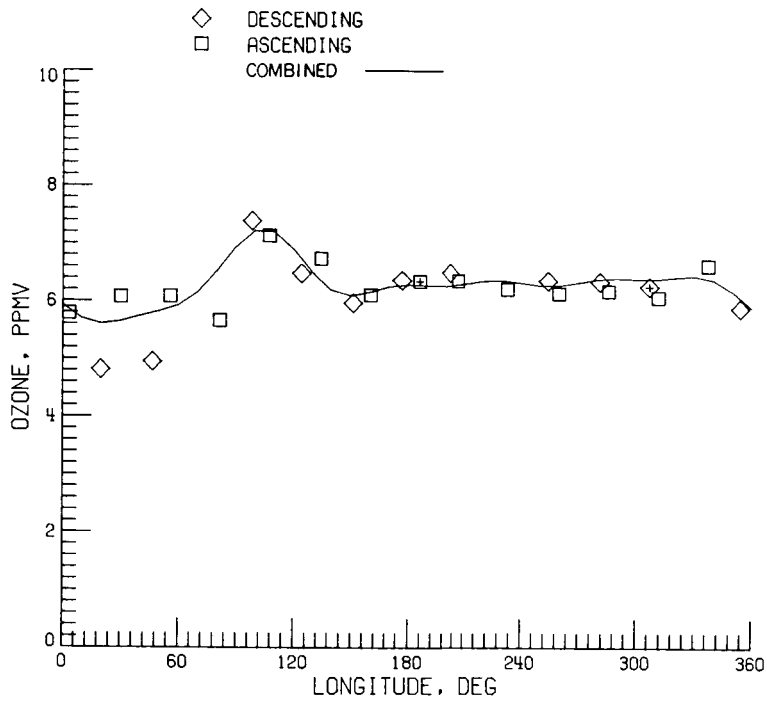
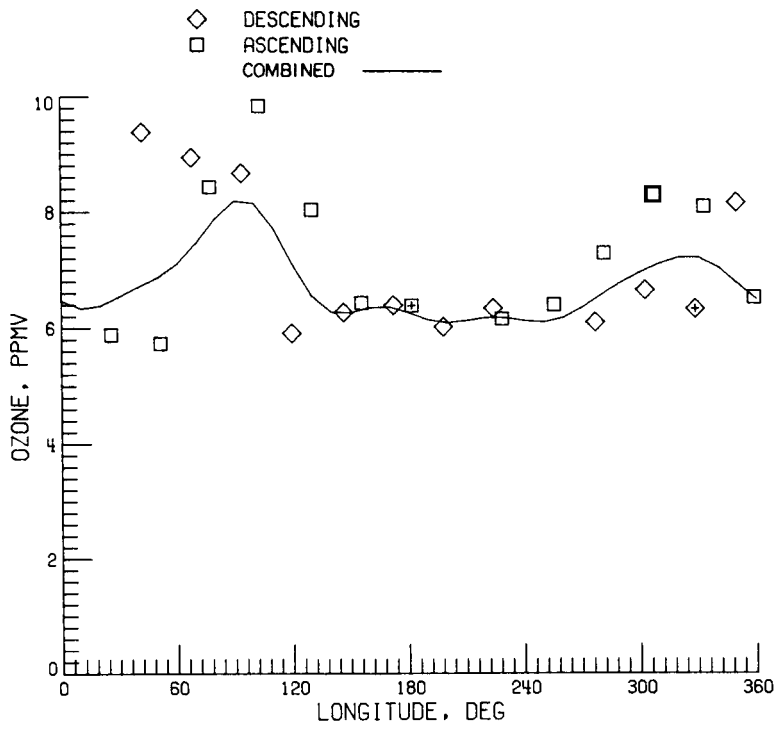


Figure 14. Kalman filter fit to ozone data for combined mode at 72°N at 3 mbar on Jan. 26. Plus signs indicate earliest data points for each mode.

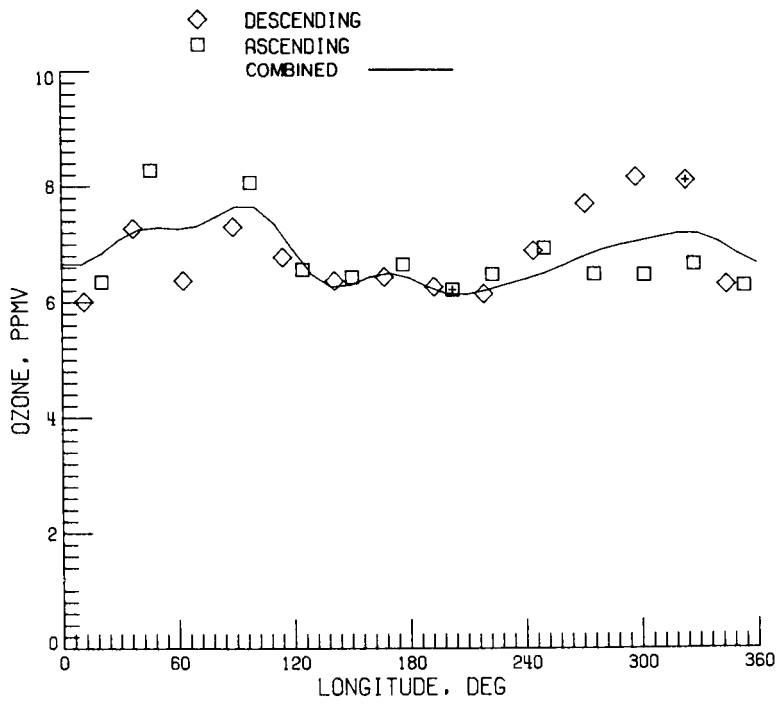


(a) Feb. 25.

Figure 15. Kalman filter fit to ozone data for combined mode at 76°N at 16 mbar. Plus signs indicate earliest data points for each mode.



(b) Feb. 26.



(c) Feb. 27.

Figure 15. Concluded.

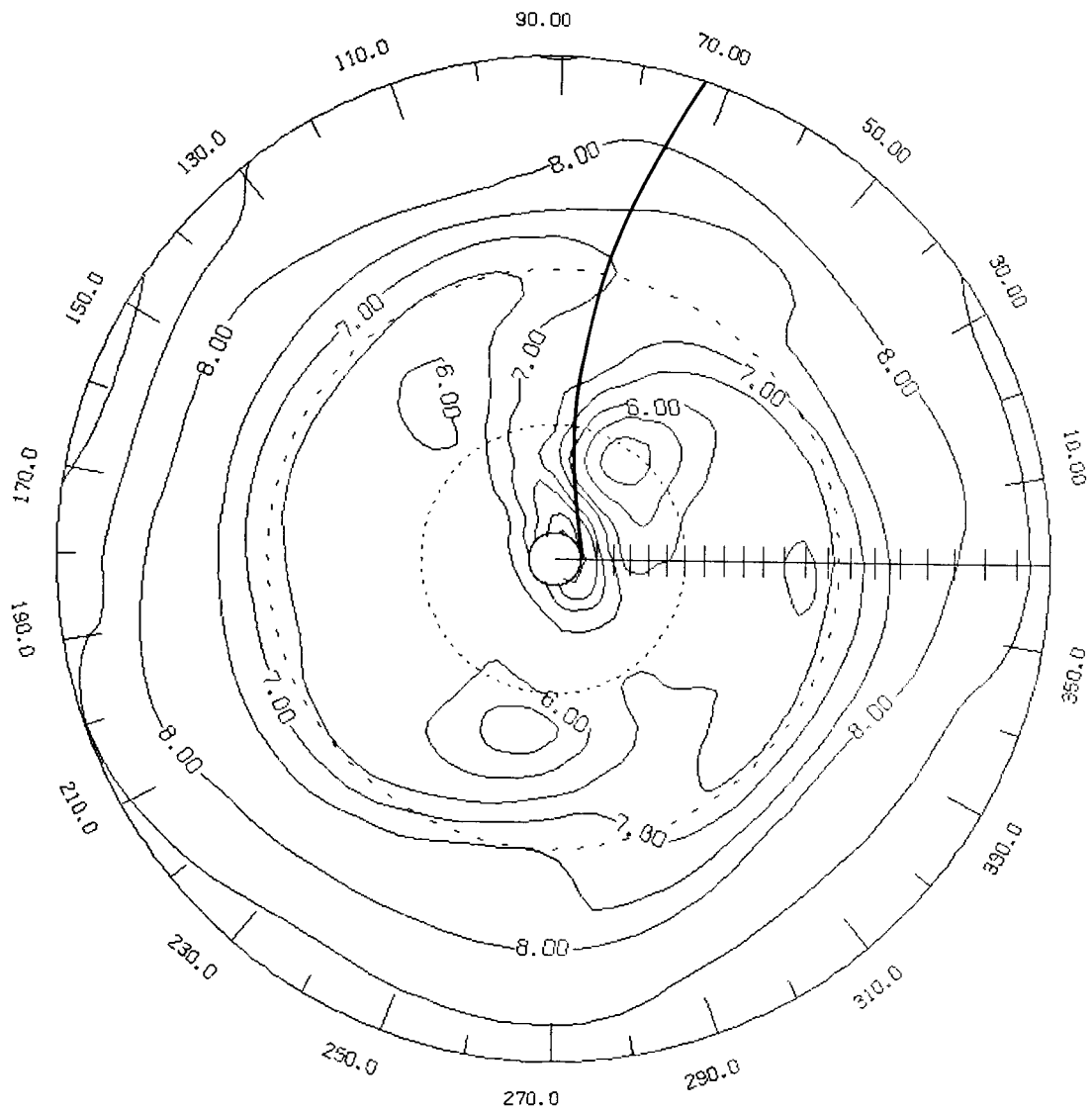


Figure 16. Combined mode LAMAT ozone mixing ratio at 16 mbar on Feb. 26, in the Northern Hemisphere with 1-2-1 latitude smoothing. Greenwich meridian is marked at 4° intervals from 0° to 84°N with dashed circles at 30°N and 60°N. Solid curve is locus of tangent points for orbit 1734. Contour spacing is 0.5 ppmv.

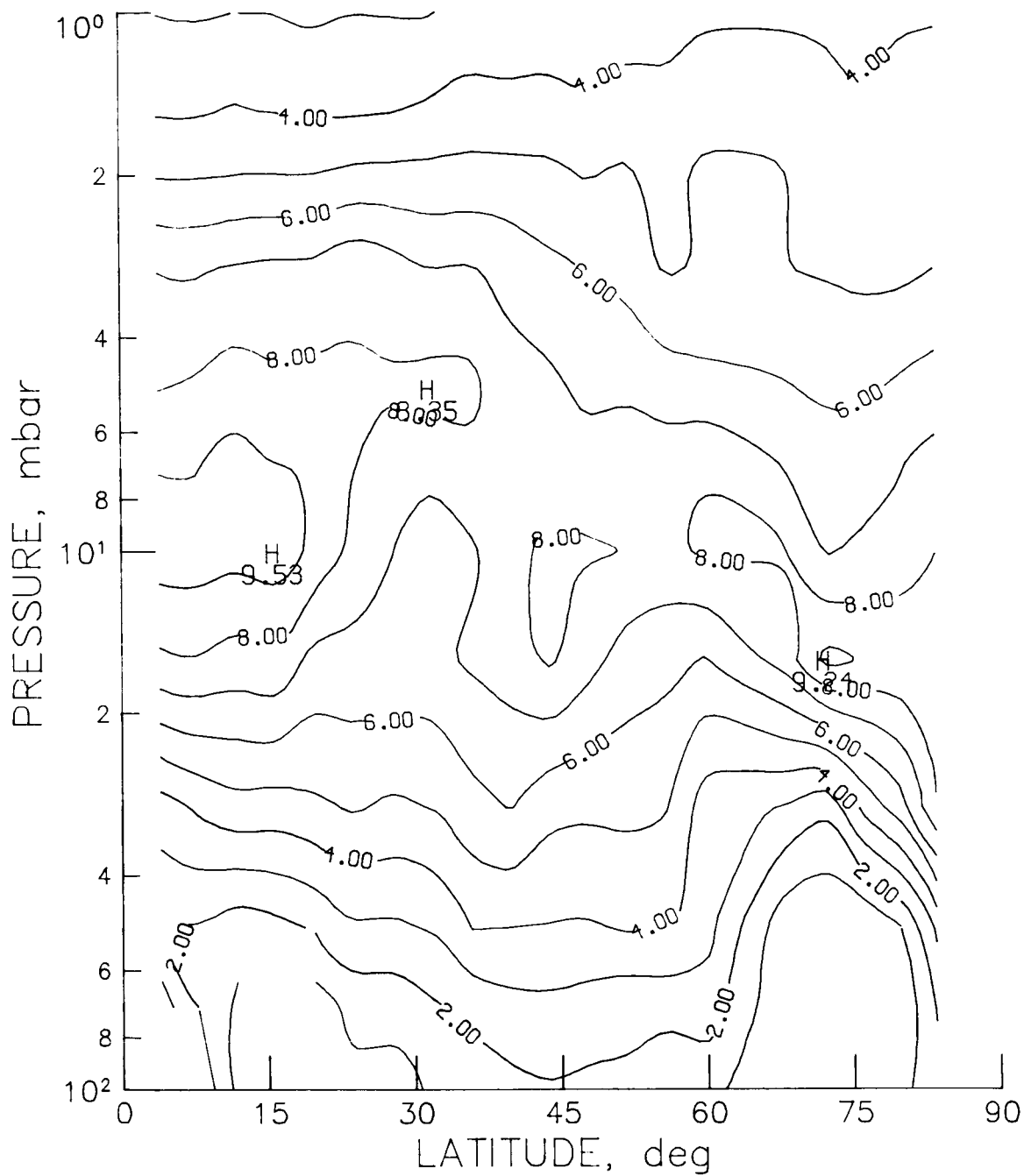


Figure 17. LIMS ozone mixing ratio for descending mode of orbit 1734 (Feb. 26, see fig. 16). There were no data between 30 and 100 mbar and 64° and 80°N. Contour spacing is 1.0 ppmv.

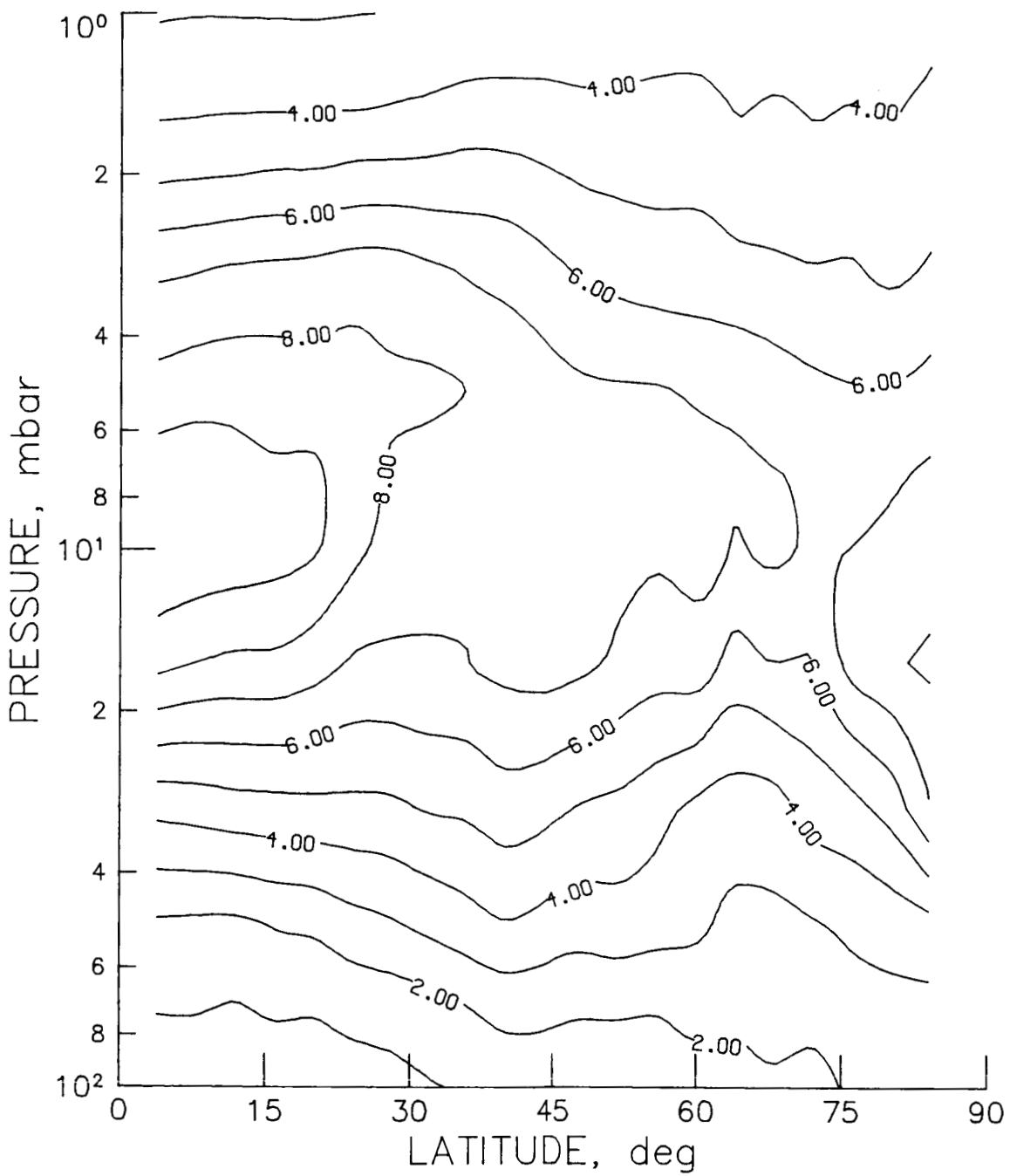
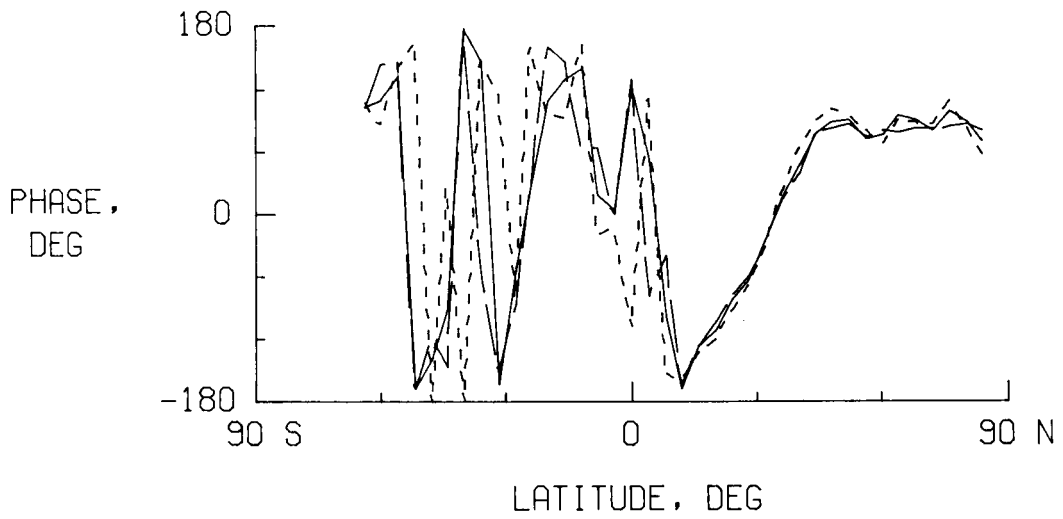
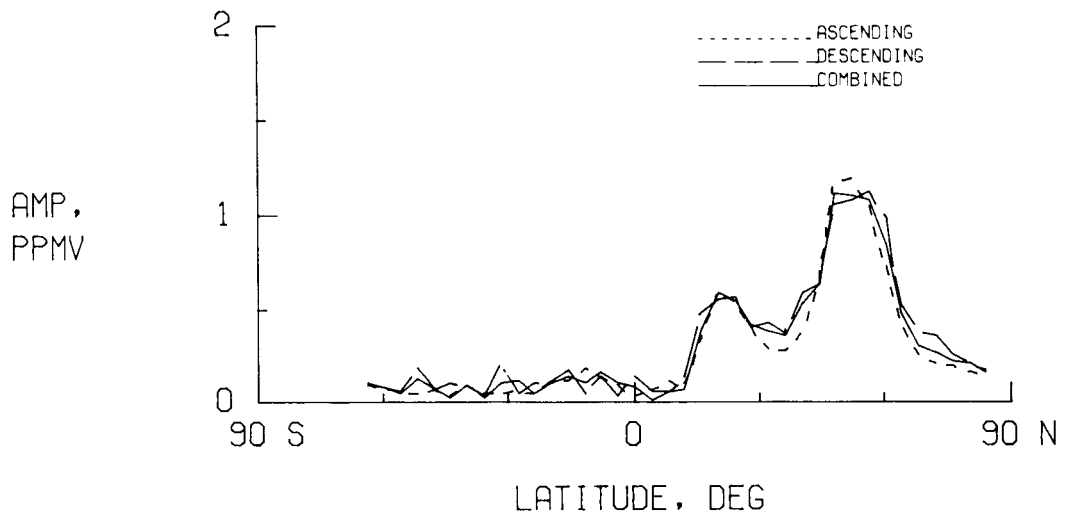
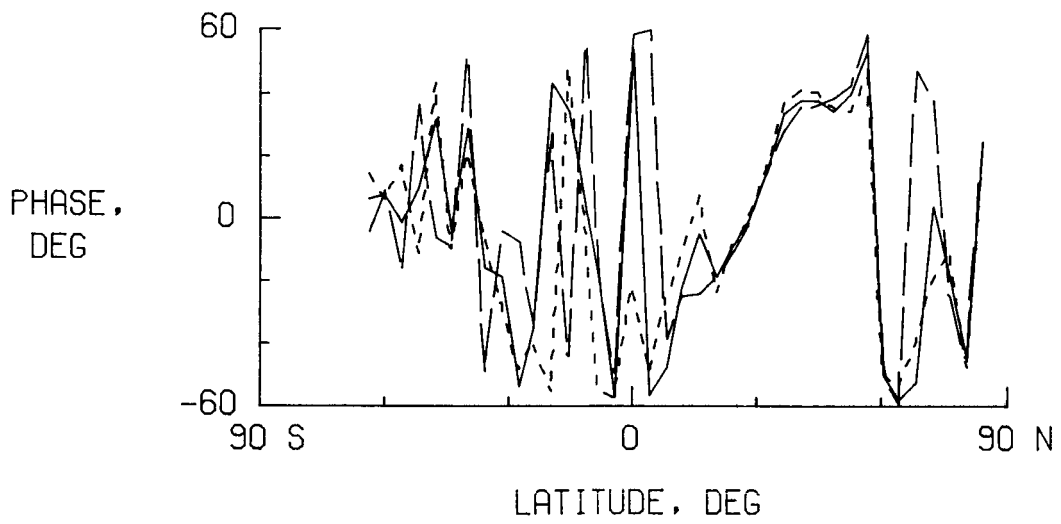
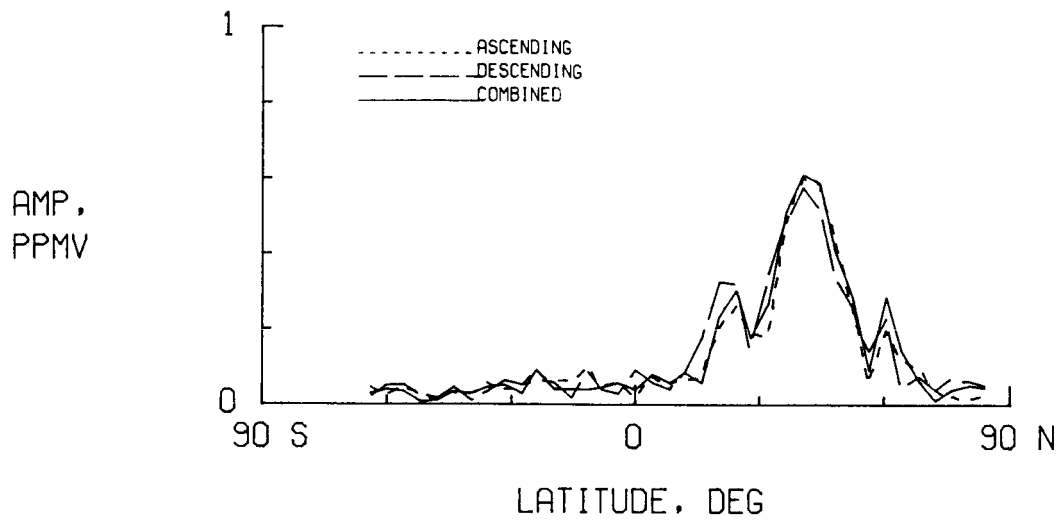


Figure 18. LAMAT ozone mixing ratio for combined mode at the longitudes of orbit 1734 (see fig. 16). Contour spacing is 1.0 ppmv.



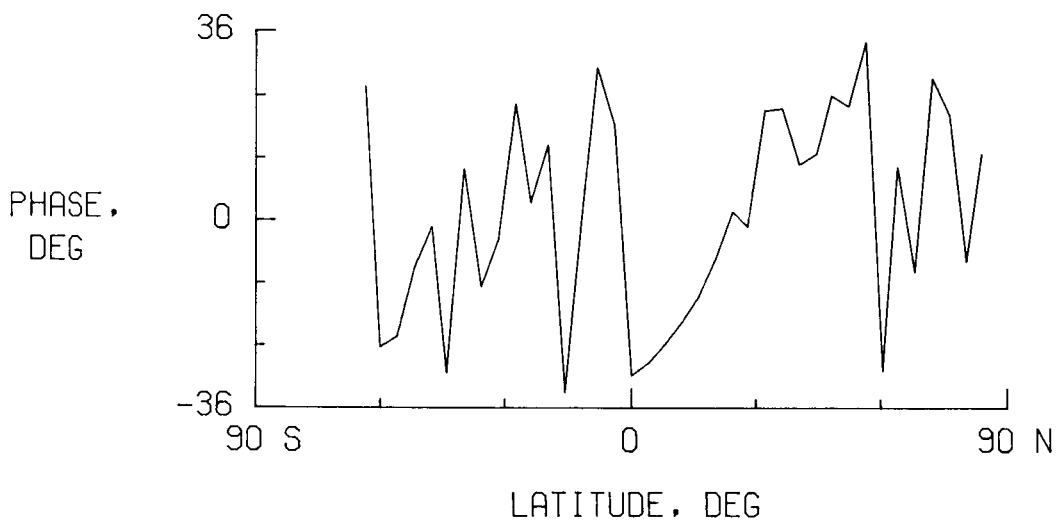
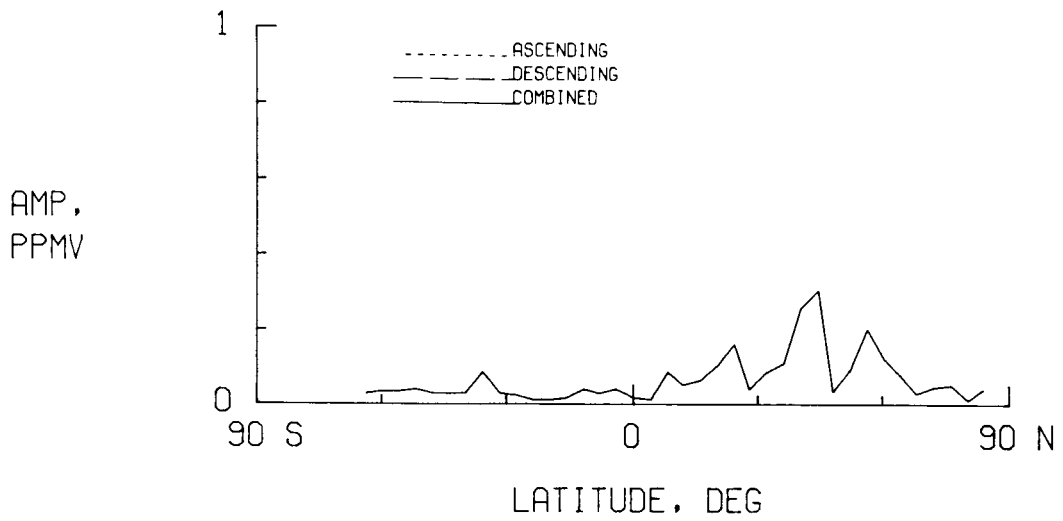
(a) Wave 1.

Figure 19. Amplitudes and phases of LAMAT ozone mixing ratio at 10 mbar on Jan. 5.



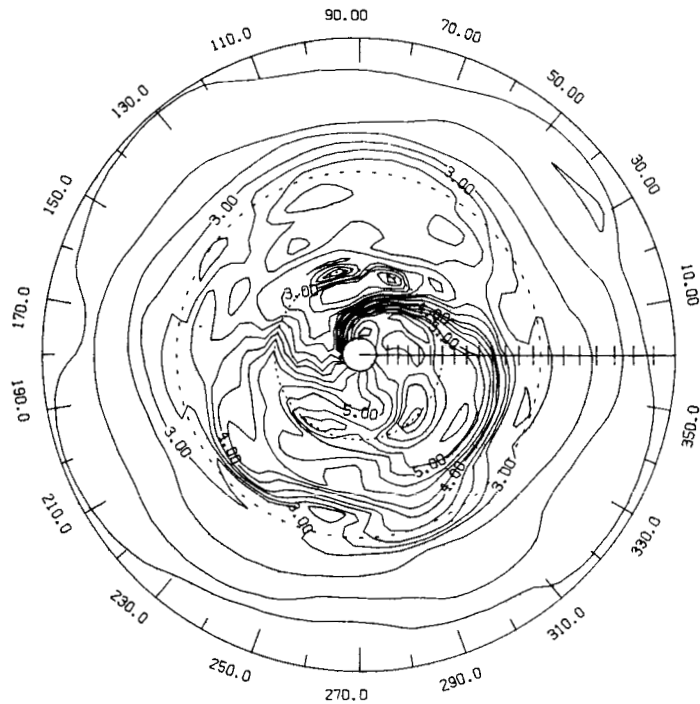
(b) Wave 3.

Figure 19. Continued.

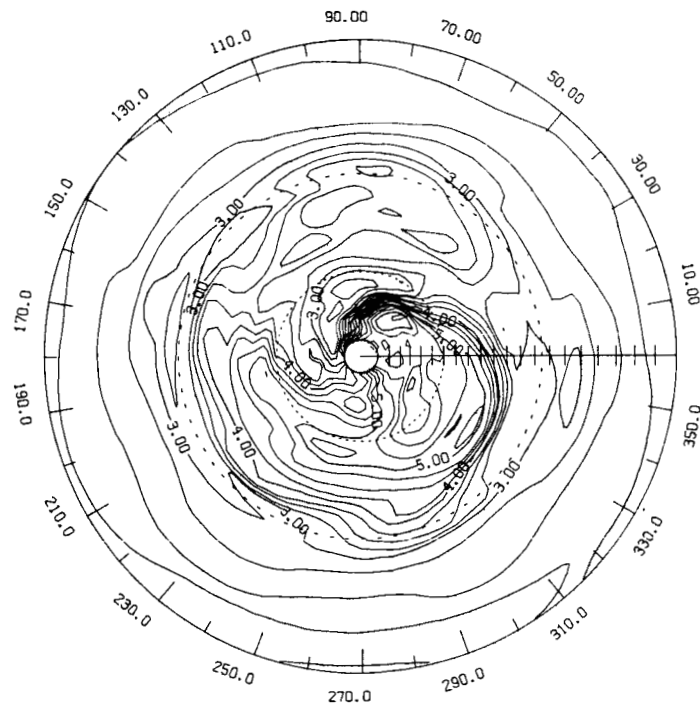


(c) Wave 5.

Figure 19. Concluded.

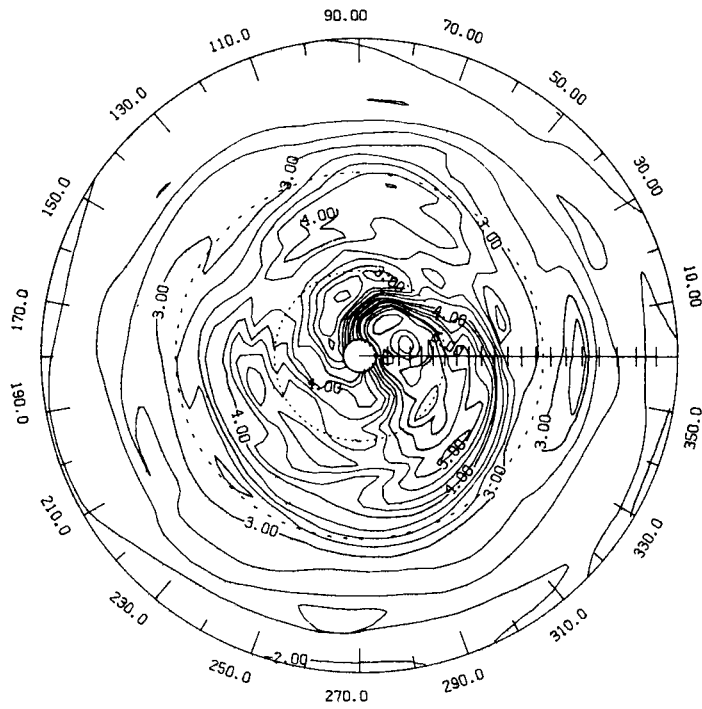


(a) Feb. 5.

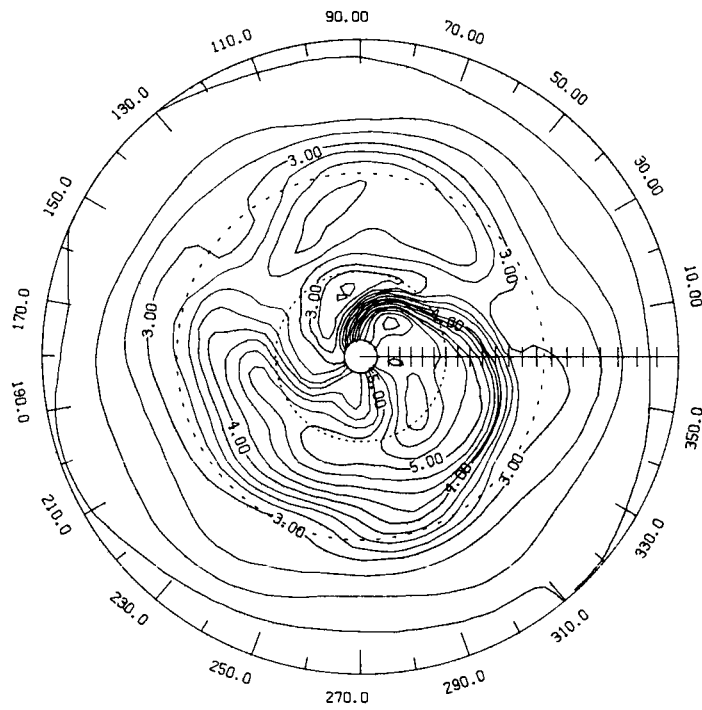


(b) Feb. 6.

Figure 20. Combined mode LAMAT nitric acid mixing ratio at 10 mbar in the Northern Hemisphere. Greenwich meridian is marked at 4° intervals from 0° to 84°N with dashed circles at 30°N and 60°N. Contour spacing is 0.25 ppbv.

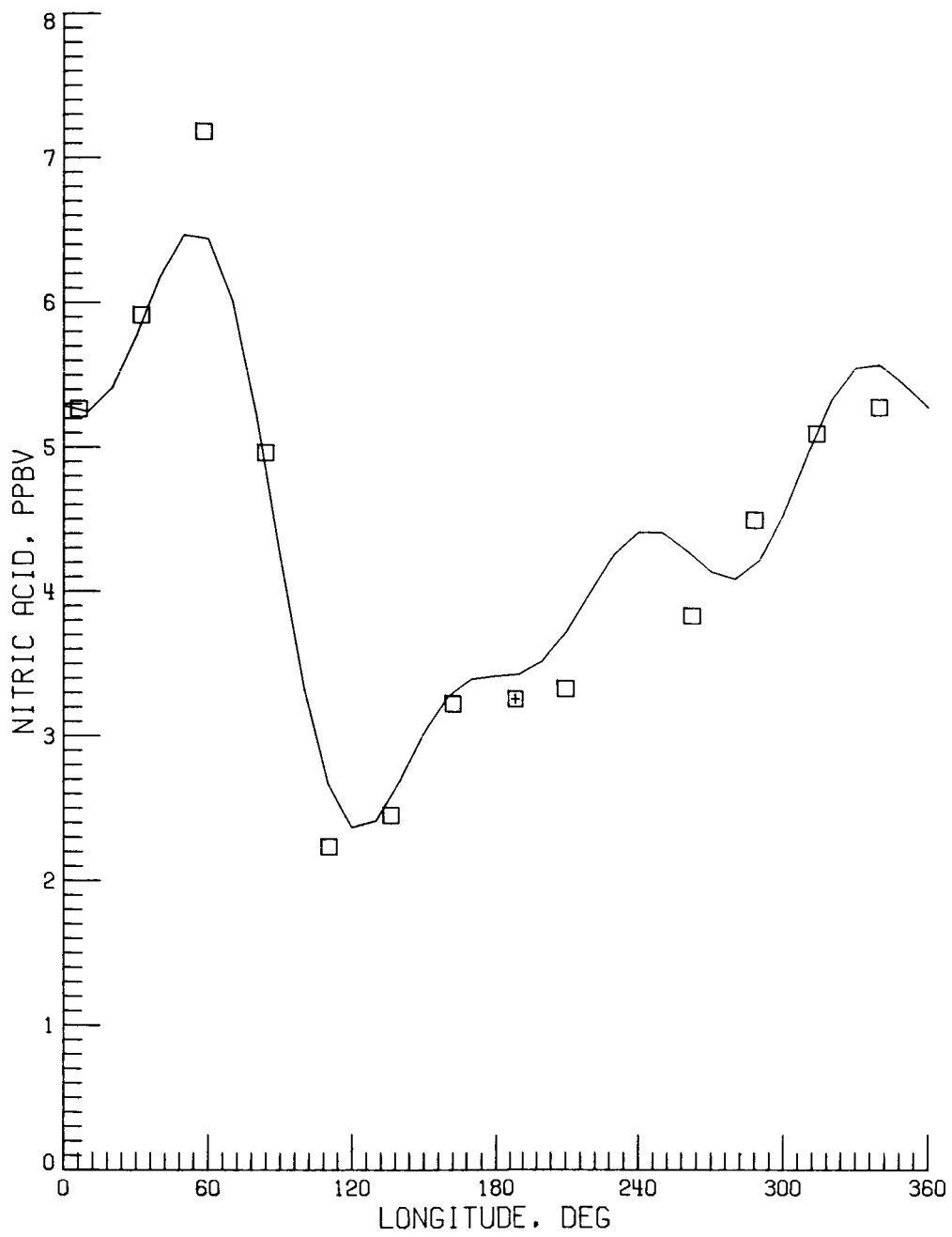


(c) Feb. 7.



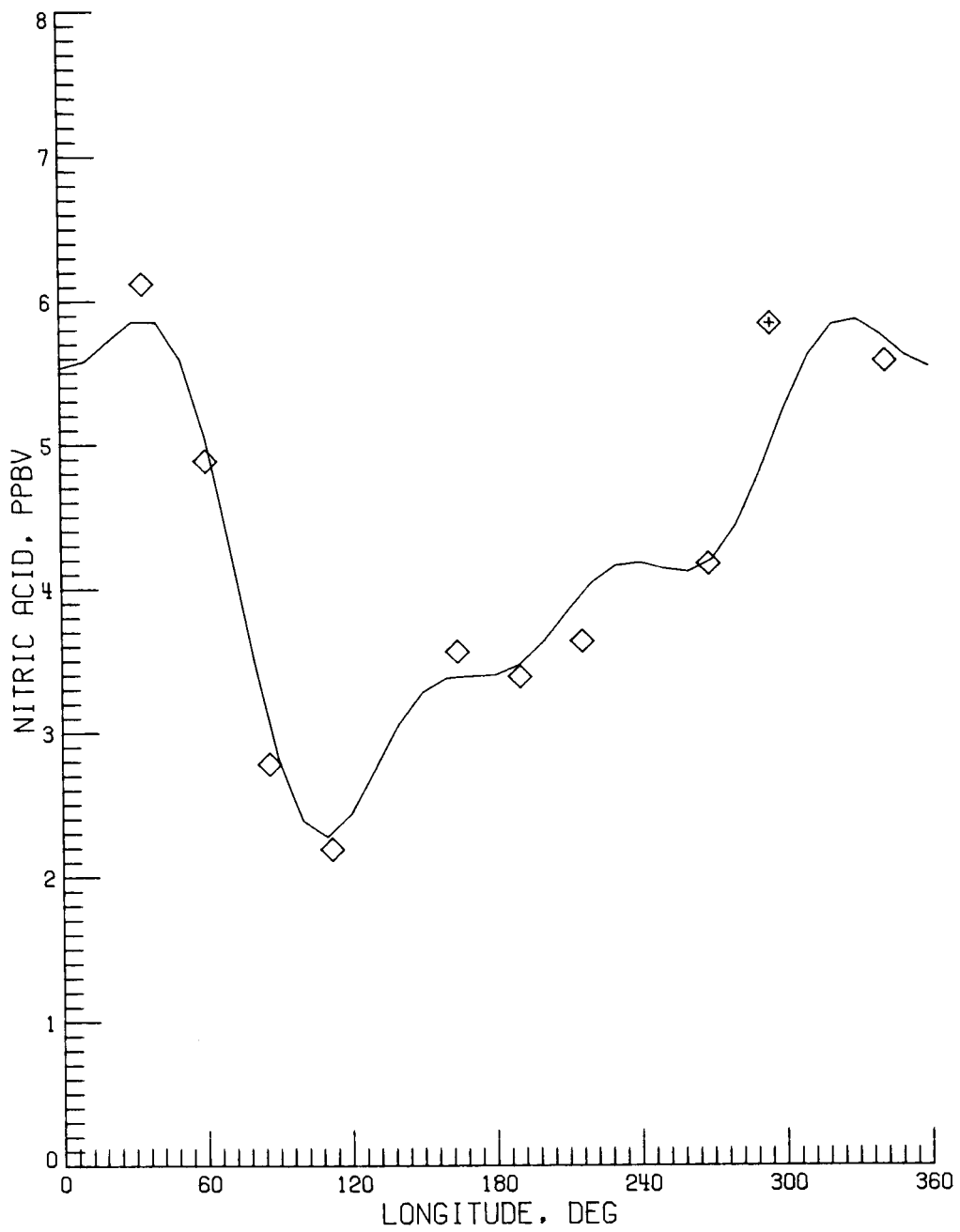
(d) Feb. 6, with 1-2-1 latitude smoothing.

Figure 20. Concluded.



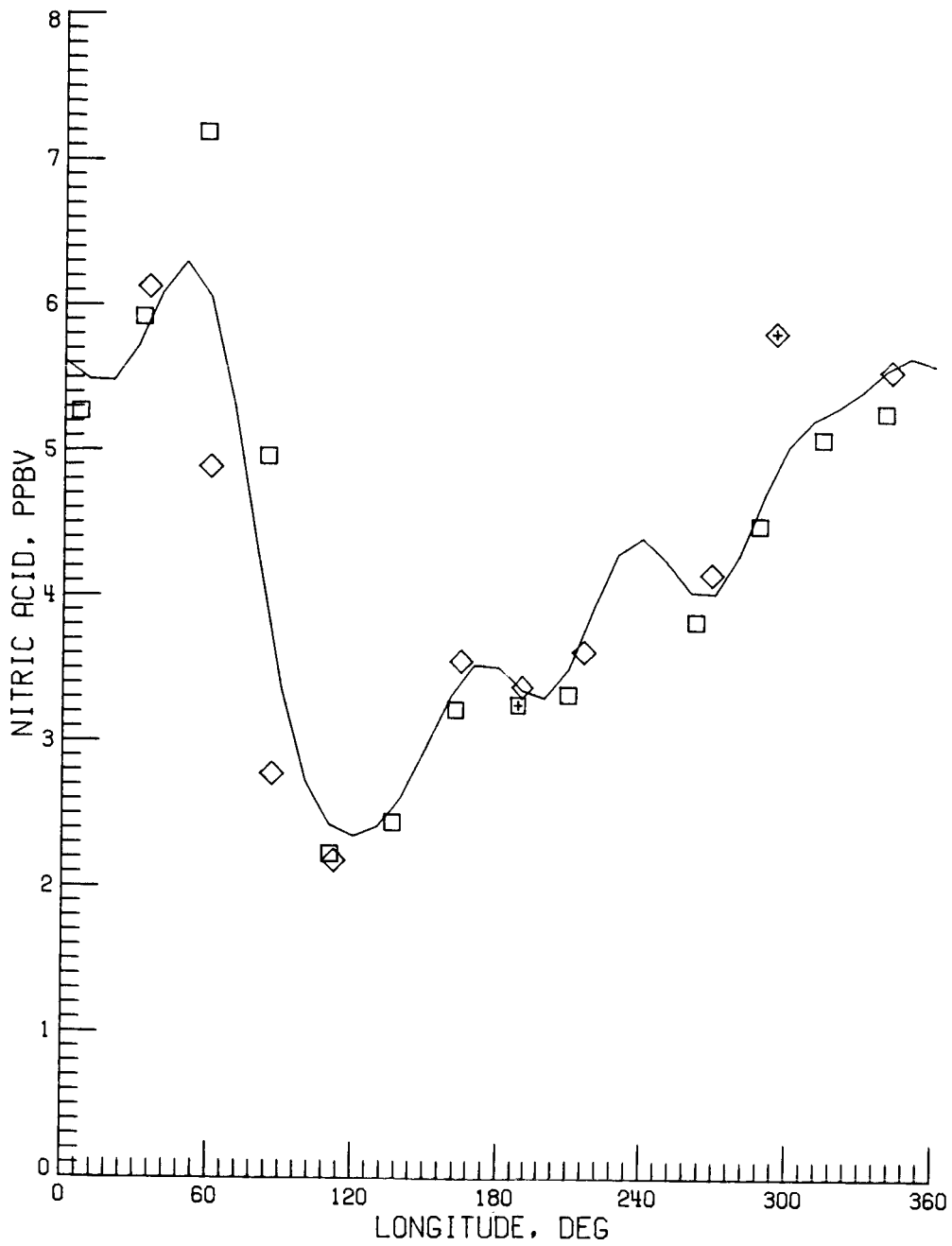
(a) Ascending mode.

Figure 21. Kalman filter fit to nitric acid data at 10 mbar at 72°N on Feb. 6. Plus sign indicates earliest data point.



(b) Descending mode.

Figure 21. Continued.



(c) Combined mode.

Figure 21. Concluded.

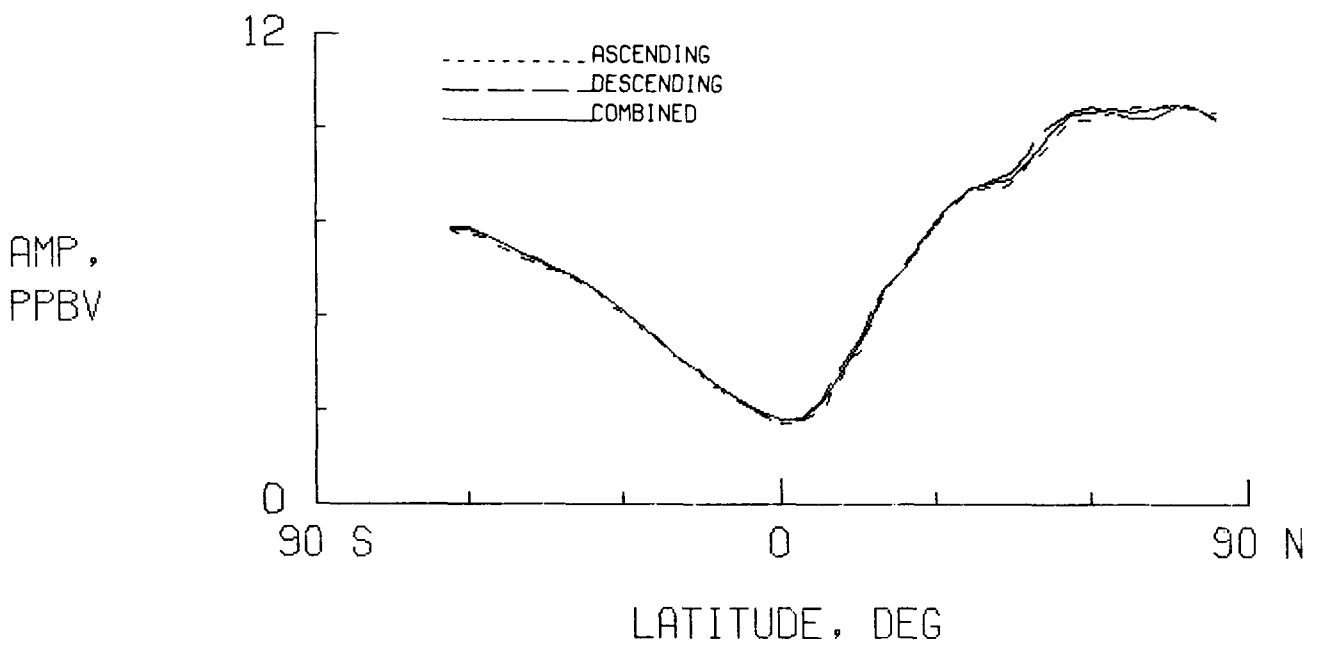
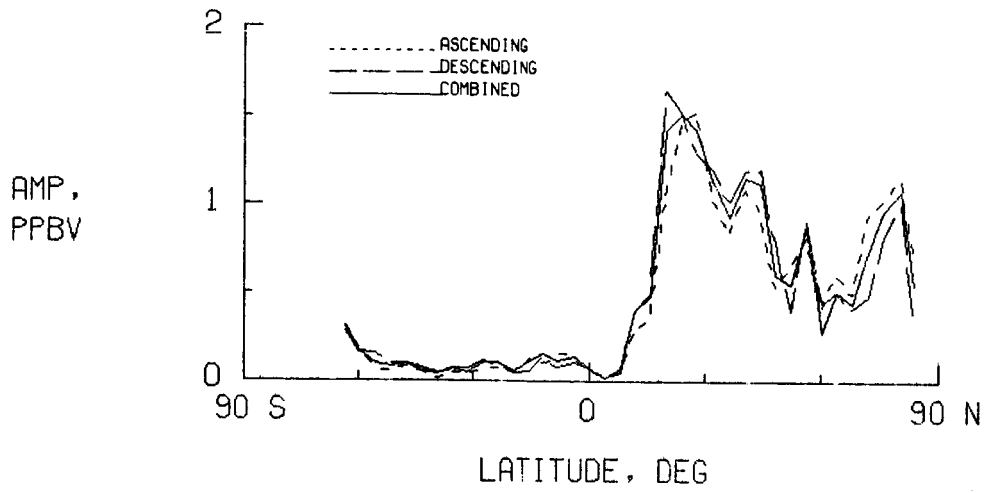
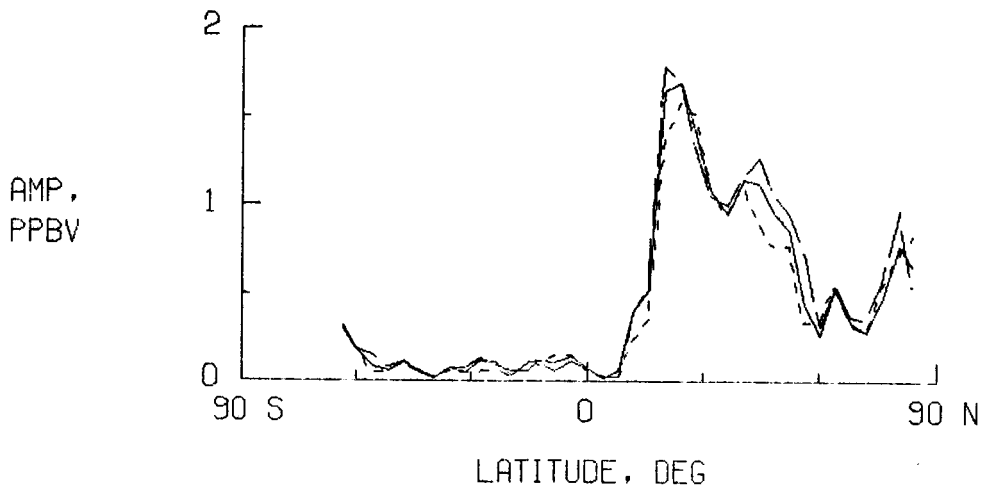


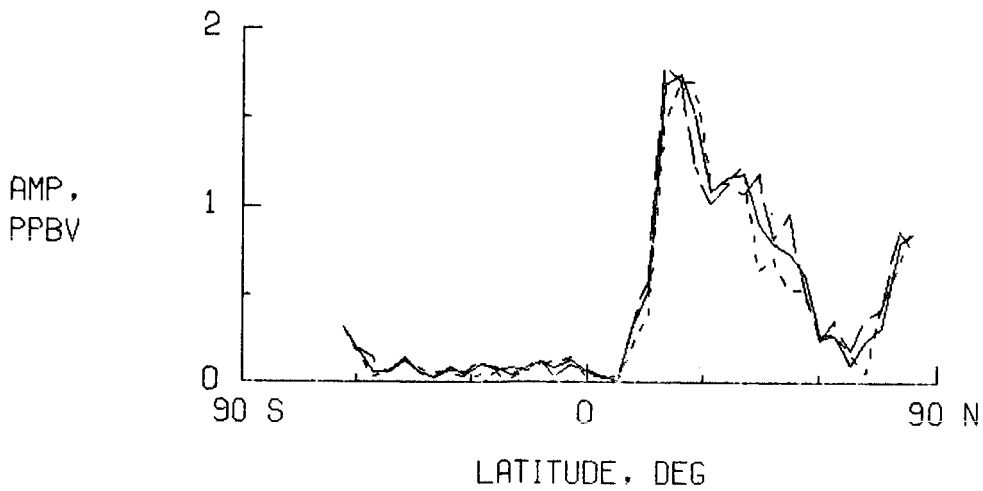
Figure 22. Zonal mean coefficient for all modes at 30 mbar for nitric acid on Jan. 25.



(a) Jan. 25.

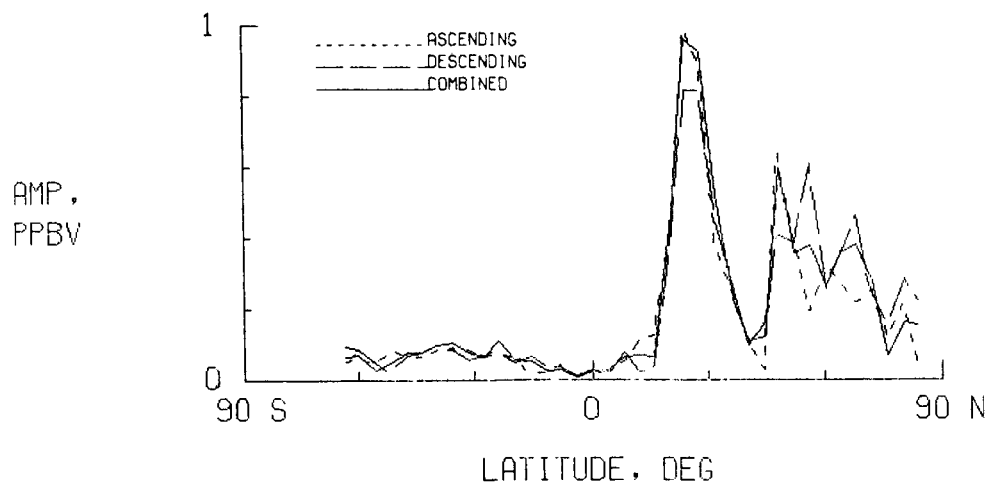


(b) Jan. 26.

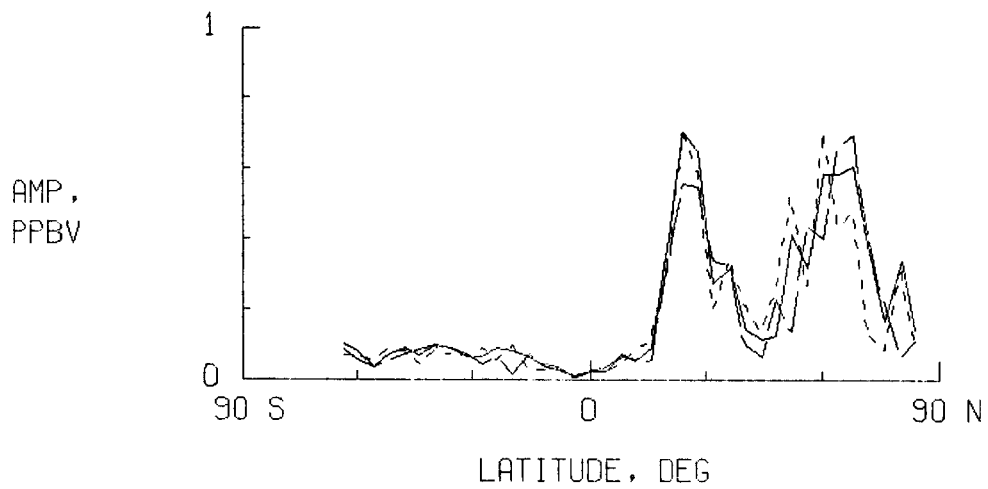


(c) Jan. 27.

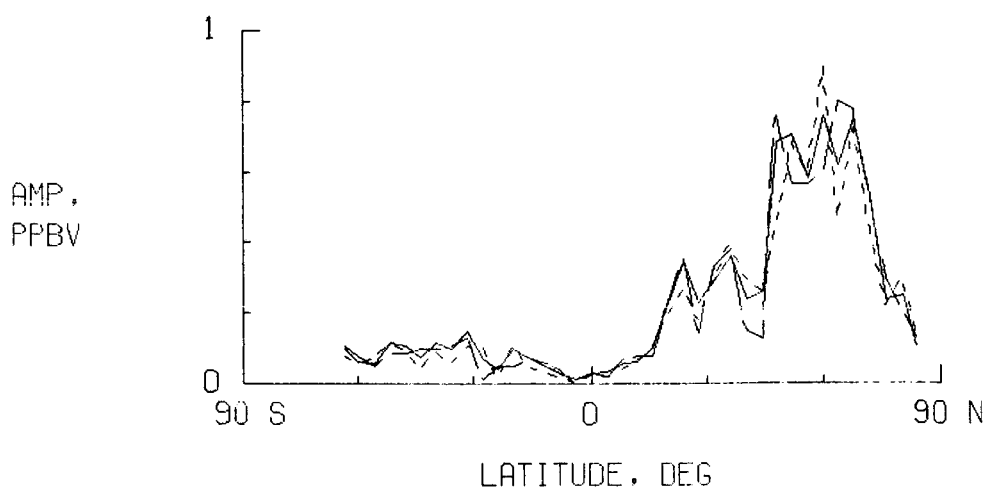
Figure 23. Variation of wave 1 amplitude at 30 mbar with mode and latitude.



(a) Jan. 25.

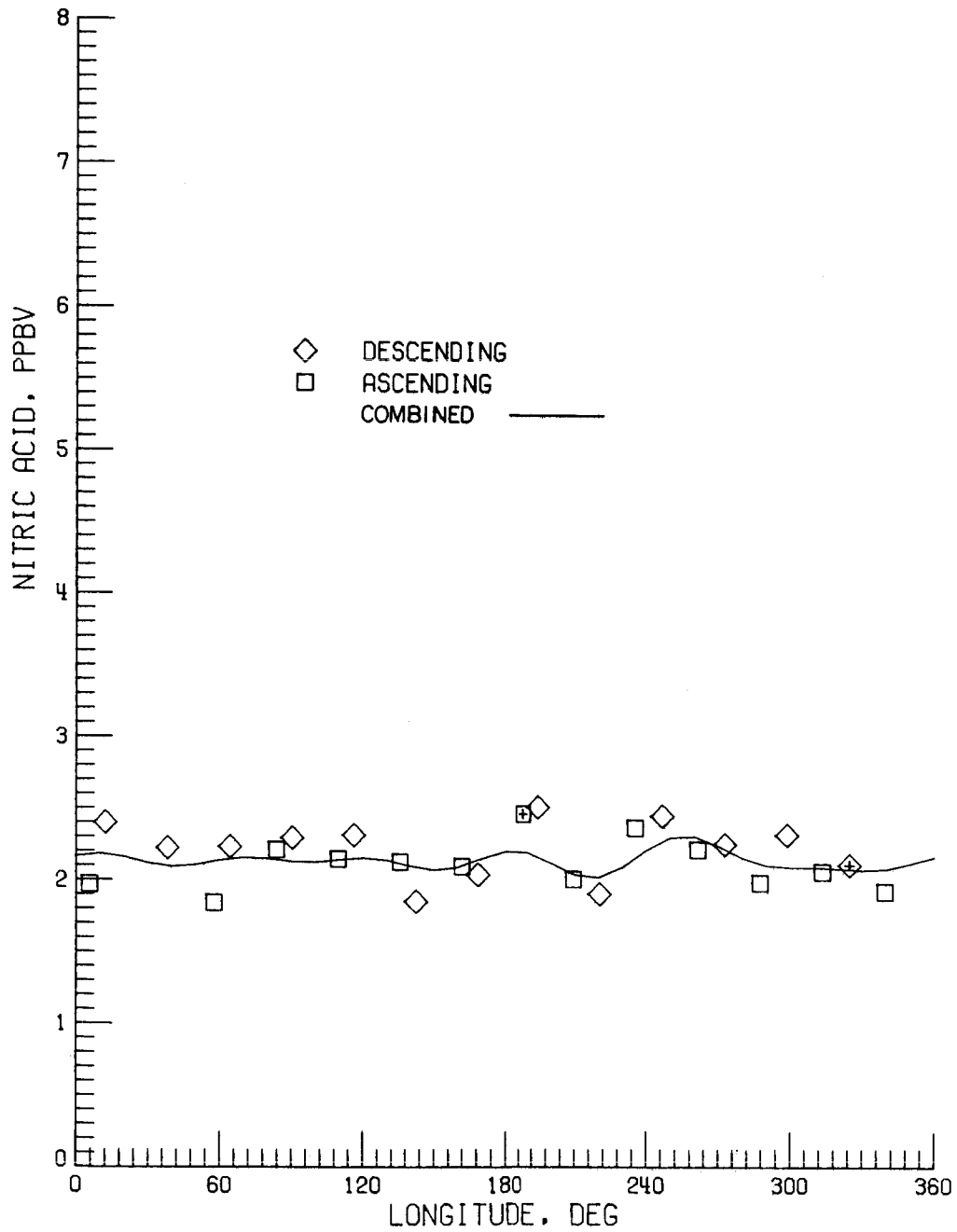


(b) Jan. 26.



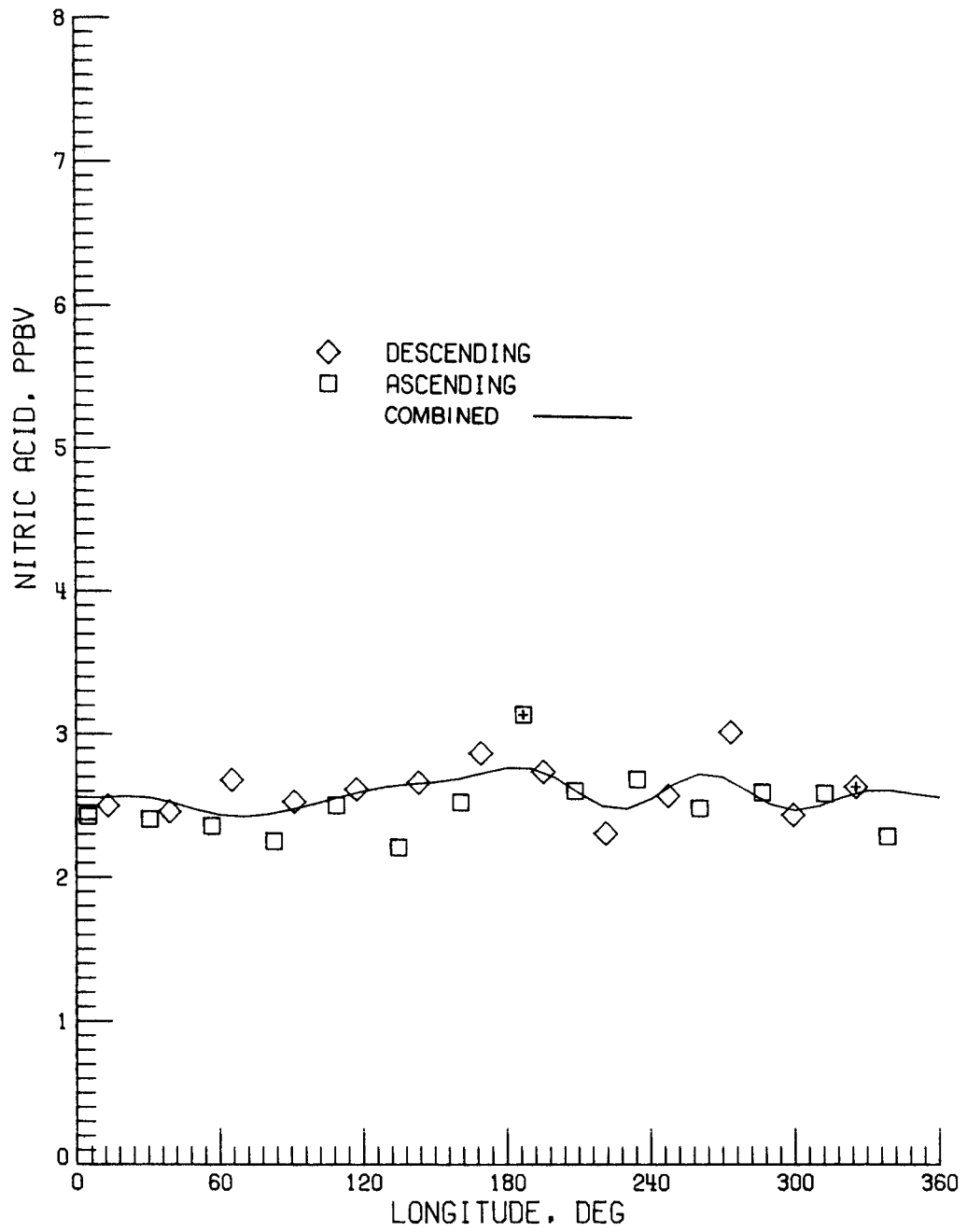
(c) Jan. 27.

Figure 24. Variation of wave 2 amplitude at 30 mbar with mode and latitude.



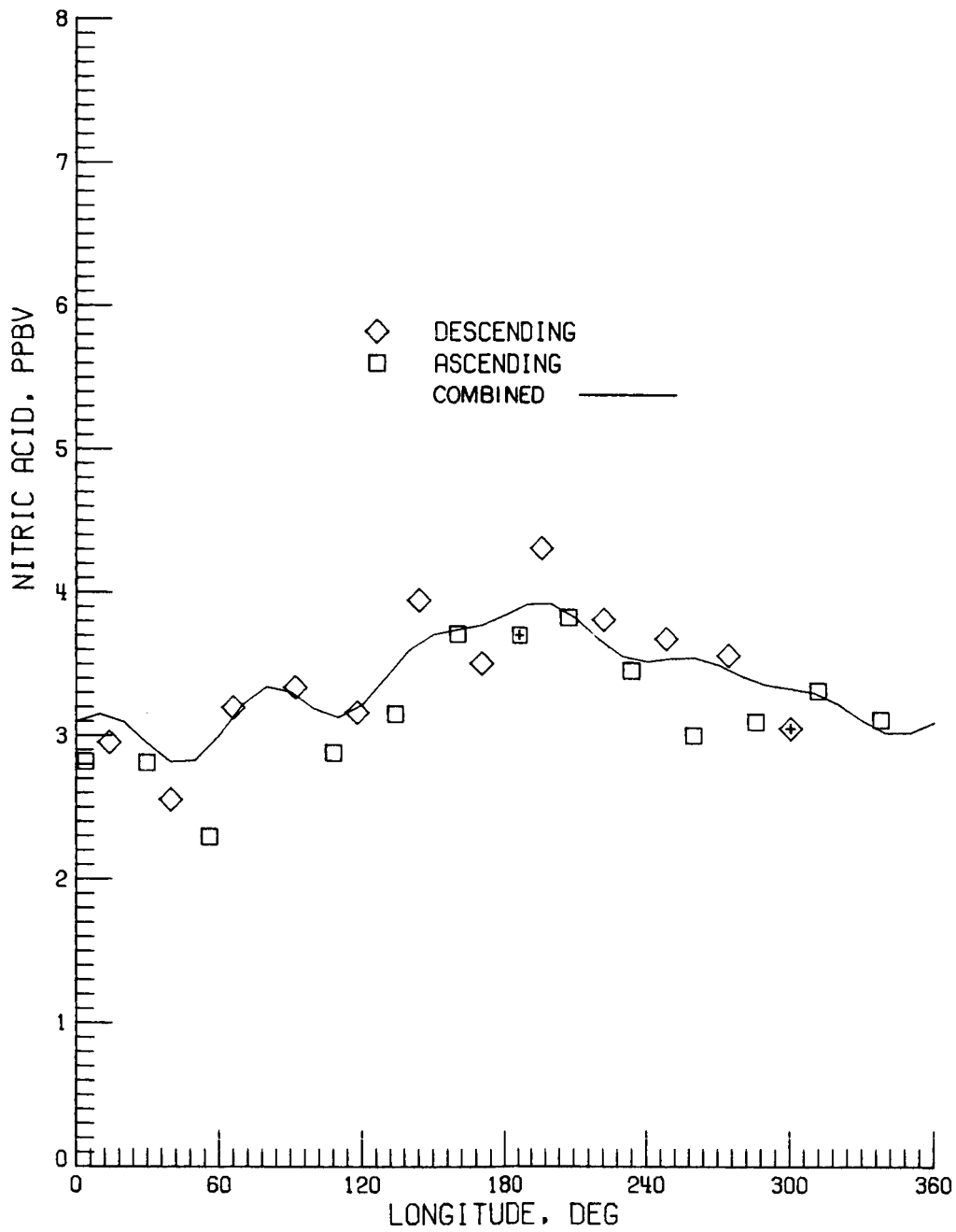
(a) 4°N.

Figure 25. Kalman filter fit to nitric acid data for combined mode at 30 mbar on Jan. 25. Plus signs indicate earliest data points for each mode.



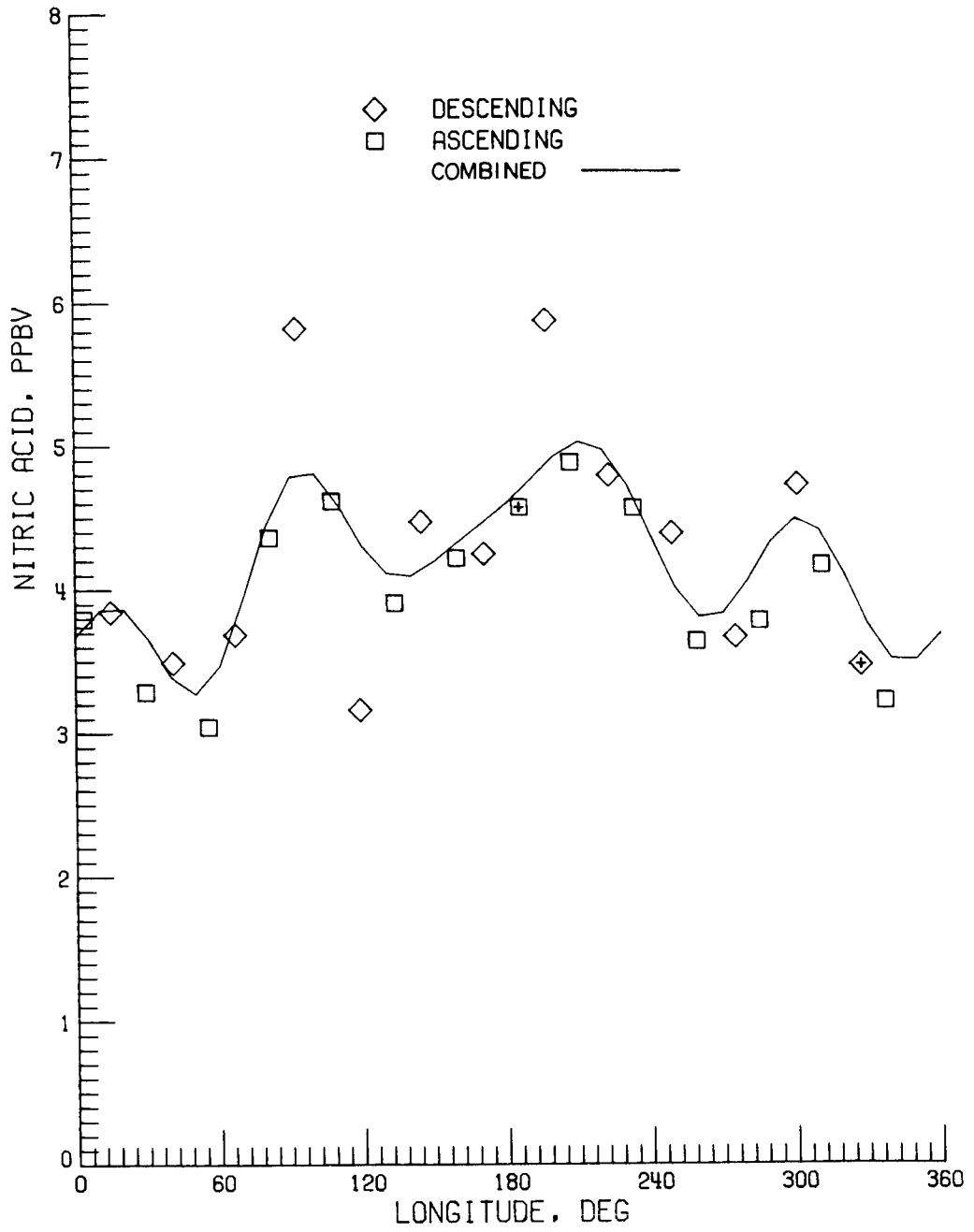
(b) 8°N.

Figure 25. Continued.



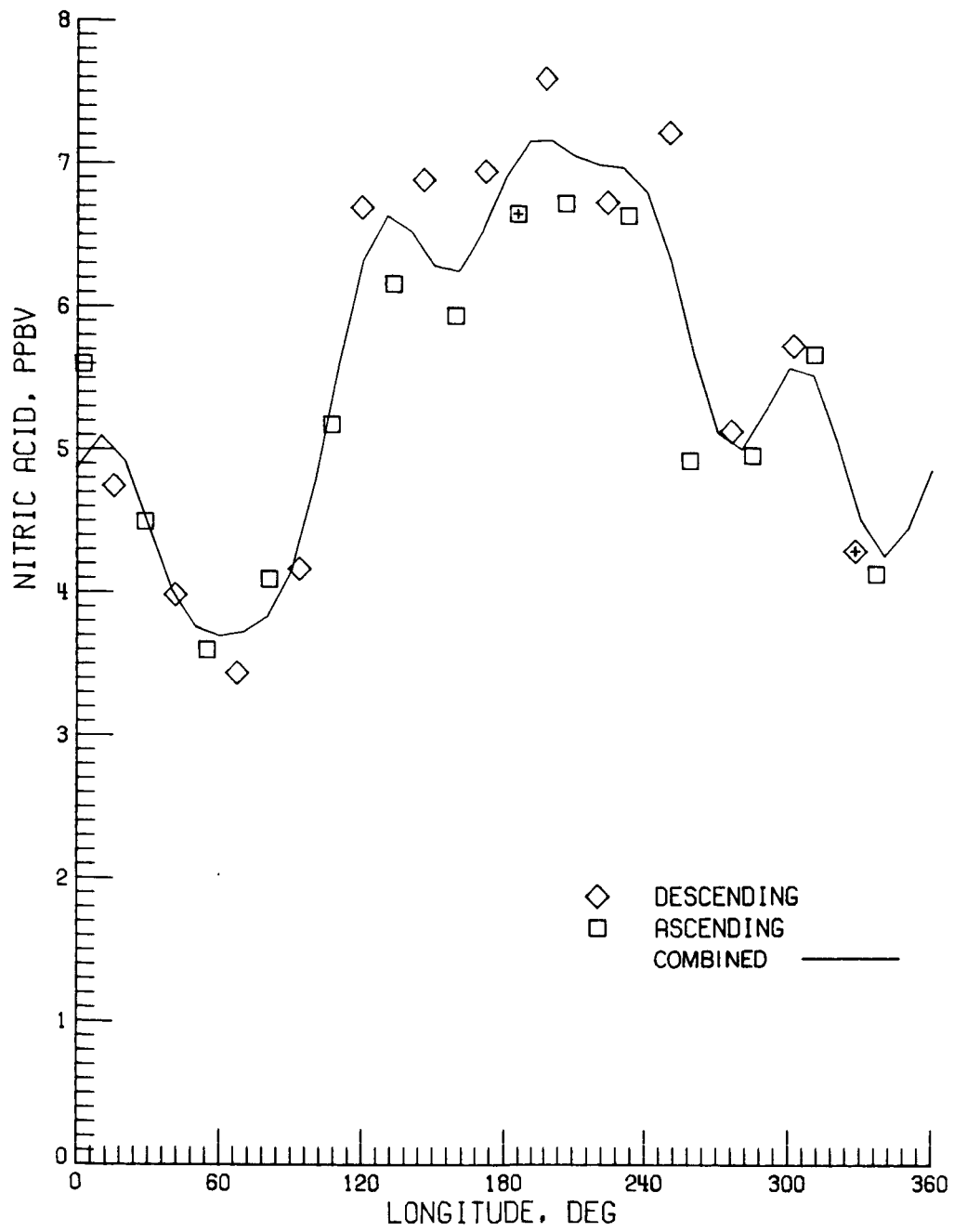
(c) 12°N.

Figure 25. Continued.



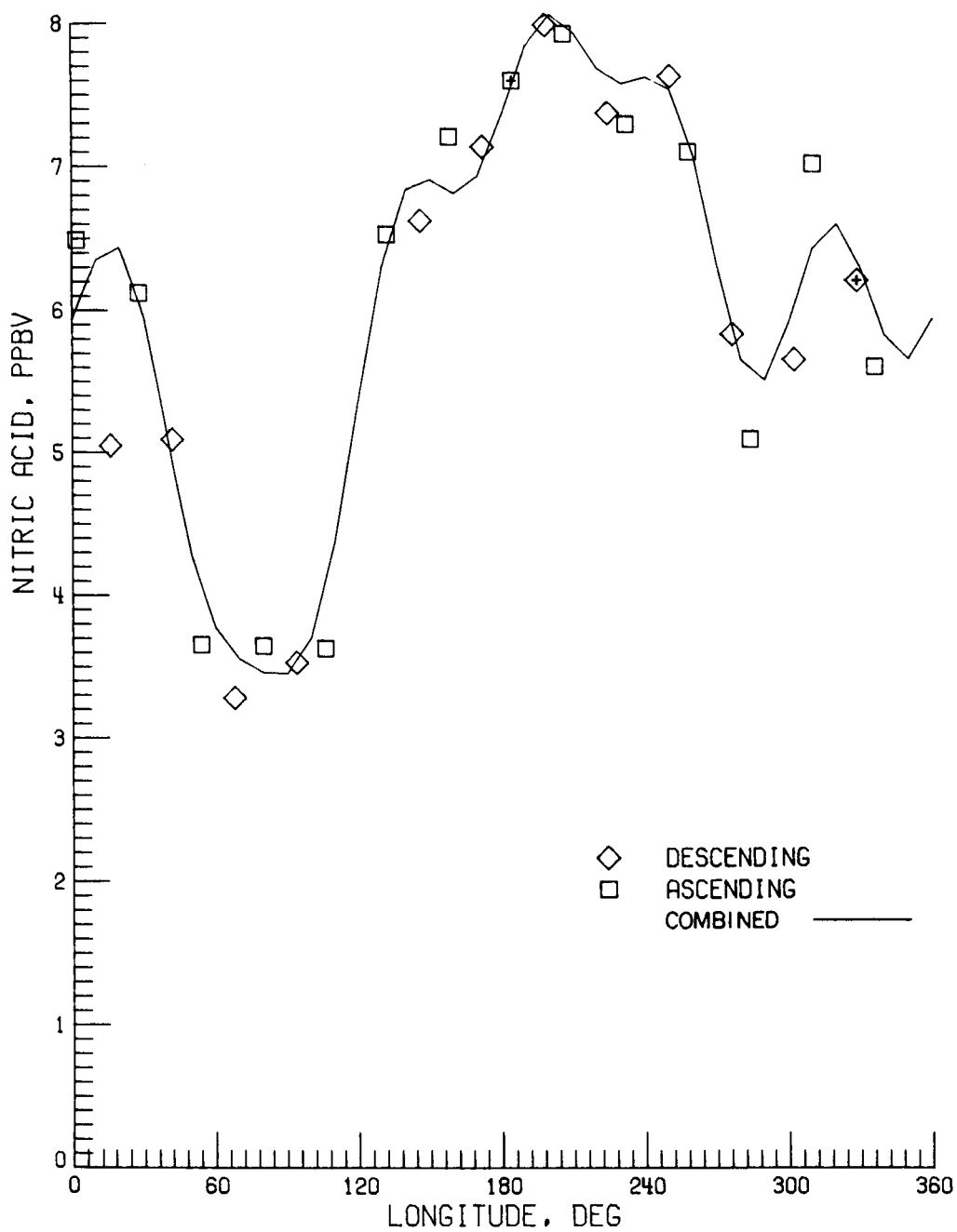
(d) 16°N.

Figure 25. Continued.



(e) 20°N.

Figure 25. Continued.



(f) 24°N.

Figure 25. Concluded.

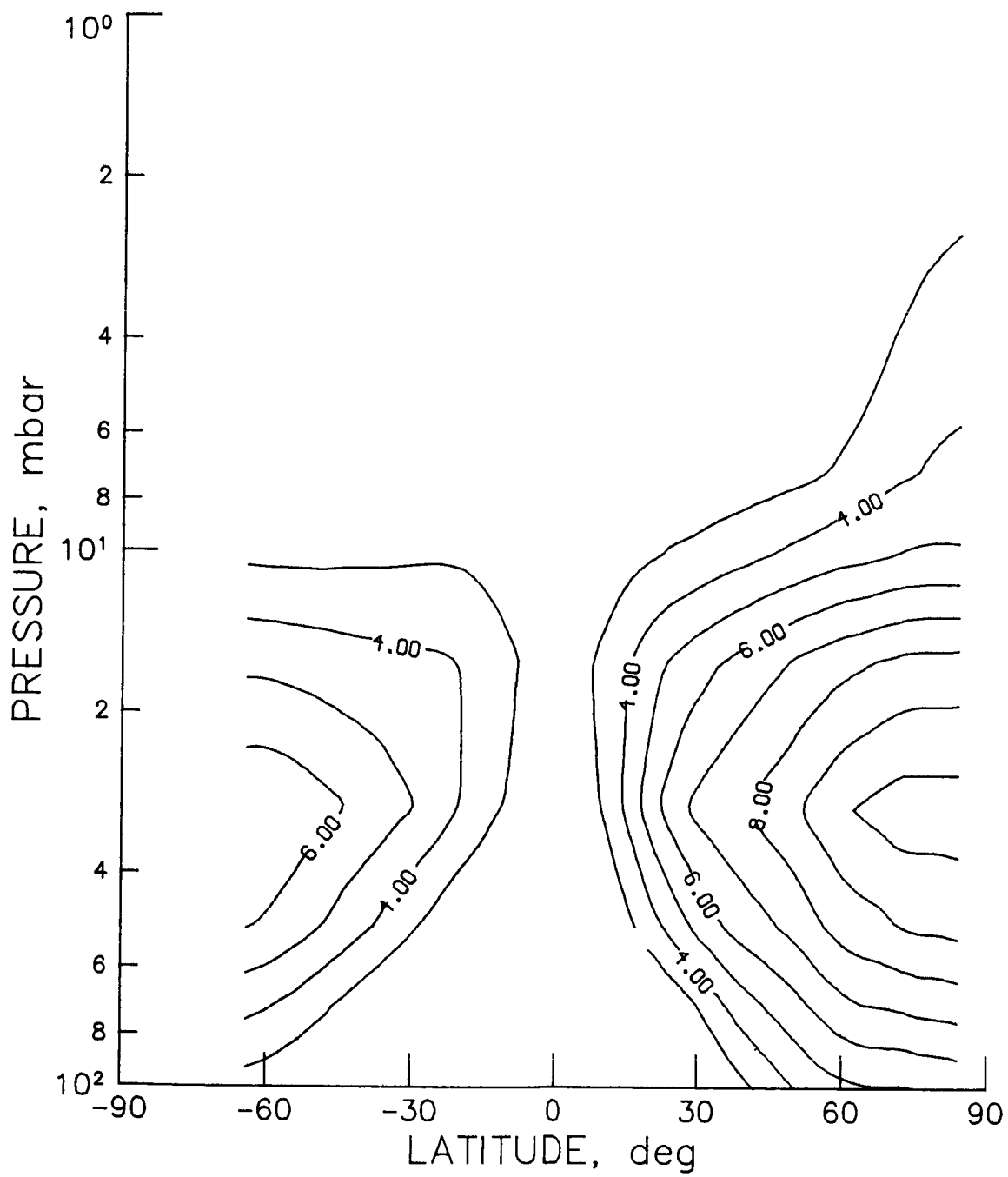


Figure 26. Zonal mean of combined mode nitric acid mixing ratio for January. Contour spacing is 1.0 ppbv.

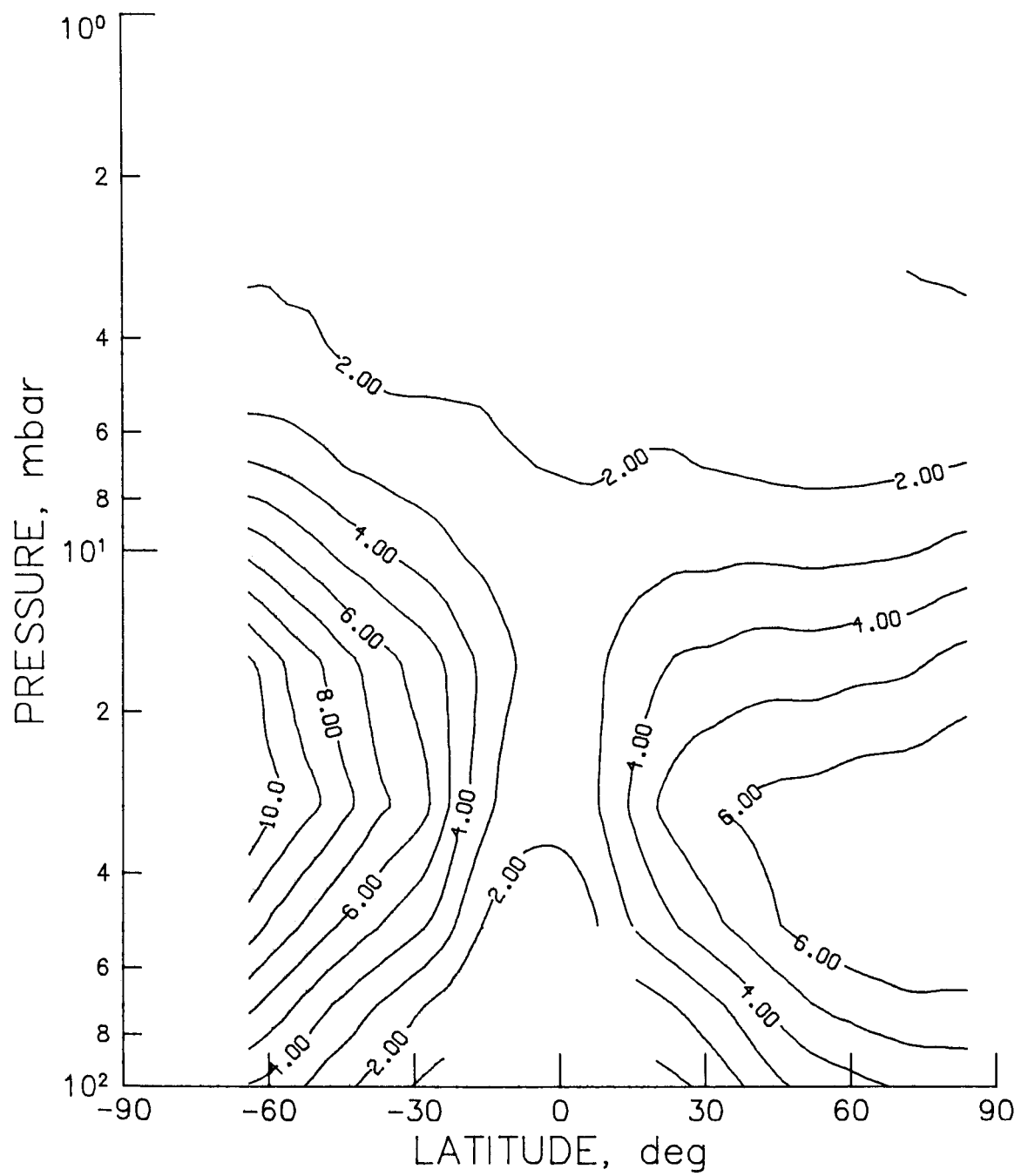


Figure 27. Zonal mean of combined mode nitric acid mixing ratio for May. Contour spacing is 1.0 ppbv.

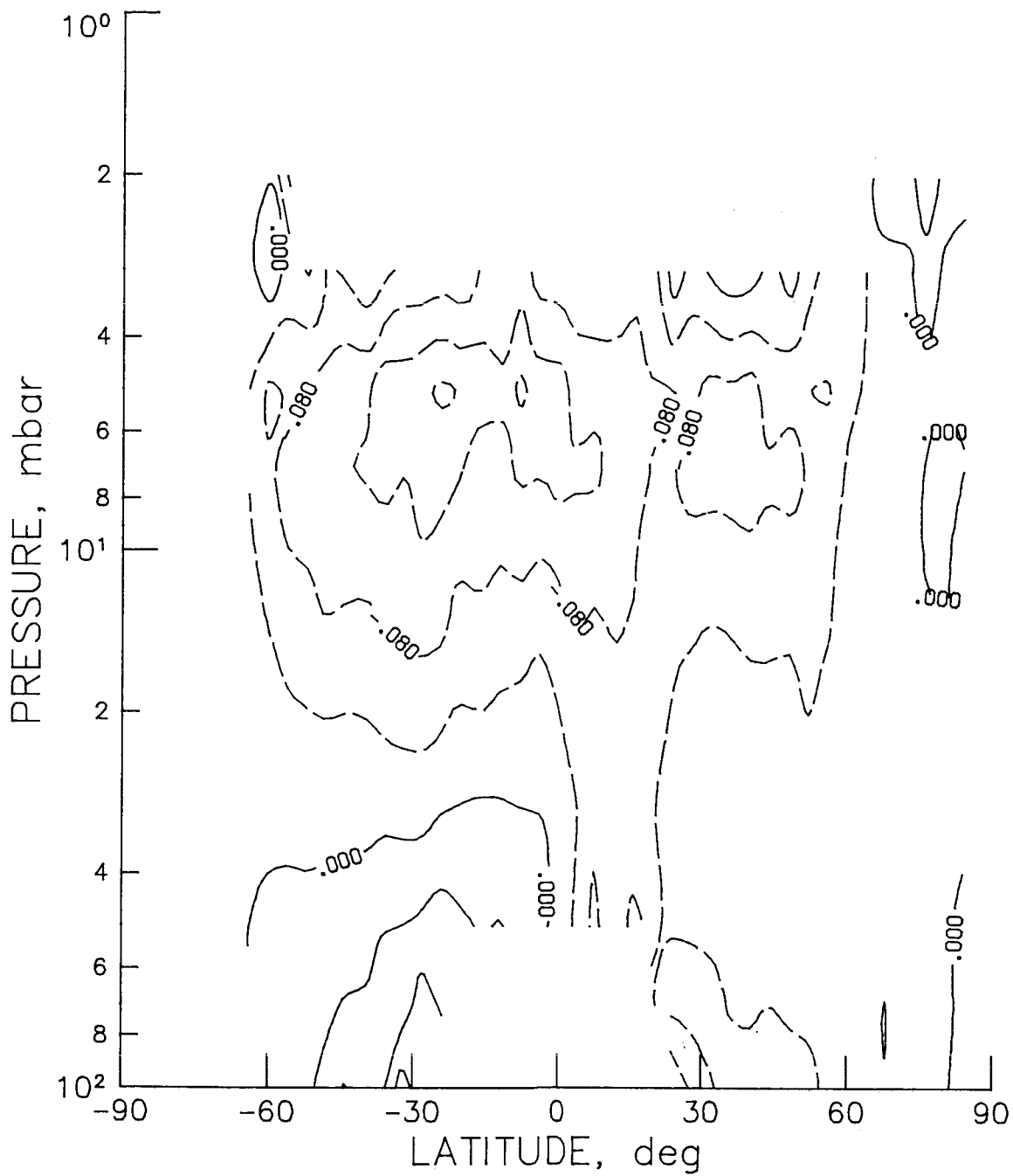


Figure 28. Ascending minus descending mode zonal mean nitric acid mixing ratio, divided by the average of the two zonal means, for January. Dashed contours are negative and interval is 0.04.

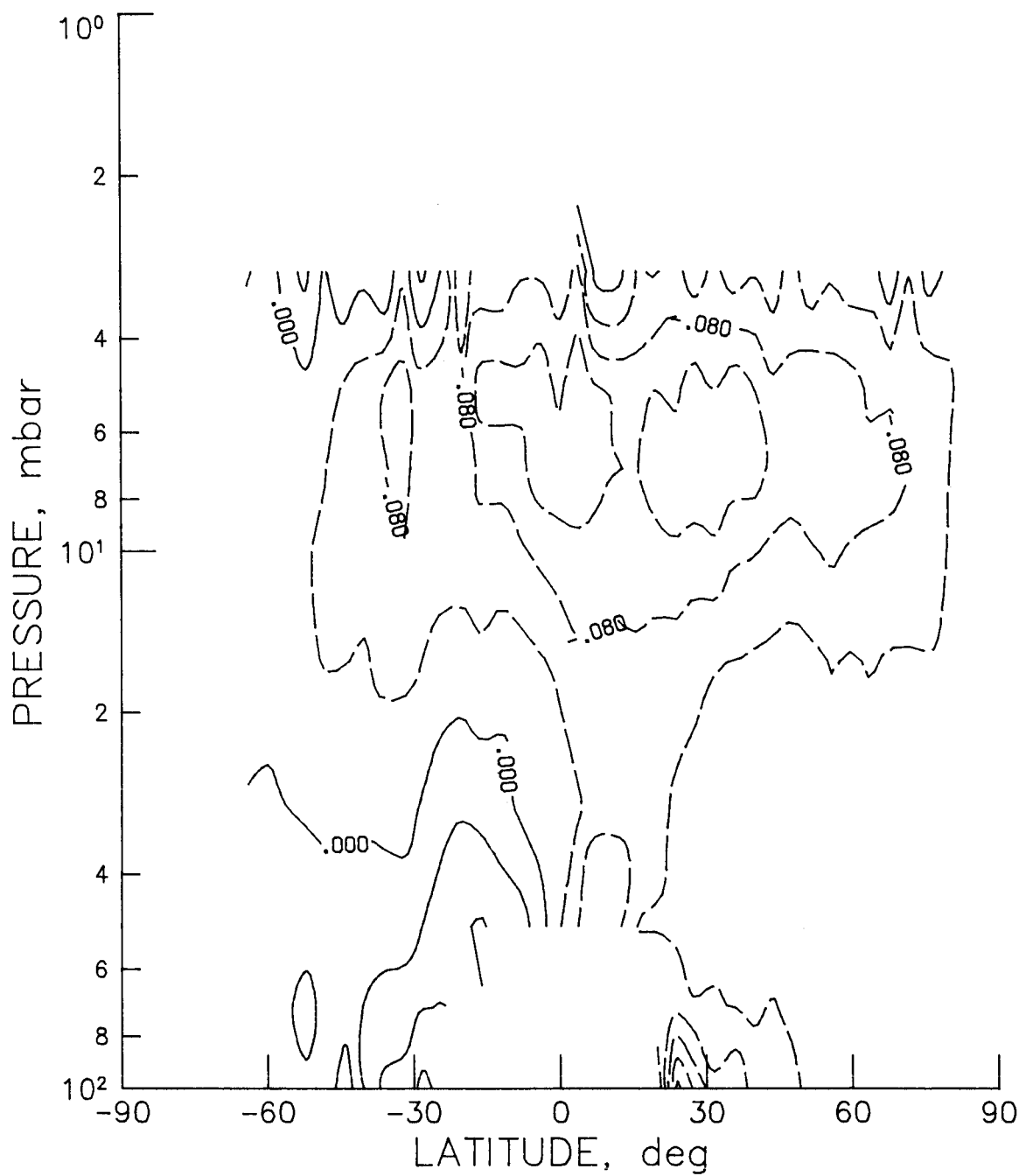


Figure 29. Ascending minus descending mode zonal mean nitric acid mixing ratio, divided by the average of the two zonal means, for May. Dashed contours are negative and interval is 0.04.

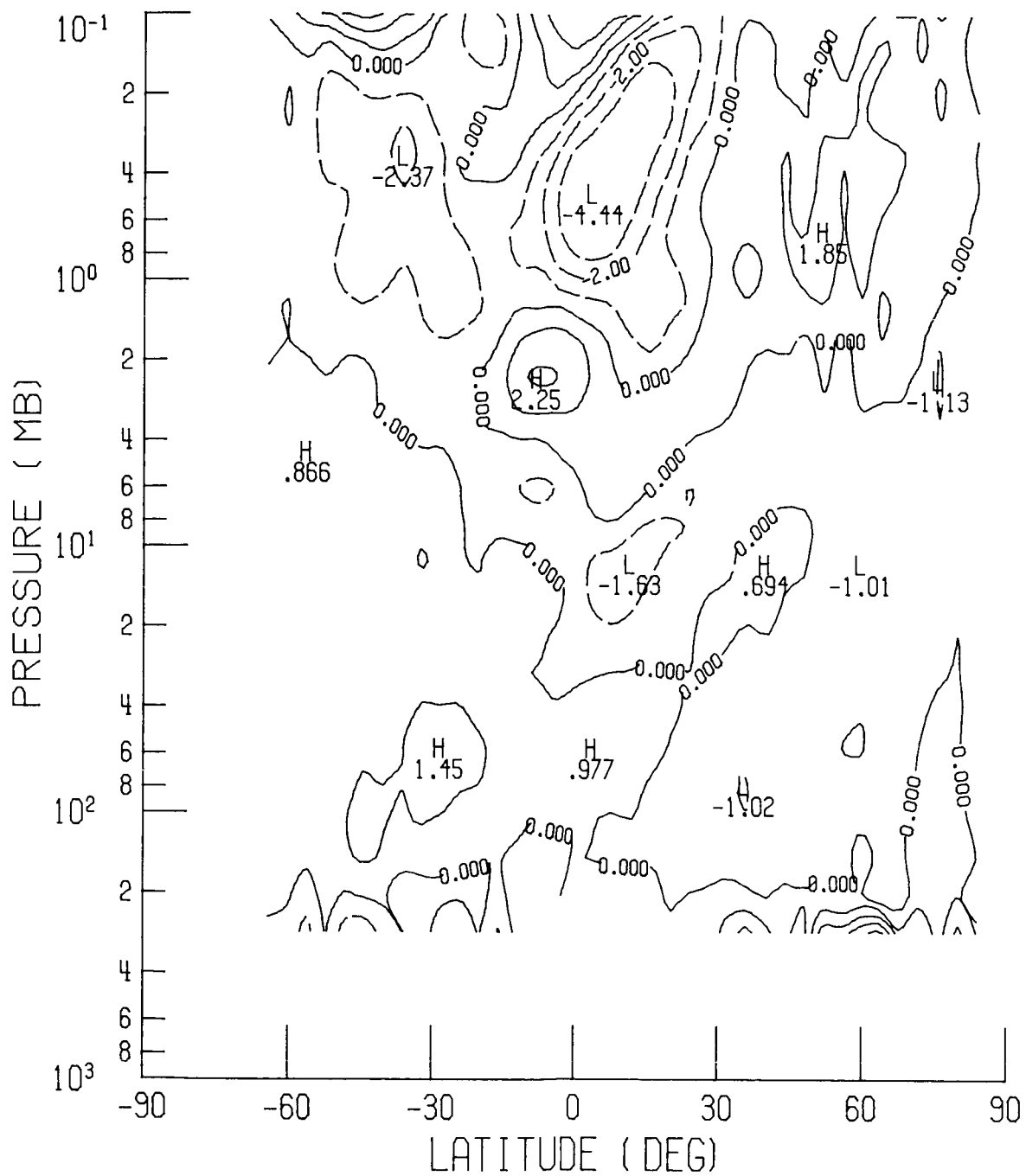


Figure 30. Ascending minus descending mode zonal mean temperature for January. Dashed contours are negative and interval is 1.0 K.

# N.H. LIMS LINE OF SIGHT

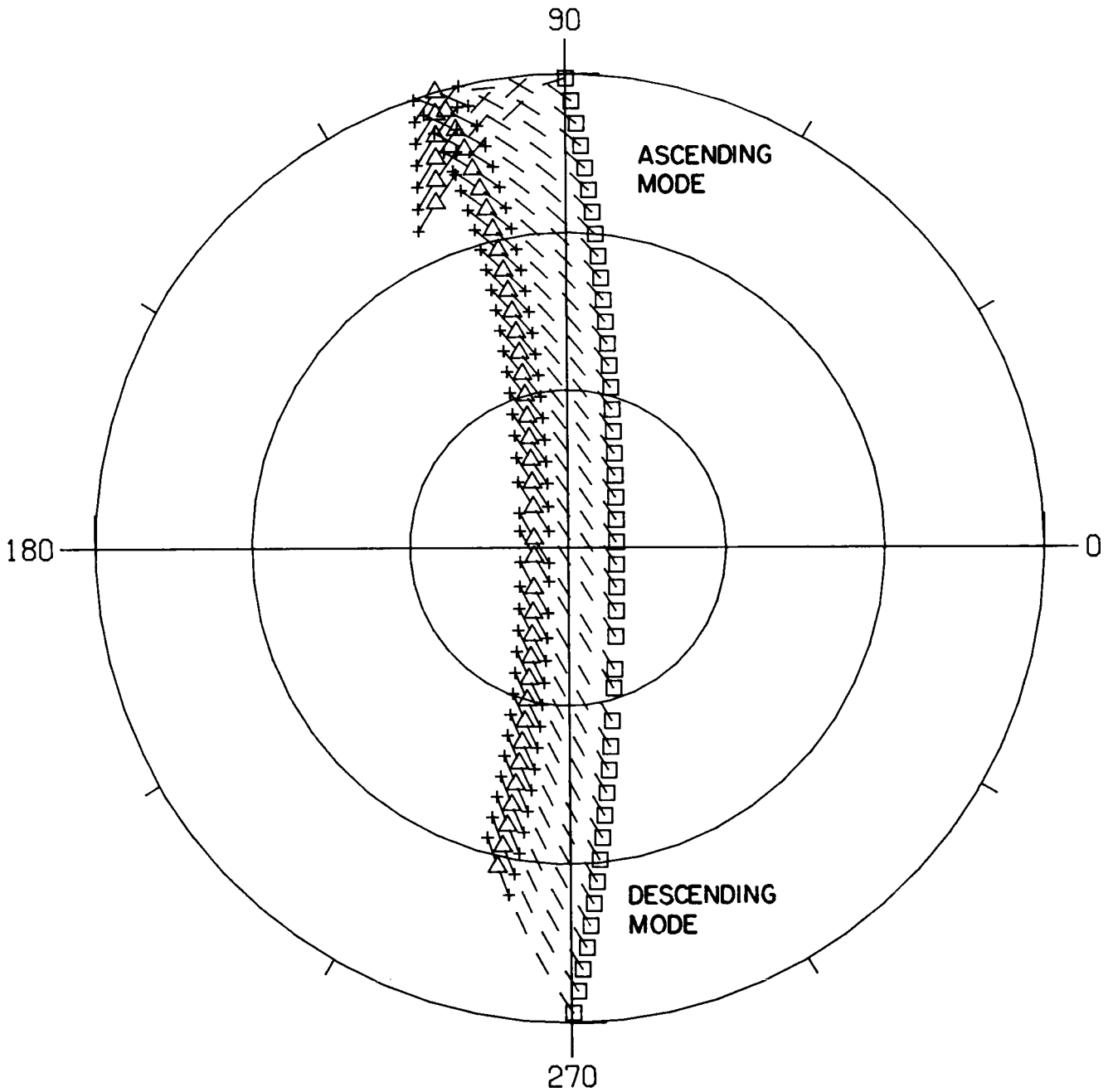


Figure 31. Polar projection of the Northern Hemisphere LIMS line of sight (dashed lines). Squares are subsatellite points; triangles are tangent points for tangent layer defined by pluses at 30 km. Ascending mode is for tangent point moving from south to north; and descending mode, the opposite.

# S.H. LIMS LINE OF SIGHT

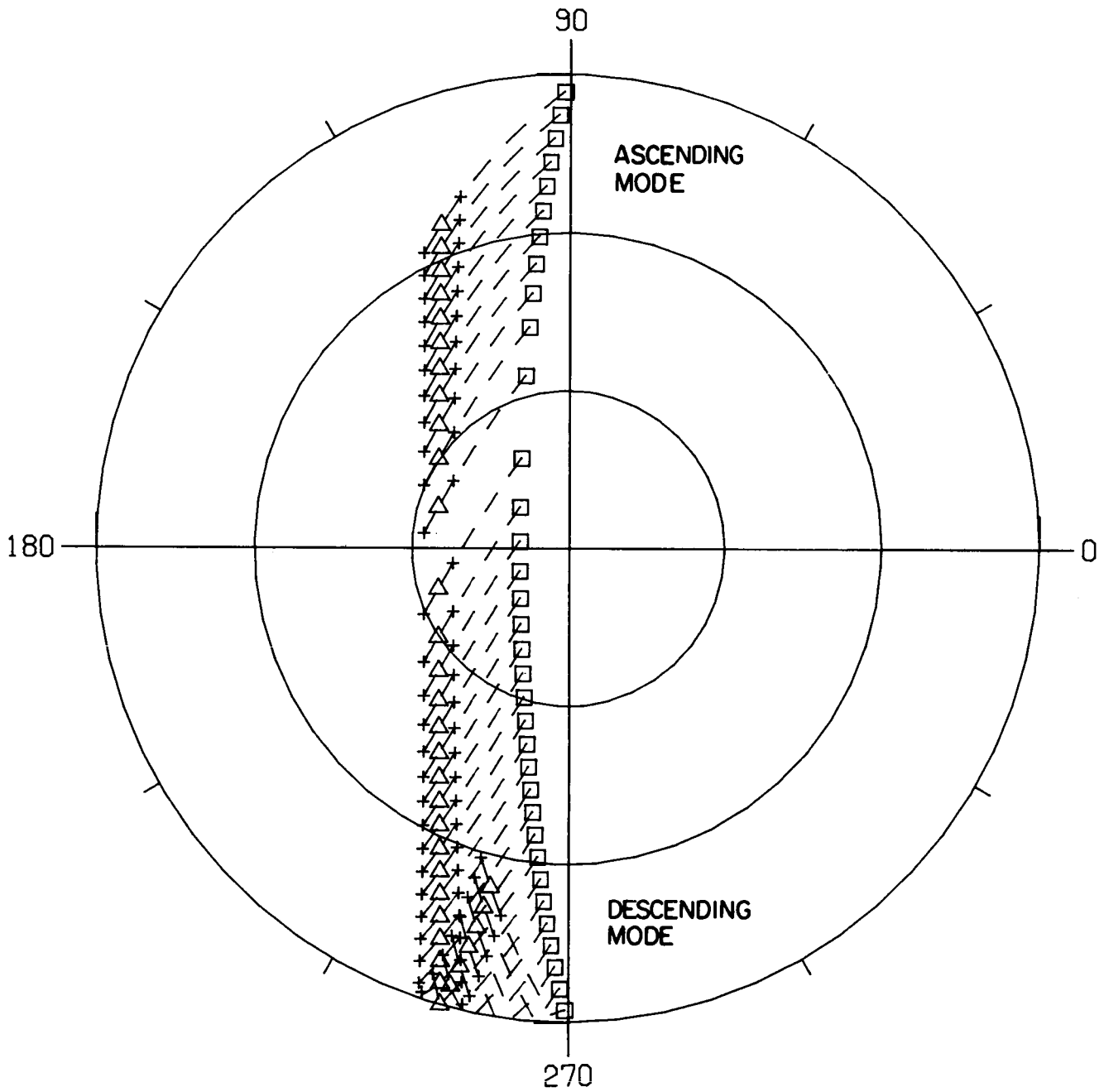


Figure 32. Polar projection of the Southern Hemisphere LIMS line of sight (dashed lines). Squares are subsatellite points; triangles are tangent points for tangent layer defined by pluses at 30 km. Ascending mode is for tangent point moving from south to north; and descending mode, the opposite.

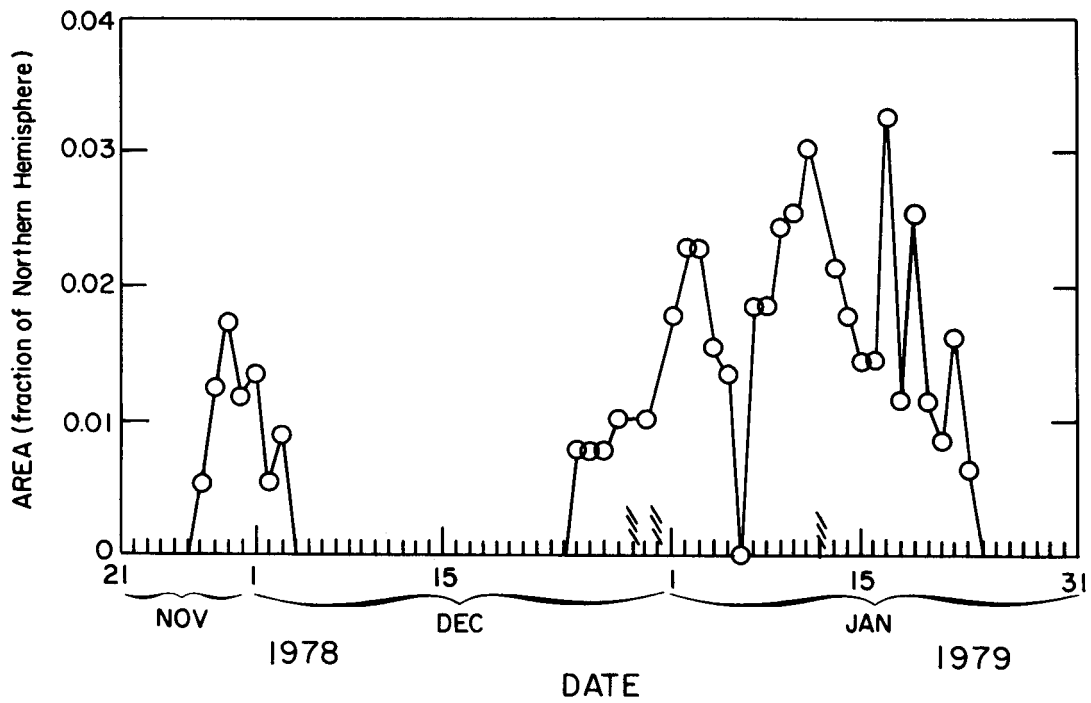


Figure 33. Area extent of polar stratospheric cloud signatures at 30 mbar. Hatched regions along the abscissa indicate dates when no data were taken.

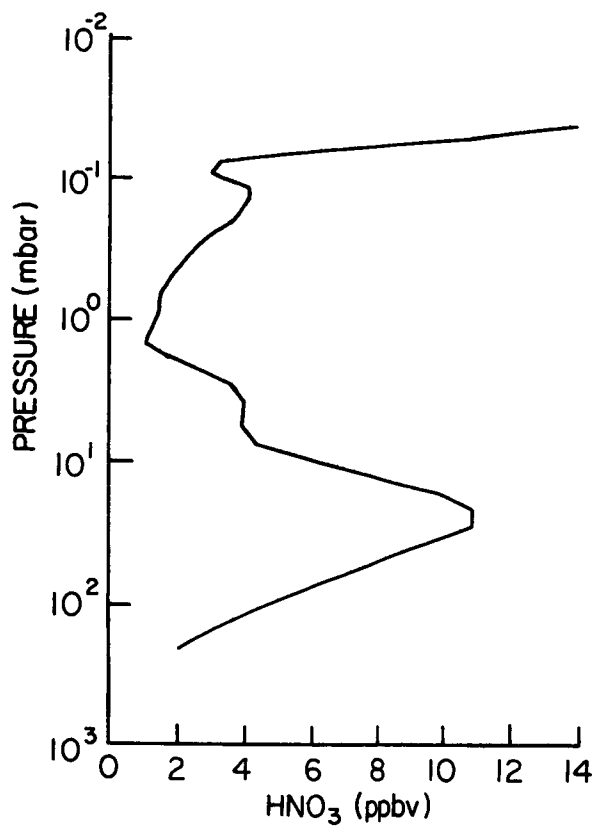
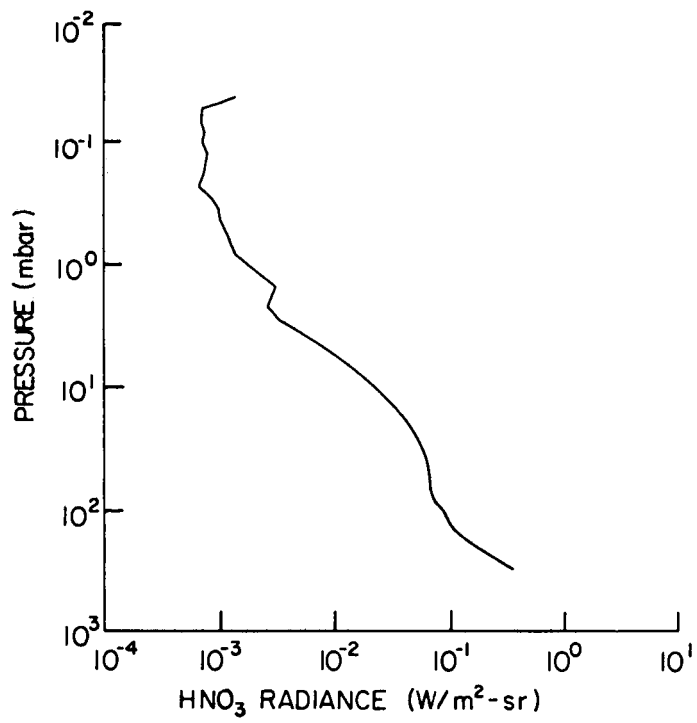
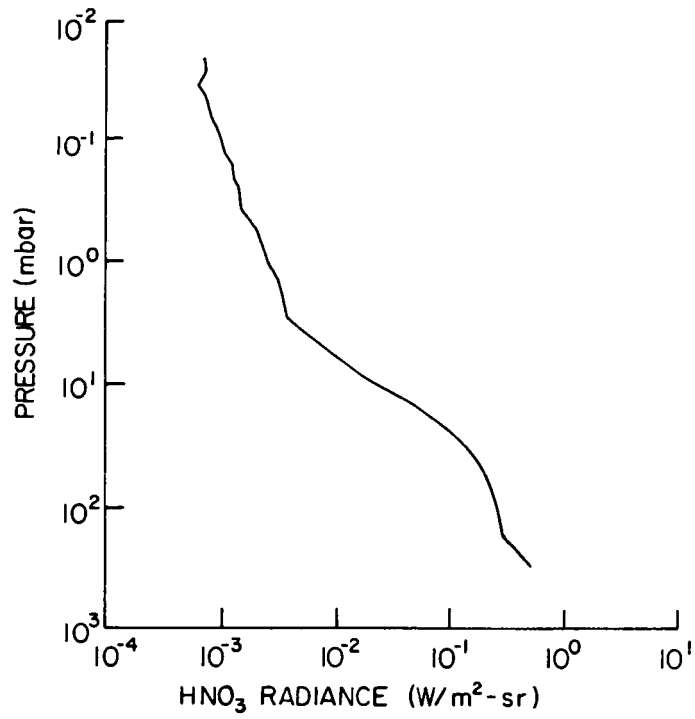


Figure 34. Sector-averaged nitric acid mixing ratio centered at 64°N, 270°E for Jan. 5-9.

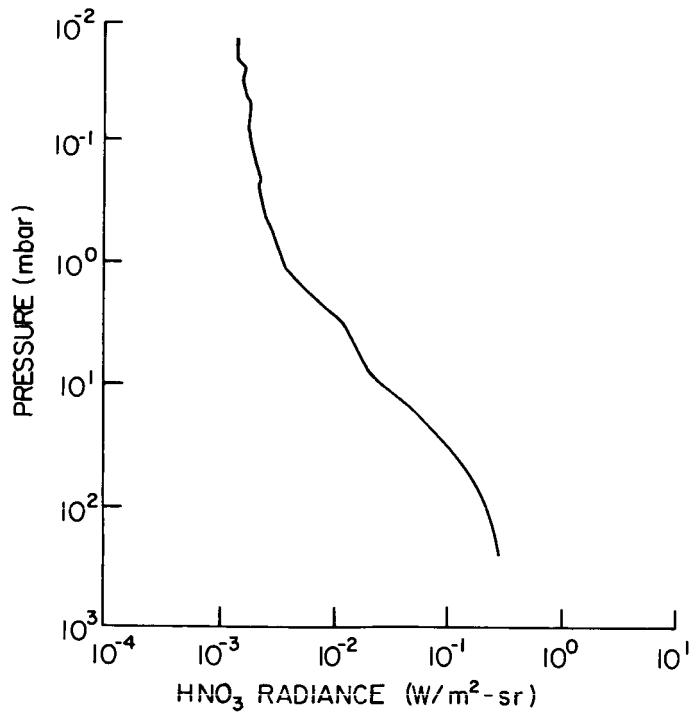


(a) 4°N, 270°E.

Figure 35. Sector-averaged nitric acid channel radiance profiles for Jan. 5-9.



(b) 44°N, 270°E.



(c) 80°N, 270°E.

Figure 35. Concluded.

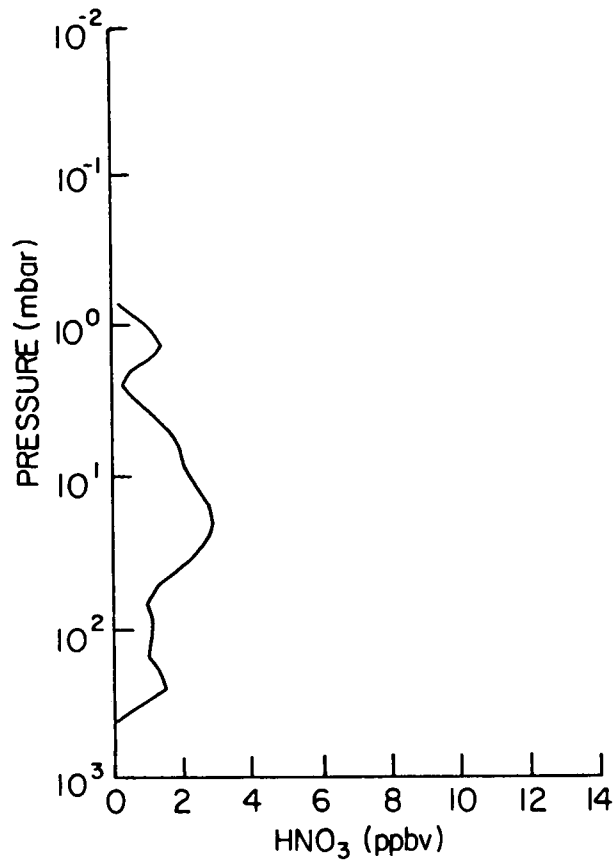


Figure 36. Sector-averaged nitric acid mixing ratio at 4°N, 270°E obtained from radiances in figure 35(a). Mixing ratio maximum near 1.5 mbar is an artifact of the incomplete removal of NO<sub>2</sub> side lobe effects (see text).

Standard Bibliographic Page

1. Report No. NASA TP-2625		2. Government Accession No.		3. Recipient's Catalog No.	
4. Title and Subtitle Description of Data on the Nimbus 7 LIMS Map Archive Tape—Ozone and Nitric Acid				5. Report Date December 1986	
				6. Performing Organization Code 673-41-10-70	
7. Author(s) Ellis E. Remsberg, Robert J. Kurzeja, Kenneth V. Haggard, James M. Russell III, and Larry L. Gordley				8. Performing Organization Report No. L-16136	
				10. Work Unit No.	
9. Performing Organization Name and Address NASA Langley Research Center Hampton, VA 23665-5225				11. Contract or Grant No.	
				13. Type of Report and Period Covered Technical Paper	
12. Sponsoring Agency Name and Address National Aeronautics and Space Administration Washington, DC 20546-0001				14. Sponsoring Agency Code	
15. Supplementary Notes Ellis E. Remsberg, Kenneth V. Haggard, and James M. Russell III: Langley Research Center, Hampton, Virginia. Robert J. Kurzeja: Savannah River Laboratory, Aiken, South Carolina. Larry L. Gordley: The College of William and Mary, Williamsburg, Virginia.					
16. Abstract The Nimbus 7 Limb Infrared Monitor of the Stratosphere (LIMS) data set has been processed into a Fourier coefficient representation with a Kalman filter algorithm applied to profile data at individual latitudes and pressure levels. The algorithm produces synoptic data at noon Greenwich Mean Time (GMT) from the asynoptic orbital profiles. This form of the data set is easy to use and is appropriate for time series analysis and further data manipulation and display. Ozone and nitric acid results are grouped together in this report because the LIMS vertical field of views (FOV's) and analysis characteristics for these species are similar. A comparison of the orbital input data with mixing ratios derived from Kalman filter coefficients indicates errors in mixing ratio of generally less than 5 percent, with 15 percent being a maximum error. The high quality of the mapped data was indicated by coherence of both the phases and the amplitudes of waves with latitude and pressure. Examples of the mapped fields are presented, and details are given concerning the importance of diurnal variations, the removal of polar stratospheric cloud signatures, and the interpretation of bias effects in the data near the tops of profiles.					
17. Key Words (Suggested by Authors(s)) LIMS (Limb Infrared Monitor of the Stratosphere) Nimbus 7 Kalman filter Ozone Nitric acid			18. Distribution Statement Unclassified—Unlimited  Subject Category 46		
19. Security Classif.(of this report) Unclassified		20. Security Classif.(of this page) Unclassified		21. No. of Pages 71	22. Price A04